Université Polytechnique HAUTS-DE-FRANCE

Thèse de doctorat

Pour obtenir le grade de Docteur de

L'UNIVERSITÉ POLYTECHNIQUE HAUTS-DE-FRANCE

Spécialité en Automatique

Présentée et soutenue par

Braulio Norberto AGUIAR COTA

Le 12/07/2019 à Valenciennes, à 10:00

Ecole doctorale :
Sciences Pour l'Ingénieur (ED SPI 072)

Equipe de recherche, Laboratoire :
Laboratoire d'Automatique, de Mécanique et d'Informatique Industrielles et Humaines (LAMIH – UMR 8201)

Pilotage automatique robuste de train sous contrainte d'enrayage-patinage

JURY

Président du jury
- El Hajjaji, Ahmed. Professeur, MIS, UPJV Amiens, France

Rapporteurs
- Manamanni, Noureddine. Professer, CRESTIC, URCA, Reims, France
- Kratz, Frédéric. Professeur, PRISME, INSA Centre Val-de-Loire, Bourges, France

Examinateurs
- Nouvelière, Lydie. Maitre de Conférences HDR, IBISC, U Evry Paris-Saclay, France
- El Hajjaji, Ahmed. Professeur, MIS, UPJV Amiens, France

Invité : Demaya, Bernard, Docteur, Ingénieur, Expert Senior, ALSTOM, Saint-Ouen, France

Directeur de thèse : Guerra, Thierry-Marie. Professeur, LAMIH, UPHF, Valenciennes, France
Co-encadrant : Berdjag, Denis, Maitre de Conférences, LAMIH, UPHF, Valenciennes, France

Doctoral Thesis

Robust Automatic Train Steering Control under Jamming and Skidding Constraints

By Braulio Norberto AGUIAR COTA

Université Polytechnique Hauts-de-France

LAMIH UMR CNRS 8201

Supervisors:

GUERRA Thierry Marie, Full Professor UPHF.

BERDJAG Denis, Associate Professor UPHF.

DEMAYA Bernard, ADM Saint-Ouen ALSTOM Transport.

Keywords: Nonlinear system, fault detection, unknown input observer, railway systems.

Mots-clés: Systèmes non-linéaires, détection de défauts, observateur à entrées inconnues, système ferroviaire.

Abstract

Millions of people use the trains every day. Therefore, rail transport and infrastructure efficiency and safety is critical, for customers and companies. A major challenge nowadays is to climb automation levels for trains, from Grade of Automation (GoA) “0” which is basically on-sight train operation all the way to GoA “4” where train operations are unattended. GoA levels are defined by the International Association of Public Transport (UITP—French acronym), and aim to provide a roadmap for the development and the integration of the so-called automatic train operation (ATO) systems. ATO are operational safety enhancement devices that help the driver by automating some operations on the train, helping him/her to be more attentive and to focus on possible safety issues or unexpected situations. Currently, the level of automation that is reached for commercial rolling stock is GoA “2”, semi-automatic train operation, when starting and stopping operations are automated. Most of the existing ATO systems are GoA 2.

As within any modern vehicle, on-board systems on a train are linked, and the ATO is working together with automatic train protection (ATP) and automatic train supervision (ATS), to ensure the respect of the speed restrictions and stop the train at the station with accuracy and within an acceptable tolerance of its timetable. The stopping task is carried out by automatic train stop control (ATSC), and all of the devices together form a package called automatic train control (ATC) (Dong et al. 2010).

All automatic systems rely on two main functions: perception and decision. The ATO device will rely heavily on the available information to ensure an accurate perception of its environment and of the operational situation, in order to carry out the right decisions. This information acquired by sensors of different technologies and made available through the communication network (bus) of the train. Obviously, sensors are limited by technology, the communication bandwidth is not infinite; and all technical systems can experience faults and failures. Those are major challenges to design efficient and robust ATO devices, because the usual way to deal with these issues is to use sensors of different technologies for each information of interest. This makes such a system more complex, possibly costly, and it increases the amount heavily of transmitted data and its supporting infrastructure.

There is a promising solution to this challenge, and it is called virtual sensors, or observers that are developed by automatic control researchers to supplement the sensors at a fraction of the cost, and embeds knowledge of the system in the automated device through analytical models of the environment. The design of a particular type of observer, and its practical exploitation for automatic train operations is the main contribution of this PhD work.

Résumé

Des millions de personnes utilisent le train chaque jour. Par conséquent, l'efficacité et la sécurité du transport ferroviaire et de l'infrastructure sont essentielles pour les clients et les entreprises. De nos jours, l'un des principaux défis est d'augmenter le niveau d'automatisation des trains, du niveau d'automatisation « 0 » (ou Goals of Automation GoA) qui consiste essentiellement à exploiter les trains à vue jusqu'au niveau « 4 », où les opérations ne sont pas surveillées. Les niveaux GoA sont définis par l'Union internationale des transports publics (UITP) et ont pour objectif de fournir une feuille de route pour le développement et l'intégration des systèmes dits « d'exploitation automatique des trains » ou ATO. Les ATO sont des dispositifs d'amélioration de la sécurité opérationnelle qui aident le conducteur en automatisant certaines opérations, lui permettant de se concentrer sur les problèmes de sécurité éventuels ou les situations imprévues. Actuellement, le niveau d'automatisation atteint pour le matériel roulant commercial est GoA « 2 », ou une exploitation semi-automatique des trains, les opérations de démarrage et d'arrêt étant automatisées. La plupart des systèmes ATO existants sont GoA 2.

Comme dans tout véhicule moderne, les systèmes embarqués sur un train sont liés et l'ATO collabore avec les organes de sécurité tels que la protection automatique des trains (ATP) et la surveillance automatique des trains (ATS). Il doit garantir le respect des limitations de vitesse et arrêter le train à la gare avec précision, tout en respectant une table horaire. La tâche d'arrêt est effectuée par le contrôle automatique de l'arrêt des trains (ATSC). L'ensemble de ces dispositifs forment le contrôle automatique des trains (ATC) (Dong et al. 2010).

Tous les systèmes automatiques reposent sur deux fonctions principales : la perception et la décision. Le dispositif ATO s'appuiera fortement sur les informations disponibles pour assurer une perception précise de son environnement et de la situation opérationnelle, afin de prendre les bonnes décisions. Ces informations sont acquises par des capteurs de différentes technologies et mises à disposition via le réseau de communication (bus) du train. De toute évidence, les capteurs sont limités par la technologie, la bande passante de communication

n’étant pas infinie. De plus, tous les systèmes techniques peuvent rencontrer des défauts et des échecs. Il s’agit là d’un défi majeur pour la conception de dispositifs ATO robustes et efficaces, car la manière habituelle de traiter ces problèmes consiste à utiliser des capteurs de technologies différentes pour chaque information source d’intérêt. Cela rend ce système plus complexe, souvent plus coûteux, et augmente considérablement la quantité de données transmises et son infrastructure de support.

Il existe une solution prometteuse à ce défi. Il s’agit de capteurs virtuels, ou observateurs développés par des chercheurs en contrôle automatique pour compléter les capteurs à une fraction du coût, et intégrer la connaissance du système dans l’automate à l’aide de modèles analytiques de l’environnement. La conception d’un type particulier d’observateur et son utilisation pratique pour l’exploitation automatique des trains constituent l’apport principal de cette thèse.

Index

CHAPTER 1. Introduction

1.1. Context of the thesis

Millions of people use the trains every day. Therefore, rail transport and infrastructure efficiency and safety is critical, for customers and companies. A major challenge nowadays is to climb automation levels for trains, from Grade of Automation (GoA) "0" which is basically on-sight train operation all the way to GoA "4" where train operations are unattended. GoA levels are defined by the International Association of Public Transport (UITP – French acronym), and aim to provide a roadmap for the development and the integration of the so-called automatic train operation (ATO) systems. ATO are operational safety enhancement devices that help the driver by automating some operations on the train, helping him/her to be more attentive and to focus on possible safety issues or unexpected situations. Currently, the level of automation that is reached for commercial rolling stock is GoA "2", semi-automatic train operation, when starting and stopping operations are automated. Most of the existing ATO systems are GoA 2.

As within any modern vehicle, onboard systems on a train are linked, and the ATO is working together with automatic train protection (ATP) and automatic train supervision (ATS), to ensure the respect of the speed restrictions and stop the train at the station with accuracy and within an acceptable tolerance of its timetable. The stopping task is carried out by automatic train stop control (ATSC), and all of the devices together form a package called automatic train control (ATC) (Dong et al. 2010).

All automatic systems rely on two main functions: perception and decision. The ATO device will rely heavily on the available information to ensure an accurate perception of its environment and of the operational situation, in order to carry out the right decisions. This information acquired by sensors of different technologies and made available through the communication network (bus) of the train. Obviously, sensors are limited by technology, the communication bandwidth is not infinite; and all technical systems can experience faults and failures. Those are major challenges to design efficient and robust ATO devices, because the usual way to deal with these issues is to use sensors of different technologies for each

information of interest. This makes such system more complex, possibly costly, and it increases heavily the amount of transmitted data and its supporting infrastructure.

There is a promising solution to this challenge, and it is called virtual sensors, or observers that are developed by automatic control researchers to supplement the sensors at a fraction of the cost, and embeds knowledge of the system in the automated device through analytical models of the environment. The design of a particular type of observer, and its practical exploitation for automatic train operation is the main contribution of this PhD work.

1.2. Research scope

Observers are efficient numerical solutions that avoid adding new sensors, providing state reconstruction and disturbance estimation. Information provided by observers are used to improve "measurements" precision and to estimate and compensate the exogenous disturbances using observer-based compensation controllers. A class of observers called unknown input observers (UIO) (J. Chen, Patton, and Zhang 1996) is used for this matter, it belongs to the so-called observer-PI family. This technique is well-known and has been successfully applied to many problems such as (Delrot et al. 2012; Lendek et al. 2010). The estimated perturbation can be efficiently taken into account with appropriate robust control techniques (Faieghi, Jalali, and Mashhadi 2014; Gao, Liu, and Chen 2016). However, if an unexpected event occurs, like a device fault or failure, the "usual" control compensation can be inadequate.

Unexpected events can be predicted through symptom detection, if the event dynamic is known and modelled. The analysis of discrepancy between estimations and measurements is the way to detect the symptoms of a possible problem. This analysis is based on the so-called model-based or model-free techniques, and is known under the name of Fault Detection, Isolation and Estimation (FDIE) or (FDI) (Gao, Cecati, and Ding 2015). FDI techniques are used for trains, for example in (Jesussek and Ellermann 2013) to capture the nonlinear characteristic of a railway vehicle, or in (Wei, Jia, and Liu 2013) to compare acceleration measurements. FDIE was also used for high-speed railway traction devices in (Y. Wu, Jiang, and Shi 2016) and to the analysis of train networks in (Verbert, De Schutter, and Babuška 2016).

A fault that often occurs in train braking systems is the wheel jamming (blocking) (Aguiar et al. 2017). This fault will hinder braking distance and position measurement, since the odometer, i.e. a frequently used sensor, is based on quantifying wheel rotation. Obviously, if the sensor is in the wheel, then when the wheel jams, the measurement will be corrupted. On another hand, if the sensor is placed on the rail, like a position beacon, then the position information is more accurate. Of course, installing the necessary beacons on all the tracks will quickly face a problem of cost and is therefore, unrealistic. Another important point is to derive fault tolerant traction and brake controls, thus, we need to detect accurately the faults, ideally missing none of them, and generating no false alarms. In view of this, H_∞ attenuation techniques helps to improve fault detection robustness with respect to modeling uncertainty (Edelmayer, Bokor, and Keviczky 1994; Zhong et al. 2003), and H_- index for fault detection sensitivity (J. L. Wang, Yang, and Liu 2007; Z. Wang et al. 2017; M. Zhou et al. 2017).

Wheel jamming, and more generally speaking, adherence issues, will lead in practice to an overestimation of the train timetable, and it is made only through collected data. An interesting topic to explore is how to improve train scheduling, by estimation of the worst case performance of observer estimation, i.e. by computing a worst case bound of the observer error. An idea to develop is to use Gronwall-like bounds theory (Dragomir 2003; Fall 2015a) to compute such a bound.

1.3. Industrial Scope and Objectives

The research project has been made together with the LAMIH laboratory and the ALSTOM Company, which is a major actor in train industry. The request of the company was about efficient numerical algorithm that will supplement odometric speed sensors for ATSC driven accurate train stopping, without knowledge of wheel-track adherence conditions and with probable intermittent wheel jamming and wheel skidding anomalies.

The first part of this work is the modeling and simulation of wheel-rail contact and actions of WSP-skid control laws. Based on this simulation model, comparisons are made with ATP and ATO level measurements acquired through experiments. The aim is to place the following studies in the context of close experimental feedback.

The second part is the study about observation of the jamming phenomenon and the action of the anti-lock control device. Taking into account the discrepancy between the measurement updates and the reaction time of ATO level systems, a continuous-discrete behavior is to be considered.

Finally, a more accurate representation of kinematics can improve existing control algorithms in variable or degraded adherence situations. Robust control must ensure accurate train stopping in all situations. Furthermore, the robust control must ensure that no ATP emergency will be triggered because of position estimation bias. A supervision system can complement the robust control autopilot device.

1.4. Outline

The thesis is organized as follows:

Chapter 2 gives a background on railways systems and automatic train control. An analysis of the mathematical model and fault interpretation for train systems is presented. In addition, a brief state of the art on robust observation and estimation for fault detection is provided.

Chapter 3 is divided in two sections: First, an active fault tolerant braking control is presented, where the main contribution is the integrated approach using an unknown input observer, fault detection, and disturbance compensation control with a reference model for train stopping, with some assumptions on the system. The design of such system and a discussion on the convergence properties is provided. The second part relaxes most of the assumptions and deals with the design of robust position estimation algorithm, based on the unknown input observer with a quasi-LPV representation. Illustrations are provided for both contributions.

Chapter 4 explores a novel Gronwall-like bound for the observer error, in continuous-discrete dynamic. The unknown input observer is considered in a quasi-LPV framework with a piecewise constant input. Practical considerations on how to improve the bound with extra information from the system are discussed. Simulations are provided for all cases.

Chapter 5 presents the results of chapters 3 and 4 applied to data acquired during real time experiments provided by ALSTOM. We present many situations, considering different speeds

and different adherence conditions. The performance of the developed observers is discussed, and strategies for observer parameters choice is proposed.

Chapter 6 concludes this work with some important remarks and future research.

CHAPTER 2. Background

This chapter presents a general knowledge about the train systems. Mathematical models used in the literature are depicted taking into account practical consideration. The behavior of sensors especially, under fault occurrences, are also described; faults due to jamming and skidding being the ones treated therein. A review of available solutions of the literature is also given. Implementation issues are discussed, especially the different operation levels and their communication: Automatic Train Control system (ATC) and its internal processes: Automatic Train Protection (ATP), Automatic Train Operation (ATO), and Automatic Train Supervision (ATS). The solutions will concern robust control, observers and fault detection analysis of different kinds depending on the assumptions made. Therefore, various observers for fault diagnosis are presented, including unknown input observers and a particular continuous-discrete time observer. A focus on jamming and skidding faults ends the chapter.

2.1. The train system

A train is composed by the locomotive and the wagons, as shown Fig. 2-1. The locomotive, among other systems, includes the motors for traction and the braking system. There are different types of railway traction, that can be divided into two groups: diesel and electric traction (Iwnicki 2006; José A. Lozano 2012; Kaller and Allenbach 1995). For diesel traction, several transmissions are available, mechanical, hydraulic and electrical. For electrical traction, there are DC (direct current) motors and AC (alternating current) motors. Nowadays, almost all the locomotives use electric traction, where the most used motors are basically (José A. Lozano 2012): DC motors with in-series or independent excitation and AC motors. The use of electric traction is considered clean and efficient.

The braking system can be categorized, depending on its mechanisms, into three groups (Fig. 2-2): pneumatic brakes (or air brakes), electric brakes, and mechanical brakes (Izumi and Seigo 1999; The Railway Technical Website n.d.). The different systems are combined on a same train. Let's consider for example pneumatic brakes: they rely on air compressors mounted into the wagons to supply pressurized air to the brakes. This technology induces a delay between the braking command and effective braking, because pressure variations cannot be

instantaneous. An improvement of this braking system is the use of electro-pneumatic brakes, using an electric signal to transmit the command. However, electro-pneumatic brakes are less reliable than a pure pneumatic system, and are used to complement the latter.

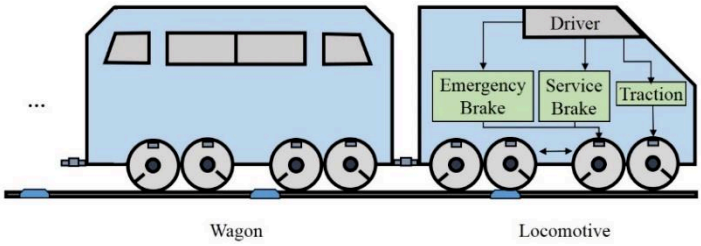

Fig. 2-1. The train system

The interaction of both systems follows some common principles as is explained in (The Railway Technical Website n.d.), for example:

- The electro-pneumatic brake operates as the service brake while the air brake is retained for emergency use
- The electro-pneumatic brake does not compromise the fail-safe or "vital" features of the air brake
- The air brake normally remains in the "release" position, even while the electro-pneumatic brake is in "application" and the same brake cylinders are used.
- Electro-pneumatic brakes are invariably used on multiple unit passenger trains.
- Electro-pneumatic brakes use a number of train wires to control the electrically operated brake valves on each wagon.
- The train wires are connected to a brake "valve" or controller in the driver's cab.

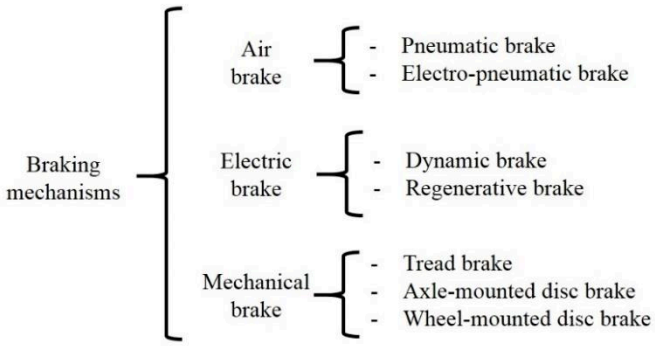

Fig. 2-2. Braking mechanisms.

The same can be said about electric and mechanic brakes. This work will not focus on braking system details, the main point here is to explain that the required braking force is a result of a combined efforts of multiple braking systems, with different dynamics that interact in a way that is difficult to model efficiently. One of the main implications is that high level systems (ATO and such) that embed control algorithms, have a poor knowledge of the braking effort that is applied in real-time for a given reference braking force.

The conditions necessary to produce the motion of the train via the traction and brake systems depend on the forces applied in the train and the adherence to tracks (the so-called rail-wheel contact), which is explained later.

2.1.1. The mathematical train model

There are many models for the analysis of separate vehicles (i.e. locomotive and wagons) and train dynamics. In general, those models can be categorized into three main groups, Fig. 2-3, (Vijay 1984).

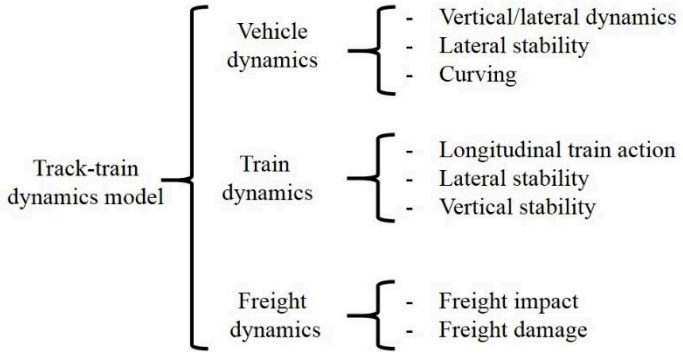

Fig. 2-3 Track-train dynamics model (Vijay 1984).

The single-point train control model is the most commonly model applied for train operation problems in the literature (Guzinski et al. 2009; Kaller and Allenbach 1995; Liu and Golovitcher 2003; Vijay 1984; Yin et al. 2017). A train with multiple vehicles is considered as single point mass object and its longitudinal motion can be approximated by a Newton equation. Therefore, the dynamic of the train can be described by the following differential equations (Guzinski et al. 2009; Kaller and Allenbach 1995; Liu and Golovitcher 2003; Vijay 1984):

$$\begin{cases} m\dot{v} = b_T(v)u_T - b_B(v)u_B - w(v) - g(p) \\ \dot{p} = v \end{cases} \tag{2.1}$$

Where v is the velocity of the train (m/s), p is position of the train (m), $b_B(v)$ is the coefficient of the braking force, u_B is the relative braking force and $b_T(v)$ is the coefficient of the traction force, u_T is the relative traction force, $g(p)$ is the tangential force to the path or the force of the declivity, $w(v)$ is the resistance to motion, and m is the mass of the train (kg). As shown in Fig. 2-4, the train dynamic along a railway slope of angle θ depends on the traction, the brake and the declivity forces, and also on the drag. Declivity force in practical cases is considered as $g(p) = g\sin(\theta(p))$, where $\theta(p)$ is the slope angle at distance p along the railway line, and g is the gravity (Howlett, Milroy, and Pudney 1994; Tan et al. 2018; Transport: Railways 2004; Vijay 1984).

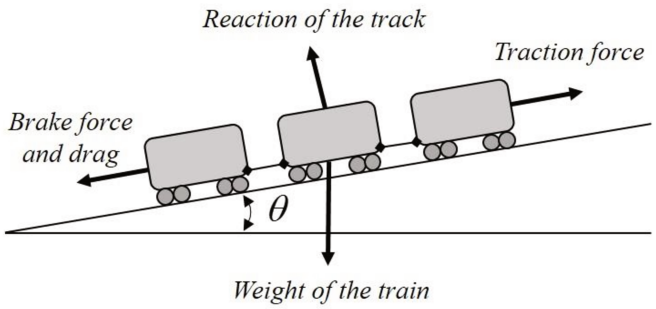

Fig. 2-4 Train dynamics

The drag or resistance to motion is assumed as a set of forces where the most important is the friction force. This force is calculated as the sum of Stribeck, Coulomb, and viscous components, Fig. 2-5. Even if the resistance to motion cannot be precisely measured by sensors, solutions using run-down tests are possible. In (Rochard and Schmid 2000) a review of the various methods applied to measurement and estimation of train resistance to motion is presented and especially the run-down tests. In these tests, the resistance is estimated either by the measurement of the deceleration versus time or by the measurement of the traction force

necessary to maintain a constant velocity at various speeds, in order to cover the working speed range. Of course, due to the experimental parameters (several speeds, different adherences) and the required conditions, these procedures are costly. Consequently, the railway transportation industry developed empirical equations that could be used to estimate the resistance to motion of a generic train. The equation is a polynomial approximation by a quadratic function that is well known, called the Davis equation. Davis equation has been applied and validated in many real time experiments, see for example (Kaller and Allenbach 1995; Rochard and Schmid 2000; Transport: Railways 2004; Douglas et al. 2017; Q. Wu, Spiryagin, and Cole 2016). The form of the equation is:

$$w(v) = w_0 + w_1 v + w_2 v^2 \tag{2.2}$$

where w_0 (N), w_1 $(\mathrm{Ns/m})$ and w_2 $(\mathrm{Ns^2/m^2})$ are real coefficients depending on train and track characteristics. Equation (2.2) shows that the most impact at lower speed is due to coefficients w_0 and w_1, representing the rolling resistance to mechanical friction, while w_2 has the major role at high speed, that is related to aerodynamic resistance. Based on the review in (Rochard and Schmid 2000), the French national railways company, SNCF (Société Nationale des Chemins de Fer français), evaluates the terms w_0, $w_1 v$ and $w_2 v^2$ as function of the rolling stock characteristics, using the following expressions:

$$w_0 = 10^{-5}\left(\varpi m_t\left(10^2\sqrt{\frac{10}{m_l}}\right)\right), \tag{2.3}$$

$$w_1 v = \left(3.6\times 10^{-7}\right) m_t v\,, \tag{2.4}$$

Where m_t is the total train mass (kg), m_l is the mass per axle (kg) and ϖ is a dimensionless parameter with values depending on the rolling stock type, e.g. for SNCF vehicles it is $0.9 \le \varpi \le 1.5$, the lower value being applicable to modern rolling stock, the higher value to nonhomogeneous freight trains. The last term is:

$$w_2 v^2 = 0.1296\left(\kappa_1\kappa_3 + \kappa_2\kappa_4 l\right)v^2\,, \tag{2.5}$$

Where the first term represents the aerodynamic resistance existing at the front and rear of the train and the second term is related to the aerodynamics resistance generated along the surface, $\kappa_4 l \ \left(\mathrm{m}^2\right)$, κ_4 is the partial perimeter (m) of the rolling stock, l is the train length (m), κ_1 $\left(\mathrm{N/m}^2\right)$ is a parameter depending on the shape of the train, front and rear, and can vary from 20×10^{-4} for conventional rolling stock to 9×10^{-4} for TGV (French High Speed Train), κ_3 is the front surface cross-sectional area $\left(\mathrm{m}^2\right)$, commonly around $10\ \mathrm{m}^2$ and κ_2 $\left(\mathrm{N/m}^2\right)$ is a parameter depending on the condition of the surface, $\kappa_4 l$, and can vary from 30×10^{-6} for conventional rolling stock to 20×10^{-6} for TGV.

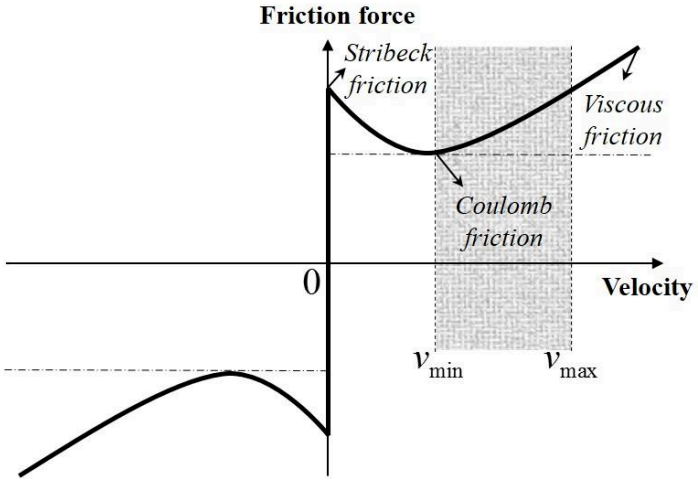

Fig. 2-5 Friction forces.

Wheel rail contact

To study the motion of the train we need to consider the wheel-track *adhesion*. *Fig. 2-6* shows the forces that are applied to the wheel and to the track. We will discuss the adhesion force F_a , since the other forces were defined previously.

The adhesion force F_a satisfies the following expression (Iwnicki 2006; José A. Lozano 2012; Kaller and Allenbach 1995):

$$F_a = \mathrm{N}\delta\,, \tag{2.6}$$

Where δ is the so-called *adhesion coefficient* and N is the vertical reaction of the track, which balances the vertical forces. This adhesion coefficient depends on temperature, humidity, dirt, speed, etc. A general expression for the approximation of δ is

$$\delta = \frac{\delta_0}{1+0.01v}, \tag{2.7}$$

where δ_0 is a real coefficient and velocity (v) is expressed in Km/h. Table. 2.1 shows typical values of δ_0 used in different regions.

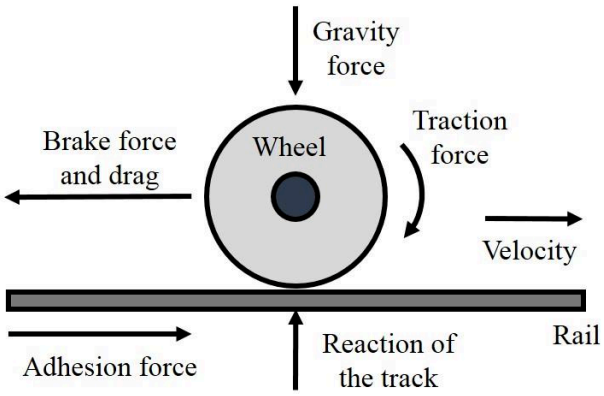

Fig. 2-6 Wheel rail contact.

A low adhesion between the wheel and the rail is an important issue for braking and traction. Poor adhesion in braking is a safety issue as it can extend the stopping distances. During traction, poor adhesion will interfere with acceleration of the locomotive, making it difficult to reach the desired speed. Mechanically, low adhesion phenomena will cause wheel jamming (when braking) and wheel skidding (when traction). Of course, this will also impact the onboard speed and position measurements of the train, because the odometers are located on the wheels. These phenomena and issues are explained in the next section.

Table. 2.1. Adhesion coefficient values for δ_0 (José A. Lozano 2012).

Adhesion coefficient values for δ_0		
SNCF (France)	Electric monophasic locomotive, multi-motor bogies	0.33
	Electric monophasic locomotive, mono-motor bogies	0.35
DB (Germany)	Diesel locomotives	0.30
	Electric monophasic locomotives	0.33
RENFE (Spain)	Diesel locomotives	0.22 - 0.29
	Classic electric locomotives	0.27
	Modern electric locomotives	0.31
USA	SD75MAC diesel and electric locomotives	0.45

Therefore, under the previous assumptions, a nonlinear continuous-time state space representation of the train system can be written as:

$$\begin{cases} \dot{x}(t) = A(x(t))x(t) - B_B(x(t))u_B(t) + B_T(x(t))u_T(t) + G(x(t)) \\ y(t) = Cx(t) \end{cases} \tag{2.8}$$

with $x(t) = \left[x_1(t) \;\; x_2(t) \right]^T$ the state vector, $x_1(t) = v(t)$ the train speed and $x_2(t) = p(t)$ its position and $y(t)$ is the output of the system. The matrices are: $A(x(t)) = \begin{bmatrix} -(w_1 + w_2 x_1(t)) & 0 \\ 1 & 0 \end{bmatrix}$, $B_B = \begin{bmatrix} b_B(x_1(t)) \\ 0 \end{bmatrix}$, $B_T = \begin{bmatrix} b_T(x_1(t)) \\ 0 \end{bmatrix}$, $G(x(t)) = \begin{bmatrix} -w_0 - g(x_2(t)) \\ 0 \end{bmatrix}$ and $C = \begin{bmatrix} 1 & 0 \end{bmatrix}$.

The nonlinear system (2.8) is the basic model considered in this work for continuous time. When a representation in discrete time will be used, it is obtained using the classical Euler transformation (Kowalczuk 1993):

$$\dot{x}(t) \approx \frac{x(k+1) + x(k)}{\Delta_t}, \tag{2.9}$$

where $k \in \mathbb{R}^+$ is the sampled instant from the sensor, and Δ_t is the sampling period. Therefore, a discrete-time nonlinear train system is:

$$\begin{cases} x(k+1) = \left(A\left(x(k)\right)\Delta_t + I\right)x(k) - \Delta_t B_B u_B(k) + \Delta_t B_T u_T(k) + \Delta_t G\left(x(k)\right) \\ y(k) = Cx(k) \end{cases}. \quad (2.10)$$

Next section is interested in the measurements available to fill in the models.

2.1.2. Sensors and faults

This work focuses mainly on the braking part of the drive, therefore, two kind of measurements are necessary: speed of the train and position. The speed sensor is embedded on the train and to get reliable information of its position, the railway track is equipped of several fixed sensors that act as markers and are usually called beacons. As shows Fig.2-7, the velocity sensor is installed on a wheel of the train. This speed sensor uses a target wheel also called phonic wheel. The sensor measures the rotation speed of the wheel by counting the teeth of the phonic wheel. The resolution of the measurement depends on the number of teeth on the wheel; the higher the number of teeth, the better the resolution is. Many technologies are used, mechanical, optical or magnetic. For further details, the reader can refer to technical documentation (Incremental encoders - Lenord+Bauer n.d.; Speed sensors - Lenord+Bauer n.d.; Saab, Nasr, and Badr 2002).

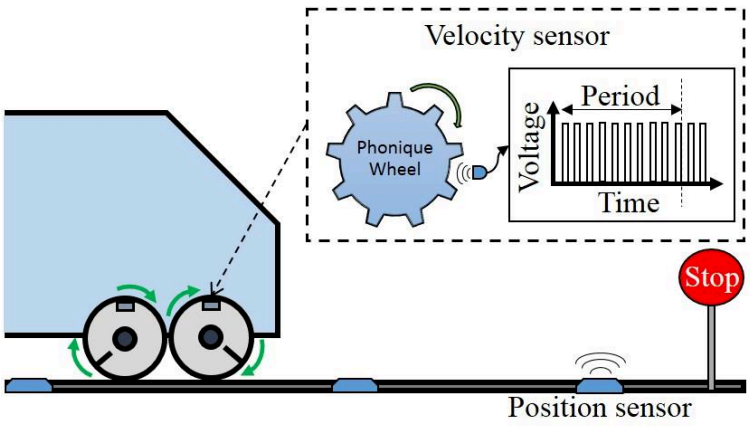

Fig.2-7. The structure of the train measurement system.

The measured velocity is obtained using wheel peripheral speed $v = \omega r$, where r is the wheel radius and ω is the wheel angular speed, that can be calculated as $\omega = \frac{2\pi}{N} \times \frac{c_i - c_{i-1}}{\Delta_t}$, where N

is the number of impulses per revolution, c_i is the current sample, c_{i-1} is the previous sample and Δ_t is the sampling period (Ridolfi et al. 2011). The train position can be estimated with the odometer sensor, but it needs also periodically a precise and reliable positioning, in order to be able to readjust the estimation and avoid excessive bias. A classical solution is to use markers set in the rail also commonly called beacons (Sandidzadeh and Khodadadi 2011; Y. W. Zhou 2012). These beacons are also commonly used for air and sea navigations (Sandidzadeh and Khodadadi 2011; Y. W. Zhou 2012). These sensors are fixed point devices, capable to transmit and receive radio signals. When the train passes over beacons, it transfers data stored inside of the beacon via data links. The data can include different information: line topography, speed restriction, distance to the next station, and beacon position. The last one corresponds to a time-to-time precise train position on the rail line that can be seen as a discrete reliable reference used to reinforce odometer-based real time estimations. Basically, there are two kinds of beacons, passive and active (The Railway Technical Website n.d.): the passive is waiting to be activated by a low frequency signal and receives its energy from a train passing over to send information; the active is powered from the railway line supply and sends continuously information to passing trains. Nevertheless, even if beacons allow precise train positioning, it can be very costly to equip all the tracks and a compromise has to be found between number of beacons (precision of the train position) and distance between two beacons (cost). Some research works deal with this topic : for example, in (Sandidzadeh and Khodadadi 2011), a solution for optimization of beacons placement in a railway track using genetic algorithm and Kalman filter was proposed .

What are the jamming and the skidding faults?

The jamming and skidding faults are phenomena that may occur depending on the train control and adherence conditions between the wheel and the track. In traction mode skidding can appear; in braking phase jamming can occur. Fig. 2-8 shows the skidding and jamming behaviors in detail (green arrows indicate the wheel rotation, the upper red arrows the movement of the train). The jamming case occurs when the brake is applied and it locks the wheel (Fig. 2-8 upper part positions 2, 4 and 5), so the wheel is sliding on the track. This happens because the braking torque is more important than adhesion torque. Similarly, skidding happens when the traction torque is more important than adhesion torque: the wheel will spin

but without moving the vehicle (Fig. 2-8 lower part positions 2, 4 and 5). In real-world conditions, these faults can occur depending on rail line conditions and any changes in conditions of adherence, i.e. for example weather conditions (rain, snow…). Another important phase where the wheel jamming occurs is during "hard" braking such as emergency braking. In this case also, the braking torque is bigger than the traction torque generated, due to adhesive force, and it results in sliding. The skidding and jamming phenomena have been studied in several articles: (Allotta et al. 2001; Allotta, Colla, and Malvezzi 2002; V. Colla et al. 2003; Valentina Colla et al. 2003; Garcia-Rivera, Sanz, and Perez-Rodriguez 1997; Malvezzi et al. n.d.; Saab, Nasr, and Badr 2002; Watanabe et al. 1997). These phenomena will damage both the wheel by creating flat spots and wearing the track. Of course, damaging wheel or rail surfaces directly impacts on maintenance costs, especially if it induces the replacement of the material (Makhortova and Vivdenko 2012). Excepted these extreme effects, the main issue of these jamming and skidding faults is that they impact directly on the measurements; thus on the estimation of both position and speed; since the sensors are based on quantifying the wheel rotation.

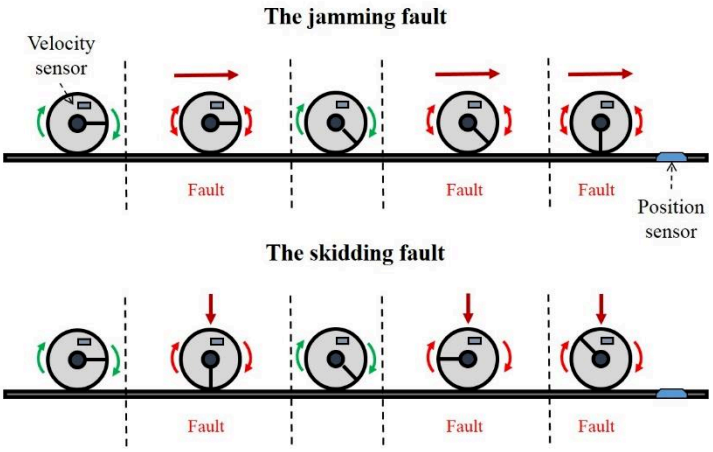

Fig. 2-8. The physical effects of the skidding and the jamming faults.

How is the sensor affected by the fault?

The effect of the wheel jamming and the wheel skidding is that the measurement from the sensor will be impacted by a bias: measured position lower than real position for the jamming case, and measured position bigger than real position for the skidding case. As result, we lose the track of the real position of the train until the next position beacon. The position error increases

proportionally with the fault duration. To exhibit the general problem, consider Fig. 2-9 and Fig. 2-10 that show real-time experiments. In these experiments, we do have the fault free velocity measurement (m/s) using a radar-base speed sensor (solid black line), whereas this measurement is not available in principle. Of course, it is used in order to validate properly the estimation results. The estimations, corresponding to the faulty signal, are based on the odometer, which is the available sensor (red dashed line). Fig. 2-10 shows the velocity difference due to jamming, i.e. when the wheel stops rotating while the train is moving, the odometer loses a percentage of the real velocity that depends on the wheel jamming duration. Fig. 2-9 shows the influence of the faulty measurement on the position estimation. The vertical lines at 90s, 98s and 107s represent positioning using the beacons and therefore the real position at these moments. The jamming, for this trial, is responsible of a measurement error of 5 meters for 200 meters spaced beacons (see zoomed part of Fig. 2-9).

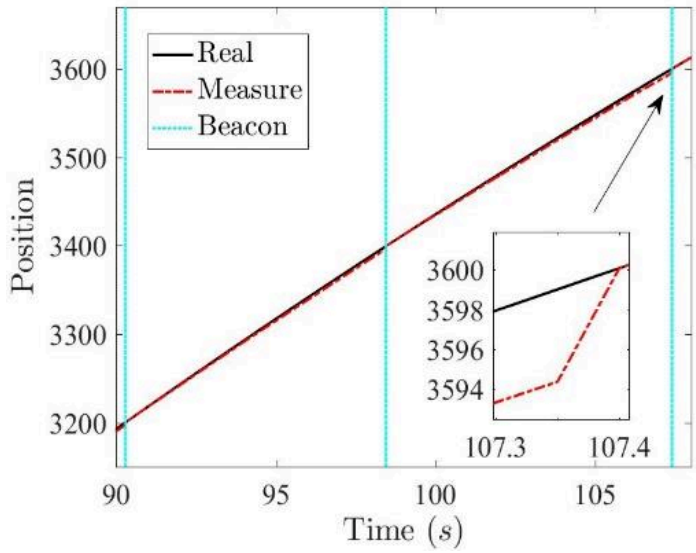

Fig. 2-9. The position estimation with wheel jamming (in meters).

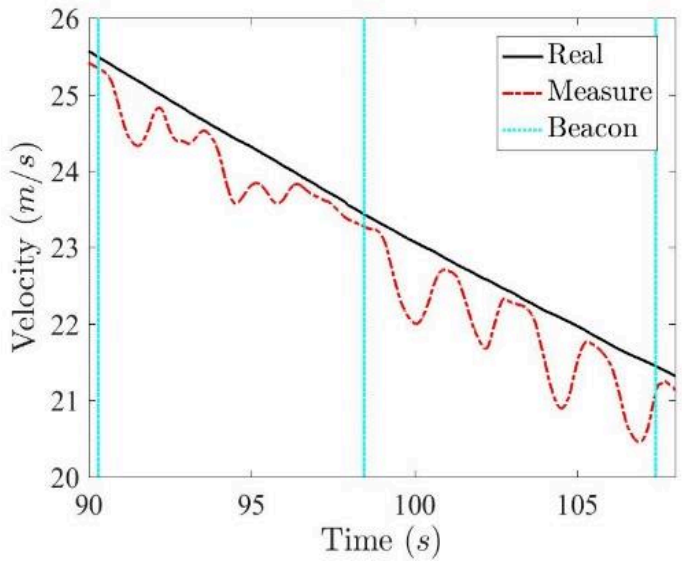

Fig. 2-10. The velocity behavior with wheel jamming.

Following the same idea, the skidding effect is presented Fig. 2-11 and Fig. 2-12; black line is the fault free signal, the red dashed is the faulty one and the blue vertical lines indicate the instants of train passing over the beacons. Fig. 2-11 shows the positive bias produced on the position with a measured velocity bigger than the real one, as shown in Fig. 2-12. For this trial the skidding represent an error around 15 meters (zoomed part in Fig. 2-11).

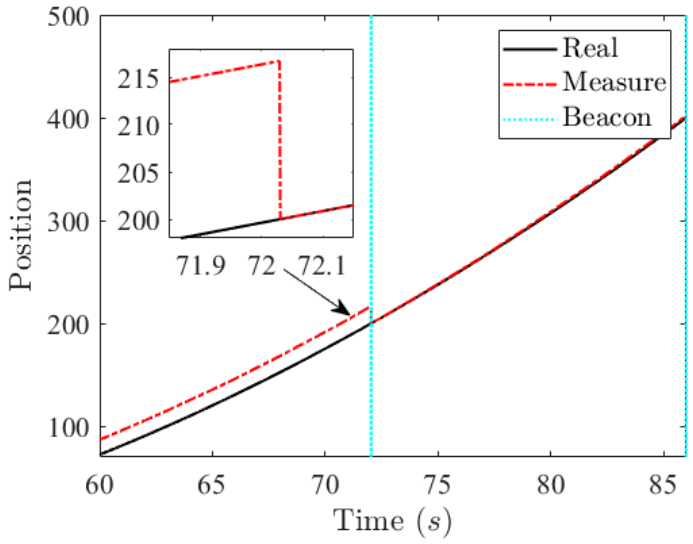

Fig. 2-11. The position estimation with wheel skidding (in meters).

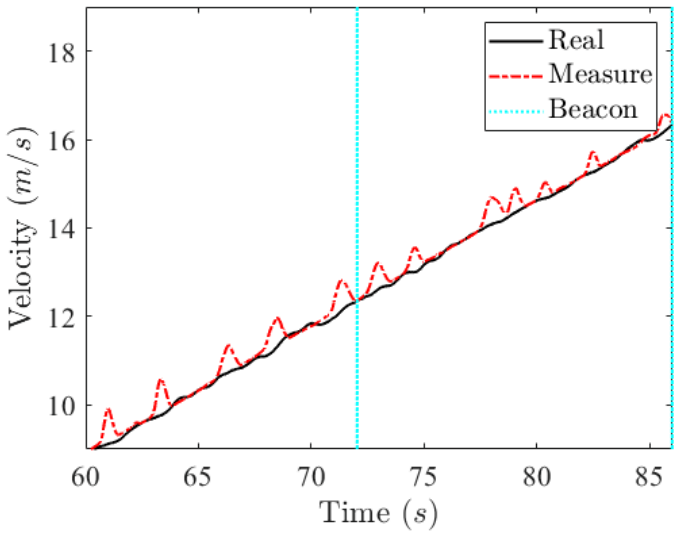

Fig. 2-12. The velocity behavior with wheel skidding.

To understand more precisely the effect on the sensor, Fig.2-13 shows the braking phase for both the fault free case (signal from sensor named s_1) and for the faulty case (signal from sensor named s_2). From s_1, the pulses coming from the fault free case are decreasing every period ending with a correct velocity calculation v_1. For the faulty case, when the jamming occurs (Fig.2-13 4th curve), there are less pulses than expected from sensor s_2; that produces a false velocity calculation v_2.

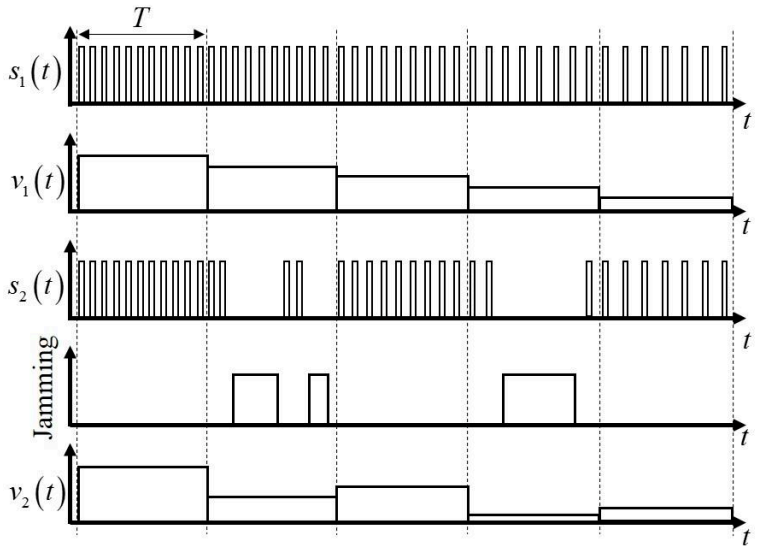

Fig.2-13 Sensor behavior with and without jamming fault.

The same effect is presented for the skidding phase, Fig.2-14. Sensor s_1 pulses are increasing every period, producing a correct velocity calculation v_1. Whereas, when the fault occurs, the number of pulses measured by s_2 is greater than the real value during the fault, and produces a false velocity calculation v_2.

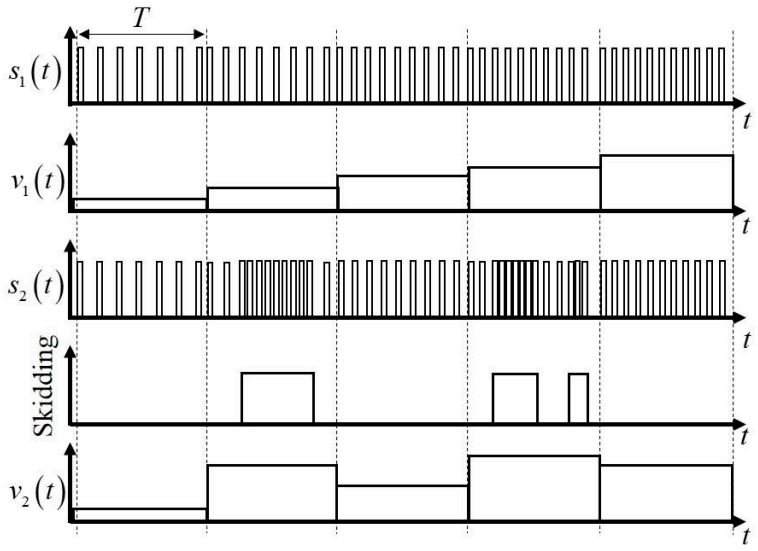

Fig.2-14 Sensor behavior with and without skidding fault.

2.1.3. Automatic Train Control (ATC)

The safe operation of the train during a travel is the goal to achieve through automatization. Some improvements have been obtained helping the train driver via the automatic train operation (ATO). The ATO system working together with the Automatic Train Protection (ATP) and Automatic Train Supervision (ATS) systems help the driver to comply with the speed restrictions, following a desired speed trajectory, and to stop the train accurately. Also, the Automatic Train Stop Control (ATSC) system helps the driver to stop the train accurately and timely at the station. All these systems together form a package called Automatic Train Control (ATC), Fig.2-15 (Dong et al. 2010).

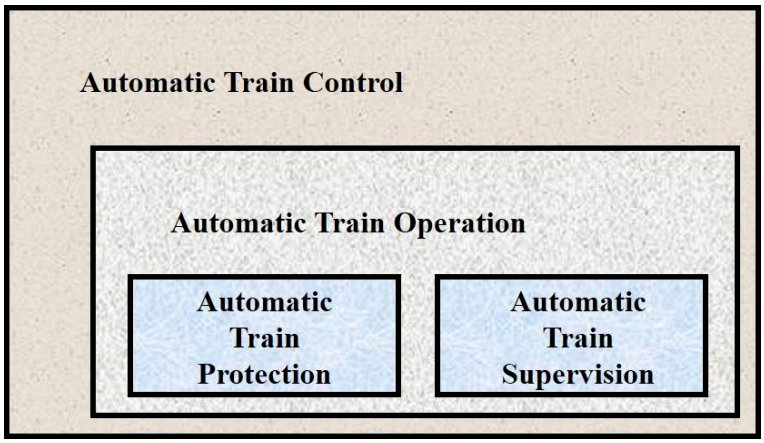

Fig.2-15. Diagram of the automatic train control system with its subsystems.

In order to understand subsystems interaction, let's consider the functions in detail (Allan and Arias 2008; The Railway Technical Website n.d.; Yin et al. 2017):

Automatic Train Protection (ATP): Safety level system, it guarantees mainly the safe stopping distance to avoid collision with the train ahead. It also insures safety limitation for speed; if a speed overrun is detected, the ATP will issue a braking (or emergency braking) order.

Automatic Train Supervision (ATS): Supervision level system that insures compliance with the expected schedule and traffic patterns. Depending on the trains, the companies and the regulations, ATS is used for: supervision of train status, schedule creation and changes, routing selection, automatic system monitoring and statistics…

Automatic Train Operation (ATO): The system that assists the driver to operate the train efficiently and safely. The system deals with speed control, comfort issues (smooth acceleration and braking) and assisted train stopping. A highest level includes energy saving-based driving assistance strategies. ATO needs ATP and ATS to be operational.

Fig. 2-16 gives an example of configuration (Allan and Arias 2008; Dong et al. 2010; Yin et al. 2017) where the ATS gives train routing and scheduling adjustments to ATO according to the train current state and schedule. ATO will gather the relevant information, such as train speed, programmed stop and dwelling time, and computes braking or acceleration rates. Meanwhile,

ATP keeps monitoring the real-time train running status, including speed limits compliance (Fig. 2-17) and corrects the train operation commands or triggers emergency brake if necessary.

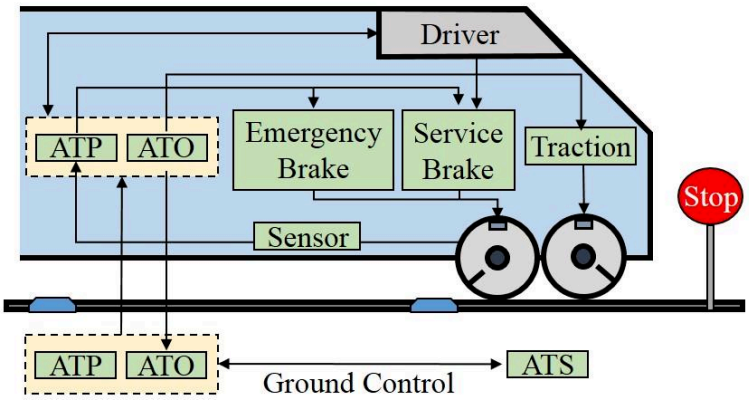

Fig. 2-16. Example of ATC structure with ATS, ATP and ATO relationships.

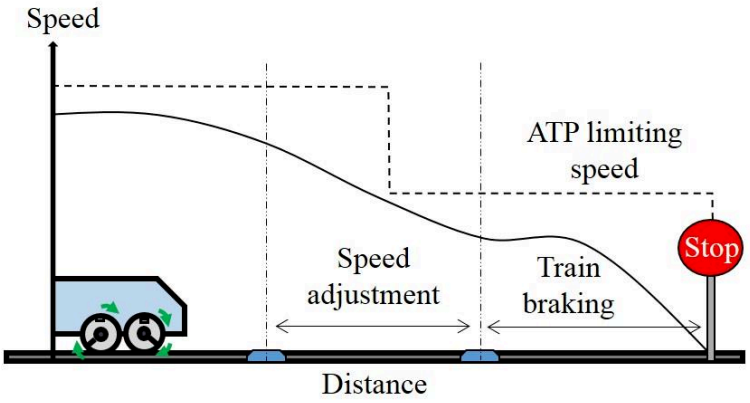

Fig. 2-17. The speed restriction by ATO.

For speed control between 2 stations, two strategies are possible for the ATO system (Yin et al. 2017): first is manual driving supported by a driver advisory system (DAS); second is a semi-automated mode or a fully-automated driving mode. For train stopping, ATO switches to the train station-stopping mode and adjusts the train braking rates dynamically, based on speed of the train and distance-to-stop.

When relying on automatic train stopping control (ATSC), the stopping accuracy could be affected by many disturbances, as is mentioned in (D. Chen et al. 2013):

- The *braking system delay* (BST) is due to a varying response time of the braking system (sensor delays, actuators response, different sampling times…);
- The *braking performance and velocity variance* (BPV) is due to the effects of temperature, humidity, abrasion, etc. on the efficiency of the braking system;
- The *basic resistance change* (BRCs) includes all resistance to motion effects, i.e. bearing, rolling, slip and air resistances.

In this work, dealing with Basic Resistance Change (BRC) is the principal issue, but the Braking System Delay (BST) will be also considered.

How the jamming and skidding faults are dealt with?

In order to reduce the impact of the jamming and skidding fault, the so-called wheel slide protection system (WSP) is used, that is analogous to the anti-lock brake systems (ABS) for cars. The WSP system adjusts the controller-issued braking torque using the dump valves, based on speed sensor readings. Each brake cylinder is filled with air or vented in order to increase or decrease the braking torque, mitigating the jamming and skidding problems when those are detected (Barna 2011). Of course, no adjustment is made in the fault free case. Following the same idea, some practical solutions have been developed and patented (Callahan and Christianson 1978; Hiscox 1976; Rath 1984; Sheppard 1969; Sutton 1977; Wood and Mazur 1990).

The WSP system is a low level system and is not meant to interact with ATO level systems. Considering that the ATO do not know actions made by the WSP, and relies solely on measurements, different approaches were proposed to improve the robustness, one of them being the multi-sensor architectures and data-fusion. For instance, the integration of odometers, accelerometers, and gyroscopes to get a better position measurement is studied in (Ridolfi et al. 2011). Another multi-sensor approach making use of odometer, radar, accelerometer, and beacons is proposed in (Y. W. Zhou 2012), where the data fusion is made via a Kalman filter algorithm.

The main issues of a multisensory architecture are feasibility and costs, which makes the single sensor approach, with appropriate post-processing, also popular. Using a single sensor

(odometer), authors of (Saab, Nasr, and Badr 2002) used a Kalman filter to detect wheel slip and/or slide using the variation of acceleration. When the fault is identified, the vehicle speed during the fault interval is then adjusted with a linear interpolation. Different algorithms based on neural networks, fuzzy logic, and crisp logic are proposed in (Allotta, Colla, and Malvezzi 2002; V. Colla et al. 2003; Valentina Colla et al. 2003; Garcia-Rivera, Sanz, and Perez-Rodriguez 1997), at the price of a high computational cost.

2.2. Virtual sensors : Observers for disturbance estimation

Under the real-world conditions, sensor measurements are noisy and induce different levels of uncertainty in the control loop as explained in previous sections. Also, a sensor will not be able to isolate the effects of a disturbance on the system. A solution that can come at hand to solve this problem is to design a disturbance observer-based control. Classically, for measurable disturbance feedforward strategies apply that allows attenuating or eliminating the influence of the disturbance on the system. For the case where the disturbance is not measured, whatever the reason is, i.e. no available sensor, sensor not adapted due to cost, size, etc., a solution is to use disturbance estimation via observers, under some rank conditions to be satisfied.

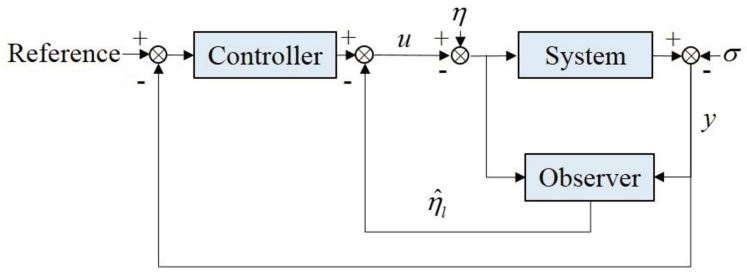

Fig. 2-18 Disturbance-observed-based control structure.

Consider the diagram Fig. 2-18 in a linear framework, i.e. with the model:

$$\begin{cases} \dot{x}(t) = Ax(t) + Bu(t) + H\eta(t) \\ y(t) = Cx(t) + N\sigma(t) \end{cases} \tag{2.11}$$

where $x \in \mathbb{R}^n$ is the state vector, $u(t)\mathbb{R}^{n_u}$, $y(t) \in \mathbb{R}^p$, $\eta(t) \in \mathbb{R}^{n_\eta}$, and $\sigma(t) \in \mathbb{R}^{n_\sigma}$ are respectively the control input, the measurement output, the external disturbance, and the

measurement noise. $A \in \mathbb{R}^{n \times n}$, $B \in \mathbb{R}^{n \times n_u}$, $C \in \mathbb{R}^{p \times n}$, $H \in \mathbb{R}^{n \times n_\eta}$ and $N \in \mathbb{R}^{p \times n_\sigma}$ are real matrices. In the case without disturbance and noise ($\eta = 0$ and $\sigma = 0$), classical tools can be used to design the controller for the system (2.11) to follow the reference signal and guarantee performances (decay rate, D-stability, H_2, H_∞ attenuation…). When dealing with unmeasured disturbances and/or noise ($\eta \neq 0$ or $\sigma \neq 0$), the solution adopted throughout this work is to estimate the disturbance η by a signal $\hat{\eta}$ while trying to minimize the error $\eta - \hat{\eta}$. A lot of work treats this problem using the so-called family of Unknown Input Observer (UIO) (Darouach, Zasadzinski, and Xu 1994) where the observer takes the form:

$$\begin{cases} \dot{z}(t) = Nz(t) + Gu(t) + Ly(t) \\ \hat{x}(t) = z(t) - My(t) \end{cases} \tag{2.12}$$

Where the matrices N, G, L and M are of appropriate dimension. Rank conditions such as a solution exists are given by $rank(CH) = rank(H)$. Extension for quasi-LPV has also been done in (Marx, Koenig, and Ragot 2007). Another family under UIO that do not decouple the disturbance is the so-called PI-observer family (C. Johnson 1968, 1970; J. Chen, Patton, and Zhang 1996) and has been adopted in our work. This technique is well-known and has been successfully applied to many problems; for example, fouling detection in a heat exchanger (Delrot et al. 2012; Lendek et al. 2010), or internal torques to explain sitting control of people living with a spinal cord injury (Blandeau et al. 2018a). The application of this technique to quasi-LPV (or so-called Takagi-Sugeno models) can be found in (Lendek et al. 2010). One of the benefits of UIO is the estimation of exogenous perturbations, that can be efficiently taken into account with appropriate robust control techniques (Faieghi, Jalali, and Mashhadi 2014; Gao, Liu, and Chen 2016).

2.2.1 Unknown Input Observer (UIO) – PI-observer form

In practice, this class of observer is relevant if the disturbance has the property to be captured by a polynomial-like input, i.e. it exists $\rho \in \mathbb{N}$ such that $d^{(\rho)}(t) = 0$, where ρ is the time derivative order (Delrot et al. 2012; Lendek et al. 2010). Therefore, we denote:

$$d_e(t) = \begin{bmatrix} d(t) \\ \vdots \\ d^{(\rho-1)}(t) \end{bmatrix}, \tag{2.13}$$

and create an extended vector of appropriate dimension:

$$x_e(t) = \begin{bmatrix} x(t) \\ d_e(t) \end{bmatrix}, \tag{2.14}$$

For example, applying the procedure to the linear system (2.11) with $d(t) = \eta(t)$ and without sensor noise $(\sigma = 0)$, (2.11) can be rewritten as:

$$\begin{cases} \dot{x}_e(t) = A_e x_e(t) + B_e u(t) \\ y_e(t) = C_e x_e(t) \end{cases}, \tag{2.15}$$

Where

$$A_e = \begin{bmatrix} A & H & 0 & \cdots & 0 \\ 0 & 0 & I & \ddots & 0 \\ & & 0 & \ddots & 0 \\ \vdots & \vdots & & \ddots & I \\ 0 & 0 & \cdots & & 0 \end{bmatrix}, \; B_e = \begin{bmatrix} B \\ 0 \\ \vdots \\ 0 \end{bmatrix}, \text{ and } C_e = \begin{bmatrix} C & 0 & \cdots & 0 \end{bmatrix}. \tag{2.16}$$

Therefore, the UIO from (2.15) (PI-observer form) is chosen as:

$$\begin{cases} \dot{\hat{x}}_e(t) = A_e \hat{x}_e(t) + B_e u(t) + L\left(y_e(t) - \hat{y}_e(t)\right) \\ \hat{y}_e(t) = C_e \hat{x}_e(t) \end{cases} \tag{2.17}$$

with $\hat{x}_e(t)$ being the estimated vector, $\hat{y}_e(t)$ the observer output, and L the observer gain matrix to derive. Defining as observer error $e(t) = x_e(t) - \hat{x}_e(t)$, the state dynamic error writes

$\dot{e} = \left(A_e - LC_e\right)e$. Usual tools to get the gain L apply; for example pole placement, quadratic Lyapunov approach, i.e. considering $V\left(e\right) = e^T Pe$ with $P = P^T > 0$ (Duan and Yu 2013), introducing performances such as decay rate, H_∞ attenuation if $\sigma\left(t\right) \neq 0$, etc.

2.2.2 Continuous-discrete time observer

As previously shown on the train signals, the measurements coming from the beacons, or the speed measurements available for the ATO correspond to discrete-time measurements with a time-varying sampling. Thus, taking into account this measurements makes the model belong to the class of continuous-discrete time models, i.e. the state is continuous and the measurement is discrete, as for example:

$$\begin{cases} \dot{x}\left(t\right) = Ax\left(t\right) + Bu\left(t\right) \\ y\left(t_k\right) = Cx\left(t_k\right) \end{cases} \tag{2.18}$$

Where the output is measured at each t_k, $k \in \mathbb{N}^+$ instant, with $0 \leq t_0 < \ldots < t_k < t_{k+1} < \ldots$ and $\lim_{k\to\infty} t_k = \infty$. We make the assumption that there is a maximum sampling interval τ_M $\left(0 < t_{k+1} - t_k \leq \tau_M < +\infty\right)$.

Therefore, the goal of the observer will be to reconstruct the continuous state, knowing only the discrete-time measurements at times t_k, $k \in \mathbb{N}^+$. Several observer designs are possible, for example, we can consider:

$$\begin{cases} \dot{\hat{x}}\left(t\right) = A\hat{x}\left(t\right) + Bu\left(t\right) + L\left(y\left(t_k\right) - \hat{y}\left(t\right)\right) \\ \hat{y}\left(t\right) = C\hat{x}\left(t\right) \end{cases} \tag{2.19}$$

Where $\hat{x}\left(t\right)$ is the estimated vector, L is the observer gain matrix, and $\hat{y}\left(t\right)$ is the observer output. Defining $e\left(t\right) = x\left(t\right) - \hat{x}\left(t\right)$ as the state error, its dynamic between two samples $t \in \left[t_k, t_{k+1}\right[$ writes:

$$\dot{e}\left(t, t_k\right) = Ae\left(t\right) - LC\left(x\left(t\right) - x\left(t_k\right)\right) = \left(A - LC\right)e\left(t\right) - LC\left(\hat{x}\left(t\right) - x\left(t_k\right)\right). \tag{2.20}$$

Therefore, invoking Input-to-State like properties (ISS) and/or Lipchitz conditions, we can prove that the convergence of the error in a ball containing the origin is possible, for a ball which radius has to be defined and will depend on the maximum sampling time interval τ_M.

In the literature, an approach using a continuous-time observer associated with a predictor, i.e. giving the prediction between two samples, is proposed in (Nadri, Hammouri, and Astorga 2004; Nadri, Hammouri, and Grajales 2013) and when the measurement is available, the predictor is updated. A continuous-discrete time observer for a multivariable nonlinear system is proposed in (M. Farza et al. 2014a; Mondher Farza, M'Saad, and Busawon 2015), where the convergence analysis provides an upper bound of the sampling as well as the rate of the observation error exponential convergence. A robust continuous-discrete time observer for internal disturbances in an electro-hydraulic actuator system is proposed in (S. A. Ali et al. 2016), where the principal characteristic is the use of an inter-sample output predictor to increase the acquisition frequency of the piston position sensor without affecting the convergence performance.

2.3. Fault detection and diagnosis

What is considered a fault? A usual definition is: "*a fault is something that changes the behavior of a system such that the system does no longer satisfy its purpose*" (Blanke et al. 2006). Since system representation describes nominal (fault-free) system behavior, faults will cause a divergence between fault-free system observer trajectories and real system state and output trajectories. The analysis of the discrepancy between estimations and measurements using the so-called model-based or model-free techniques is known under the name of Fault Detection and Diagnosis (FDD), or Fault Detection Isolation and Estimation (FDIE or FDI) (Gao, Cecati, and Ding 2015).

Generally, a fault is classified as sensor fault (f_s), actuator fault (f_a), and plant or component/parameter fault (f_c). Therefore, we can introduce them into the state space representation of a model; for example, if we consider the system (2.11) with the different types of fault, the expression becomes

$$\begin{cases} \dot{x}(t) = (A + \Delta A)x(t) + (B + \Delta B)u(t) + B_a f_a(t) + B_c f_c(t) + H\eta(t) \\ y(t) = (C + \Delta C)x(t) + N\sigma(t) + C_s f_s(t) \end{cases} \quad (2.21)$$

where B_a, B_c, and C_s are known constant matrices of appropriate size, and ΔA, ΔB, and ΔC are unknown parameter matrices. Faults, disturbances and model uncertainties will alter the plant behaviour. In order to quantify this alteration, we follow the approach from (Blanke et al. 2006) for the system (2.21): faults are usually represented as additional external signals or as parameter deviations. In the first case, the faults are called *additive faults*, in the second case, the faults are called *multiplicative faults* because the system parameters depending on the fault size are multiplied with the input or system state. Moreover, faults have to be detected and removed by corrective actions, since a fault can lead to a system failure, whereas disturbances and uncertainties will not harm the system directly, and are only attenuated, compensated or decoupled from the control loop by a filter or a robust design (H_∞ attenuation, decoupling observer…) (Blanke et al. 2006).

The fault diagnosis approach includes fault detection (FD), fault isolation (FI), and fault estimation. The fault detection aims to determine the moment when the fault occurs, the fault isolation aims to identify the fault type and location and the fault estimation aims to determine the severity of the fault (amplitude or duration). Based on the information obtained from the fault diagnosis, a supervision system can take fault-tolerant actions to make sure that the objectives are fulfilled even with faults or to reconfigure the objectives with respect to the current "health" of the system, and relies on actuator complete or partial redundancy. The whole approach is called fault-tolerant control Fig. 2-19 (Gao, Cecati, and Ding 2015).

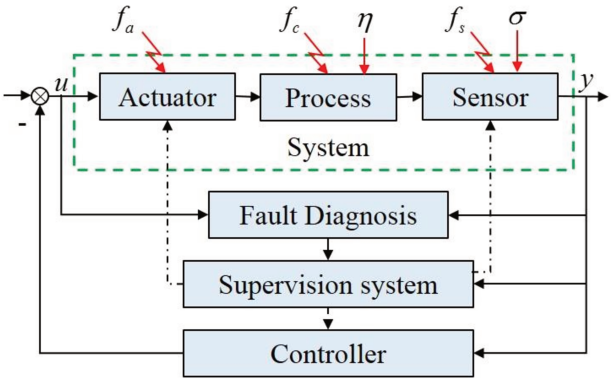

Fig. 2-19. The fault tolerant control scheme (Gao, Cecati, and Ding 2015).

The fault diagnosis methods can be categorized as:

- Model-based methods.
- Signal-based methods.
- Knowledge-based methods.
- Combined methods.

In this work, the model-based method is preferred, because a model is available and as we are working also on security issues (braking is one of them), some guarantees have to be settled. For more details about the other methods, the reader can refer to (Blanke et al. 2006; Cecati 2015; Gao, Cecati, and Ding 2015; Gao, Ding, and Cecati 2015; Isermann 2006; J. Zhang, Swain, and Nguang 2016). The model-based methods can be categorized depending on the type of the model used: deterministic or stochastic, time-based, event-based or hybrid, etc.

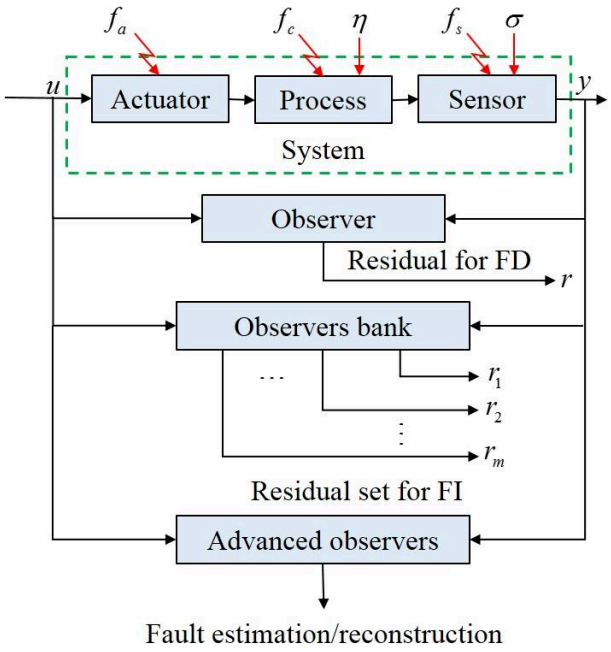

Fig. 2-20. The model-based fault diagnosis scheme (Gao, Cecati, and Ding 2015).

Deterministic fault diagnosis applies in our case and we propose to solve model-based fault diagnosis using observers. Fig. 2-20 presents a general scheme including several observers with fault detection, fault isolation and fault identification (Gao, Cecati, and Ding 2015). Note that the "residual" refers to a signal that is sensitive to the fault of interest, or to a set of signals

related to different faults. An observer-based fault detection for system (2.21), has the following form

$$\begin{cases} \dot{\hat{x}}(t) = A\hat{x}(t) + Bu(t) + L_o\left(y(t) - \hat{y}(t)\right) \\ \hat{y}(t) = C\hat{x}(t) \\ r(t) = L_r\left(y(t) - \hat{y}(t)\right) \end{cases} \tag{2.22}$$

Where $\hat{x}(t)$ is the estimated state vector, L_o is the observer gain matrix, $\hat{y}(t)$ is the observer output, $r(t)$ is the residual, and L_r is the residual gain. Defining the state error $e = x - \hat{x}$, its dynamic writes:

$$\begin{cases} \dot{e}(t) = (A - L_o C)e(t) + B_a f_a(t) + B_c f_c(t) + H\eta(t) + \Delta A x(t) + \Delta B u(t) \\ \qquad -L_o\left(\Delta C + N\sigma(t) + C_s f_s(t)\right) \\ r(t) = L_r\left(Ce(t) + N\sigma(t) + C_s f_s(t) + \Delta C x(t)\right) \end{cases} \tag{2.23}$$

From (2.23), we can see that the error dynamics appears to be sensitive to disturbances, to unknown parameters matrices, and to faults, and the same applies to the residual expression as well. Therefore, another important point is to be able to design conditions to ensure robustness of the residual to everything but the faults. In view of this, H_∞ attenuation can be added for fault detection observer to filter faults in uncertain dynamical systems (Edelmayer, Bokor, and Keviczky 1994; Zhong et al. 2003), mixed with H_- index to improve fault sensitivity (J. L. Wang, Yang, and Liu 2007; Z. Wang et al. 2017; M. Zhou et al. 2017).

Following (J. L. Wang, Yang, and Liu 2007; M. Zhou et al. 2017), the synthesis of observer (2.22) is called H_-/H_∞ if the following conditions hold:

a) The state estimation error from (2.23) is asymptotically stable.
b) The residual $r(t)$ from (2.23) is robust to the disturbances and measurement noise, $\eta(t)$ and $\sigma(t)$, respectively. Therefore, if the signals belong to L_2 space, an H_∞ attenuation can be proposed:

$$\|r(t)\|_2 < \gamma \left\| \begin{bmatrix} \eta(t) \\ \sigma(t) \end{bmatrix} \right\|_2 \tag{2.24}$$

c) The residual $r(t)$ from (2.23) is sensitive to the faults $f_s(t)$ and $f_c(t)$. Therefore, if the signals belong to L_2 space, H_- index approach can be proposed:

$$\|r(t)\|_2 > \beta \left\| \begin{bmatrix} f_c(t) \\ f_s(t) \end{bmatrix} \right\|_2 . \tag{2.25}$$

Several solutions were proposed in the literature: for deterministic models, the most studied are sensor faults and actuator faults. For linear systems, to cite some of them, results can be found with actuator fault detection in (Q. Zhang 2002), for both sensor and actuator faults in (J. L. Wang, Yang, and Liu 2007), and using an UI observer for actuator fault estimation under disturbance for a wind turbine in (Witczak et al. 2015).

Extensions of the works on linear models to LPV and/or Takagi-Sugeno (T-S) models are also common. We are interested in the so-called LMI-based fault diagnosis family, i.e. the methodology ends up with LMI constraints problems. For T-S models approaches, simultaneous state and process faults estimation for uncertain dynamics system can be found in (Pazera and Witczak 2016); robust techniques for sensor and actuator fault detection in (Chibani et al. 2017; Jee, Lee, and Joo 2012; Li et al. 2018). For linear parameter varying (LPV) system results using a bank of observers for sensor fault detection and isolation are presented in (Theilliol and Aberkane 2011), and actuator fault detection using a generalized output for LPV in (M. Zhou et al. 2017). Some works focus on residual evaluation, and the determination of a static or dynamic threshold detection, like in (Z. Wang et al. 2017).

Jamming and the skidding faults modelling for FDD.

To represent the faults in the mathematical model of train proposed in the previous section, we have different options to consider: actuator, system or sensor faults. As we can see from the previous sections, the principal difference of the jamming and the skidding faults is the effect on measured velocity: positive bias for skidding and negative bias for jamming. Moreover, the jamming fault occurs only during the braking phase (when $u_B > 0$ and $u_T = 0$), whereas the skidding occurs during the traction phase (when $u_B = 0$ and $u_T > 0$). We consider that when fault happens, the wheel cannot transmit traction and braking forces anymore. Different

approaches to represent the faults and to complete the model of the train system (2.8) are presented below.

Case 1: hybrid system with fault induced switches: the system without fault is:

$$\begin{cases} \dot{x}(t) = A(x(t))x(t) + B_T u_T(t) - B_B u_B(t) + G(x(t)) \\ y(t) = Cx(t) \end{cases} \tag{2.26}$$

and with fault occurrence, the system will be

$$\begin{cases} \dot{x}(t) = A(x(t))x(t) + G(x(t)) + Ff(t) \\ y(t) = Cx(t) \end{cases} \tag{2.27}$$

Where F represents fault related coefficients and $f(t) \in [1,-1]$ is the fault occurrence, being positive or negative based on the fault type.

Case 2: exogenous input: in this case, the complete model includes an extra term driven by fault occurrence:

$$\begin{cases} \dot{x}(t) = A(x(t))x(t) + B_T u_T(t) - B_B u_B(t) + G(x(t)) + F(u,t)f(t) \\ y(t) = Cx(t) \end{cases} \tag{2.28}$$

with $F(u) = -(B_T u_T(t) - B_B u_B(t)) + \xi(t)$, $\xi(t) \in \mathbb{R}$ and $f(t) \in [0,1]$. When $f(t) = 1$ the fault is total, and the control is completely inhibited. The term $\xi(t)$ is related to the "residual" resistive force and is practically unknown.

***Remark 2-1*:** it is also possible to model the fault as a multiplicative term of the input, and in this case, the fault is an **actuator fault.** Moreover, it is important to take into account that when the fault occurs, for the cases 1 and 2, the train will practically lose control of the jammed or the slipping wheel if the fault.

Case 3: Sensor fault: the model will include the fault term in the output

$$\begin{cases} \dot{x}(t) = A(x(t))x(t) + B_T u_T(t) - B_B u_B(t) + G(x(t)) \\ y(t) = Cx(t) + Ff(t) \end{cases} \tag{2.29}$$

Where $F \in \mathbb{R}^{n\times n}$ is the fault matrix and $f(t) \in [-\xi_1, +\xi_2]$; $f(t) > 0$ when skidding and $f(t) < 0$ in jamming situation. Coefficients $\xi_1, \xi_2 \in \mathbb{R}$ relate the severity of the fault, with $\xi_1 \leq \max(x(t))$ and a finite ξ_2.

Conclusion

The first section presented the description of the train system and its mathematical model, as well as the analysis of the jamming and skidding faults. Their physical effects on the sensors and their possible representation included in the mathematical have been shown. The principal issues to be kept in mind are:

- The friction force coefficients cannot be precisely measured by a sensor or precisely calculated in practice.
- The locomotive velocity is measured via a sensor on the wheel (odometer) and its position via time-to-time sensors fixed in the railway line, called beacons.
- The main effect of wheel skidding/jamming is to corrupt the sensor measurement and, therefore to lose the train position (between two beacons); the fault consists in an overestimation in the case of skidding, an underestimation for jamming.
- The sampling measurements from the sensors have to be at sufficiently high frequency to detect the fault occurrences accurately.
- The data transmission between the internal process of ATO and lower level devices (like sensors) works at a different sampling time and it has to be considered in the controller design.

Section 2.2 summarized the disturbance-observed-based control approach. This methodology allows the attenuation or the decoupling of the influence of disturbance with respect to the system. We recalled the unknown input observer (UIO) technique and especially the well-known PI-observer form.

Last part, section 2.3, presented fault detection and diagnosis techniques. Based on the behavior of the jamming and skidding faults, we propose models to categorize them as a sensor or actuator faults. The basis of the proposed approaches in this thesis is the application of model-

based methods using an UIO in the form of a PI-observer, coupled with robust approaches such as H_∞ attenuation, and H_- for fault detection sensitivity.

CHAPTER 3. Actuator and sensor fault detection with unknown input observer-based approach

3.1. Introduction

This chapter proposes different approaches for train speed and position estimation that are resilient to faults caused by wheel jamming or skidding. The proposed algorithms are meant to be used in high level modules (ATC/ATO level), and will improve the accuracy of the ATSC function, i.e. make the train stop at the expected position in the station. The proposed approaches are based on two representations, with respect to fault modeling: we consider actuator fault-based and sensor fault-based problem formulations. In the first case, we consider that the fault will result in degraded control of the train speed during the "faulty" period. This hypothesis is based on the supposition that degraded adherence conditions that impact the wheel with the speed sensor (making the wheel jam or slip), will be more or less similar on the other actuated wheels on the same cart, and to some extent to other carts as well. This hypothesis is realistic for traction (acceleration) phase, i.e. for skidding faults, but less realistic for braking (deceleration) phase and jamming faults. This is due to the fact that only the locomotive is providing the traction effort, while the braking effort is provided by all vehicles. In the particular scope of this study, we consider the train as a material point, and the experiments were made on a single locomotive, which strengthens the proposed hypothesis. When dealing with a multi-vehicle train model, this assumption is to be made on a per vehicle basis, and this is an expected development of this PhD results in the future.

Returning to this chapter scope, we deal specifically with jamming faults: obviously train stopping occurs after the braking phase, which is only impacted by jamming faults. Nevertheless, the results are easily transposed for the skidding fault detection, since fault models differs mostly by the sign of the fault signal, and of course, the driving scenario will be different, which will change some assumptions.

For the first case (actuator fault formulation), we model the physical effects of the wheel jamming by an "all-or-nothing" behavior that alternates randomly through fault duration. The

severity of the fault will depend on the jam/no-jam ratio during the considered period. This behavior can also be reproduced by a variable amplitude and continuous-time fault signal, but we believe that this is less accurate. The second case, based on the sensor fault formulation, considers that the fault will corrupt sensor measurements without direct impact on the control, with a variable amplitude and a variable duration of the fault, which is more challenging than the first case. In both cases, the fault detection filter is based on an unknown input observer in continuous-time, where the unknown input includes mechanical and aerodynamic resistive to motion forces, that are unmeasured and usually approximated by empirical equations (as explained in section 2.1.1, along with perturbations and noise.

Based on the previous discussion, this chapter is divided in two sections, each section being dedicated to a problem formulation, and the contributions are developed separately, along with illustrations. This reflects the chronology of the work, and the evolution from actuator centered to sensor centered representation of the fault that we believe to be more accurate considering the available experimental data, and the possible implementations of this work in the short term, having only access to acquisition modules without to inject controls in experiments.

3.2. Active Fault Tolerant Control for accurate train stopping.

In this section, we propose a solution to deal with actuator faults under the assumption that the control signals are available. The proposition is based on an integrated fault tolerant control approach, based on perturbation estimation and compensation, and on a fault detection module. If a fault is detected, then the controller will be switched into a "safe mode", effectively reducing the fault duration. Then the system will wait for fault disappearance and the return to a fault free-situation, to switch the controller to the "nominal" mode. As a result, the fault duration is minimized, and the train will improve its ability to stop at the expected position.

The proposed approach is developed for automatic train stop control (ATSC) module, and includes an unknown input observer for disturbance estimation and for fault detection, and a robust PI controller with an active fault tolerant mechanism. More specifically, we design the control law based on a reference tracking objective (Miyatake and Ko 2010; Yang et al. 2014). Using the estimation from the UI-observer, we estimate the perturbation and compute a fault sensitive residual, i.e. a fault indicator.

The fault detection relies on the comparison of the residual with a threshold, and will follow a cyclic behavior, based on fault occurrence and system recovery:

- In the nominal (fault-free) case, the reference system matches the fault-free real system, and the residual converges to zero.
- If a fault happens, the nominal reference systems will no longer match the reality, and the residual diverges. When the residual will be higher than the threshold, then a fault will be detected.
- Consequently, the reference system will then switch to a "faulty" reference system, matching the real system, and the control will go into the "safe" configuration. The residual will then converge to zero until the fault disappears, then increase again because the "faulty" reference system will no longer match the real system which has recovered from the fault.

- When the threshold is crossed again by the residual, the reference system switches back to nominal, matching the reality, and the residual converges again. The cycle resumes then with a new reference control and speed adjusted with respect to the fault duration.

The design procedure for observers and controllers, is expressed in terms of linear matrix inequalities (LMI), which are efficiently solved using convex optimization techniques (Boyd et al. 1994). This solution is tested only in simulation as control signals are not available from the available real-time data collected during experiments.

3.2.1. Problem statement and methodology

Based on the train dynamic analysis in in section 2.1.1, we consider the following train motion model (Guzinski et al. 2009; Kaller and Allenbach 1995; Liu and Golovitcher 2003; Vijay 1984)

$$\begin{cases} \dot{v} = -w(v) - b_B(v)u_B + b_T(v)u_T - g(p) \\ \dot{p} = v \end{cases} \tag{3.1}$$

where v is the velocity (*m/s*), p is the position of the vehicle (in *meters*), $b_B(v)$ is the braking force coefficient, u_B is the braking force, $b_T(v)$ is the traction force coefficient, u_T is the traction force, $g(p)$ is the tangential force to the path (the force due to the declivity), and $w(v)$ is the resistance to motion. Some assumptions on the model are made prior to the design: as stated in section 2.1.1, the resistance to motion can be approximated via a second order speed-dependent polynomial $w(v) = w_0 + w_1 v + w_2 v^2$; we also consider the maximum braking and traction forces via a single constant value b, such that u will be the unique control signal, where $u < 0$ and $u > 0$ correspond to u_B and u_T respectively. The specific external force is neglected in this study, because we are concerned with train stopping at parking stations, and usually stations are on flat ground and on a straight path to maximize visibility and other safety-based considerations. Therefore, the train model without fault is written in the following state space model:

$$\begin{cases} \dot{\bar{x}} = A\bar{x} + Bu + D(v) \\ \bar{y} = C\bar{x} \end{cases} \tag{3.2}$$

where $\bar{x} = \begin{bmatrix} v & p \end{bmatrix}^T$ is the state vector, $A = \begin{bmatrix} -w_1 & 0 \\ 1 & 0 \end{bmatrix}$, $B = \begin{bmatrix} b \\ 0 \end{bmatrix}$ and $C = \begin{bmatrix} 1 & 0 \end{bmatrix}$ are constant matrices, $D(v) = \begin{bmatrix} d(v) \\ 0 \end{bmatrix}$ with $d(v) = -w_0 - w_2 v^2$, is the part of the dynamic friction which is not included in A, and $\bar{y}$ is the output of the system.

In this section, the additive fault form is used for the controller design that corresponds, in section 2.3, to the second case 2 where fault is considered as an exogenous input. Therefore, the model with the fault included has the following form:

$$\begin{cases} \dot{\bar{x}} = A\bar{x} + Bu + D(v) + F(u,t) f(t) \\ \bar{y} = C\bar{x} \end{cases} \tag{3.3}$$

Where $F(u,t) = -Bu(t) + \xi(t)$, with $\xi(t)$ being the residual resistive force. The fault $f(t) \in [0,1]$ is jamming related only, and we consider that $f(t) = 0$ for all traction phase, i.e. for $u > 0$. Skidding faults are not considered for brevity, since in that case the model changes slightly. As discussed before, when $f(t) = 1$, then the fault is total and the control on the wheel is lost. We consider that during the fault duration, $f(t)$ will be varying randomly. For the dynamic friction part $d(v)$, neither it cannot be precisely measured by sensors, nor the parameters w_0, w_1 and w_2 are known precisely. Thus, its dynamic will be captured using the unknown input observer technique. Another issue in (3.3), is when the fault occurs and the system loses the ability to brake, thus not allowing dynamic friction compensation by the control law. Therefore, we want to detect the fault occurrence as fast as possible, to trigger the control action that will inhibit the fault.

3.2.1.1. Methodology

Considering that the principal part of the train model is estimated, an ideal system is used as a reference system. The reference system will produce a speed reference trajectory to be followed by the real train to ensure safety requirements. This architecture and behavior replicates the way the ATP works (see section 2.1.3), monitoring that the speed remains in some safety interval around a reference set point. The general structure of the integrated design is shown Fig. 3-1: the Unknown Input Observer (UIO) in a PI form is designed to estimate the speed, the position

and the dynamic friction. A controller is thus designed to track the reference with a friction compensation using the unknown input estimation obtained from the UIO.

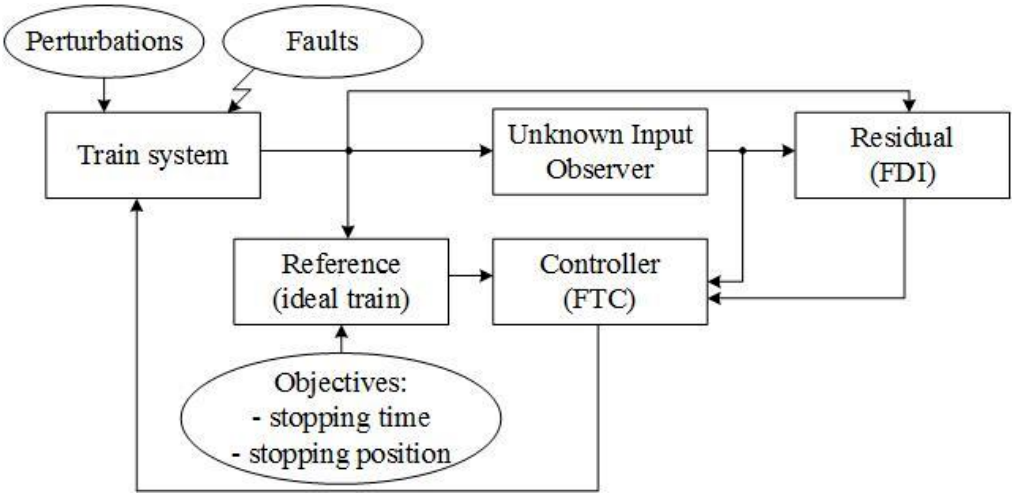

Fig. 3-1 Controller and observer scheme.

To detect the jamming fault, a residual is computed based on the measurement velocity of the train and the estimated velocity of the observer. This residual signal is filtered and used to detect fault occurrence and recovery instants, via threshold triggering conditions. At the end, a fault tolerant control (FTC) is obtained, integrating all the discussed modules.

3.2.1.2. Wheel jamming effect

In order to clarify our idea for the reader, we reproduce a similar figure as Fig. 2-10 of chapter 2 about the speed behavior with wheel jamming, left part of Fig. 3-2. The right part presents the absolute error $\left|v(t)-\hat{v}(t)\right|$ between the real speed $v(t)$ and the estimated one $\hat{v}(t)$, and we define the following variables:

- Δt_{jam} is the fault duration (red arrow);
- Δt_{ds} is the delay on detection when the fault starts;
- Δt_{de} is the delay on detection when the fault ends.

Fig. 3-2 gives one example, recalling that the sampling period is $\Delta_t = 0.2s$, and as explained in chapter 2, the fault can take place in "jam/no jam" periods ratio of this sampling period, i.e. a 20% fault means a jamming occurring during $40ms$, a 40% fault corresponds to a jamming during $80ms$ …

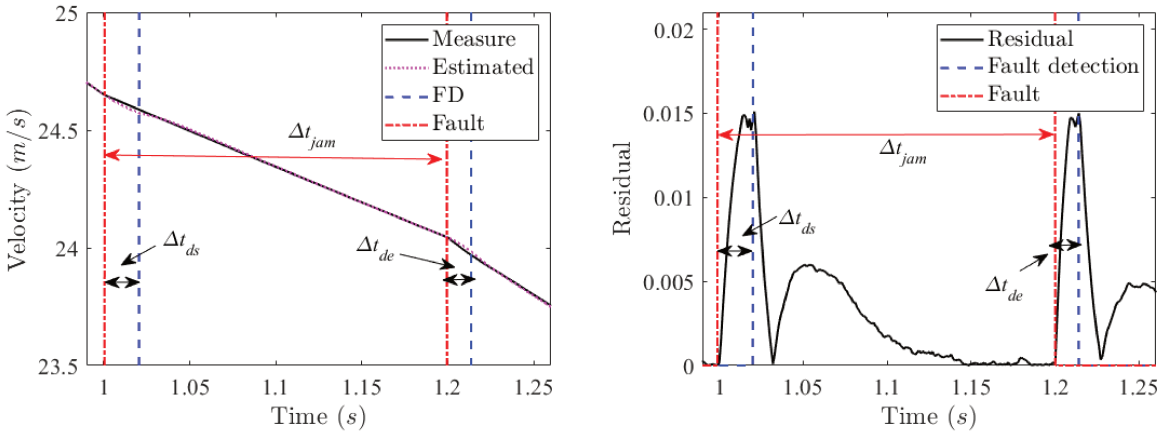

Fig. 3-2. The jamming effect: on the speed (left), on the residual (right).

3.2.2. Contribution

3.2.2.1. Controller design

For the controller design, let us first introduce a reference model based on an ideal train system, i.e. parameters perfectly known and no faults. We also set objectives for the final stopping position and the recommended braking amplitude. The proposed reference system has the following structure:

$$\begin{cases} \dot{\bar{x}}_r = A^* \bar{x}_r + B^* u^* \\ \bar{y}_r = C\, \bar{x}_r \end{cases} \tag{3.4}$$

where $\bar{x}_r = \begin{bmatrix} v_r & p_r \end{bmatrix}^T$ is the state vector with the reference velocity v_r and the reference position p_r, the matrices A^*, B^* and C are constants, u^* is an ideal control and $\bar{y}_r$ is the output. The notation $*$ stands for ideal constant values. In ideal conditions, from (3.4) it is possible to find the stopping position of the train, i.e. considering as a constant the input u^*:

$$v_r(t) = \left(v(t_0) + \frac{b^* u^*}{w_1^*} \right) e^{-w_1^*(t-t_0)} - \frac{b^* u^*}{w_1^*} \tag{3.5}$$

t_0 is the initial instant, the time when ATSC is activated and $v(t_0)$ is the initial velocity at t_0. Now it is possible to get the final position and the final time from the previous expression:

$$t_f = \frac{1}{w_1^*}\ln\left(\frac{w_1^* v(t_0) + b^* u^*}{w_1^* v(t_f) + b^* u^*}\right) + t_0 \tag{3.6}$$

Integrating (3.5) gives directly with $p(t_0)$ is the initial position at t_0:

$$p(t) = \frac{1}{w_1^*}\left(v(t_0) + \frac{b^* u^*}{w_1^*}\right)\left(1 - e^{-w_1^*(t-t_0)}\right) - \frac{b^* u^*}{w_1^*}(t - t_0) + p(t_0) \tag{3.7}$$

Noting that $\left(v(t_0) + \frac{b^* u^*}{w_1^*}\right)e^{-w_1^*(t-t_0)} = v(t_f) + \frac{b^* u^*}{w_1^*}$ and the final position being known, we obtain from (3.7) $p(t_f) = -\frac{v(t_f) - v(t_0)}{w_1^*} - \frac{b^* u^*}{w_1^*}(t_f - t_0) + p(t_0)$ or equivalently:

$$-b^* u^*(t_f - t_0) = w_1^*\left(p(t_f) - p(t_0)\right) + v(t_f) - v(t_0) \tag{3.8}$$

And finally:

$$-b^* u^* \frac{1}{w_1^*}\ln\left(\frac{w_1^* v(t_0) + b^* u^*}{w_1^* v(t_f) + b^* u^*}\right) = w_1^*\left(p(t_f) - p(t_0)\right) + v(t_f) - v(t_0) \tag{3.9}$$

Of course, for the special case of stopping $v(t_f) = 0$ and therefore (3.9) can be written as:

$$\frac{b^* u^*}{w_1^*}\ln\left(1 + \frac{w_1^* v(t_0)}{b^* u^*}\right) = v(t_0) - w_1^*\left(p(t_f) - p(t_0)\right) \tag{3.10}$$

Notice that there is always a solution to (3.10). Effectively, let us denote $x = -\frac{w_1^*}{b^* u^*} > 0$ and $\alpha = -w_1^*\left(p(t_f) - p(t_0)\right) \geq 0$, therefore finding a solution to (3.10) is equivalent to find a solution to $\mathrm{f}(x) = 0$ with:

$$\mathrm{f}(x) = \ln(1 - x v_0) + x(v_0 + \alpha) \tag{3.11}$$

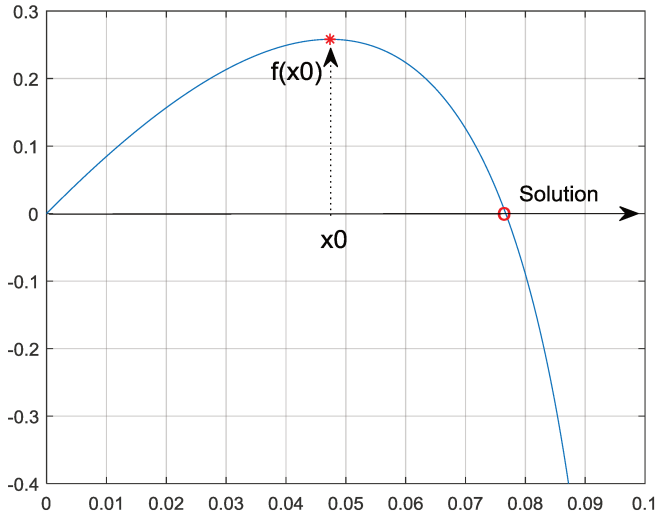

Fig. 3-3: example of function $\mathrm{f}(x)=\ln(1-xv_0)+x(v_0+\alpha)$

With this notation the domain of definition of $\mathrm{f}(x)$ is $x\in\left]0,\frac{1}{v_0}\right[$, and $\lim_{x\to\frac{1}{v_0}^-}\mathrm{f}(x)=-\infty$, $\mathrm{f}(0)=0$. An example of such a function is given Fig. 3-3. The derivative writes $\mathrm{f}'(x)=\frac{xv_0(v_0+\alpha)-\alpha}{xv_0-1}$ which is null if $x_0=\frac{\alpha}{v_0(\alpha+v_0)}$. Notice that $x_0\in\left]0,\frac{1}{v_0}\right[$, and that $\mathrm{f}(x_0)=\frac{\alpha}{v_0}-\ln\left(\frac{\alpha}{v_0}+1\right)>0$. Therefore ,using the Rolle's theorem, we know that $\mathrm{f}(x)$ crosses 0 once and only once on the interval $\left]0,\frac{1}{v_0}\right[$; the solution will be such that $x\in\left]\frac{\alpha}{v_0(\alpha+v_0)},\frac{1}{v_0}\right[$ and equivalently the solution satisfies: $u^*\in\frac{w_1^*v_0}{b^*}\times\left]-1-\frac{v_0}{\alpha},-1\right[$.

Thus the procedure from (3.5) to (3.10) can give from any initial position $(t_0,p(t_0),v(t_0))$ the constant control $u^*(t_0)$ to apply to reach the final position $(t_f,p(t_f),0)$. Nevertheless, if any disturbance arrives or a fault occurs, this ideal $u^*(t_0)$ is no more true; and the larger the fault, the bigger the error is. Therefore, $u^*(\cdot)$ must be recomputed after the faulty instants and the procedure is:

Algorithm 3-1 to design the reference trajectory:

Repeat

- Follow $u^*(t_k)$ reference control, while monitoring fault occurrence.
- A fault is detected, fault tolerant action is made, and then the system has recovered.
- After recovery at time t_k, compute $u^*(t_{k+1})$ solving the nonlinear equation (3.10) with $(t_0, p(t_0), v(t_0)) = (t_k, p(t_k), v(t_k))$
- Recalculate the final time as: $t_f = \frac{1}{w_1^*} \ln\left(\frac{w_1^* v(t_0) + b^* u^*(t_{k+1})}{w_1^* v(t_f) + b^* u^*(t_{k+1})}\right) + t_0$

Until $p(t_f)$ is reached

Thus, system (3.4) produces a reference signal u^* that will be piecewise constant, i.e. $u^*(t) = u^*(t_k)$ when $t \in [t_k, t_{k+1}[$, then produces a smooth reference trajectory $\overline{y}_r$ via (3.4) to be followed by the train system (3.3). The controller then writes with a state $p_i(t)$ corresponding to its integral part:

$$\begin{cases} u(t) = \frac{1}{b^*}\left(L_1\left(v(t) - v_r(t)\right) + L_2 p_i(t) + \hat{d}(t)\right) + u^* \\ \dot{p}_i(t) = v(t) - v_r(t) \end{cases} \tag{3.12}$$

where L_1 and L_2 are the controller gains to be designed. For the controller input, the error is the speed difference $e(t) = v(t) - v_r(t)$. Then, taking the assumption that $w_1 = w_1^*$, the dynamic of this error writes

$$\dot{e}(t) = -w_1^* e(t) + b^*\left(u(t) - u^*\right) + d\left(v(t)\right) + F\left(u(t)\right) f\,. \tag{3.13}$$

Introducing the control law (3.12) in the previous expression without the fault, we obtain

$$\begin{bmatrix} \dot{e} \\ \dot{p}_i \end{bmatrix} = \begin{bmatrix} -w_1^* - L_1 & -L_2 \\ 1 & 0 \end{bmatrix} \begin{bmatrix} e \\ p_i \end{bmatrix} + \begin{bmatrix} d(v) - \hat{d}(v) \\ 0 \end{bmatrix}. \tag{3.14}$$

As $w_1^* > 0$, it is easy to design a controller such that $\begin{bmatrix} -w_1^* - L_1 & -L_2 \\ 1 & 0 \end{bmatrix}$ is Hurwitz stable. Input to State Stability (ISS) property is direct, as $d(v) - \hat{d}(v)$ is bounded. Moreover, without faults,

the unknown input error $d(v)-\hat{d}(v)$ will converge towards 0 and reference tracking will be ensured.

3.2.2.2. Observer design

As explained previously, for the estimation of the dynamic friction, we consider Unknown Input Observer (UIO) in the PI form. Therefore, the train system (3.2) is extended, considering that a polynomial approximation $d^{(\rho+1)}(v)\approx 0$ is enough to capture the dynamic of the friction. Therefore, it can be rewritten as:

$$\begin{cases}\dot{\bar{x}}_t = A_t\bar{x}_t + B_t u\\ \bar{y}_t = C_t\bar{x}_t\end{cases} \tag{3.15}$$

where $\bar{x}_t=\begin{bmatrix} v & d(v) & \dot{d}(v) & \cdots & d^{(\rho)}(v)\end{bmatrix}^T$ is the extended state vector, $A_t=\begin{bmatrix}-w_1^* & I_\rho\\ 0_{\rho\times 1} & 0_\rho\end{bmatrix}$ and $B_t=\begin{bmatrix}b^*\\ 0_{\rho\times 1}\end{bmatrix}$ are constant matrices, and $\bar{y}_t$ is the output with $C_t=\begin{bmatrix}1 & 0_{1\times\rho}\end{bmatrix}$. An UIO PI-observer can be defined as:

$$\begin{cases}\dot{\hat{\bar{x}}} = A_o\hat{\bar{x}} + B_o u + K\left(\bar{y}_t-\hat{\bar{y}}\right)\\ \hat{\bar{y}} = C_o\hat{\bar{x}}\end{cases} \tag{3.16}$$

where $\hat{\bar{x}}=\begin{bmatrix}\hat{v} & \hat{d}(v) & \dot{\hat{d}}(v) & \cdots & \hat{d}^{(\rho)}(v)\end{bmatrix}^T$ is the estimation vector, $A_o=A_t$ and $B_o=B_t$ are constant matrices, $K\in\mathbb{R}^{\rho+1}$ is the observer gain, and $\hat{\bar{y}}$ is the output observer with $C_o=C_t$. Therefore, in this ideal case, the time derivative of the error $e_0=\bar{x}_t-\hat{\bar{x}}$ is

$$\dot{e}_o=(A_o-KC_o)e_o. \tag{3.17}$$

And the convergence of the error is guaranteed $\lim_{t\to\infty} e_0(t)=0$ if the gain K is designed such that A_o-KC_o is Hurwitz stable; pole placement, quadratic synthesis, with or without additional performance criteria, any technique can come at hand.

3.2.2.3. Fault detection

Since only one type of fault is considered, the wheel jamming, the isolation is not required and the Fault Detection Isolation (FDI) module is reduced to FD functionality. Adding more faults, such as skidding for example will require an isolation mechanism. Now, with the estimation of the velocity from the observer $\hat{v}(t)$ and the velocity measurement from the train system $v(t)$, the following residual $r(t)$ is considered

$$r(t) = \left| v(t) - \hat{v}(t) \right|, \tag{3.18}$$

As usual, fault detection thresholds will be used to detect the fault occurrence and fault recovery instants. Their tuning is done in such a way that discrepancy in measurements on a real system with uncertainties would not trigger false detections, and will not miss the detection of any fault. In order to reduce the measurement noise, a low pass filter is also added. The main idea of the algorithm is presented Fig. 3-4, with two main parts, detection of a fault with a delay Δt_{ds} and detection of the end of a fault with a delay Δt_{de}.

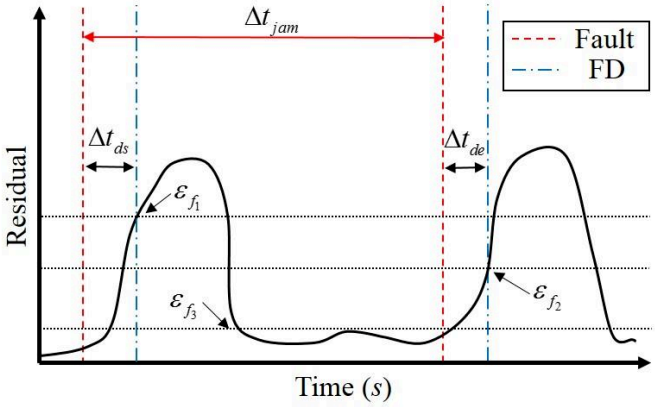

Fig. 3-4. Fault detection mechanism.

These detections need three thresholds named ε_{f_1} (non-faulty-to-faulty), ε_{f_2} (faulty-to-non-faulty), and ε_{f_3} (faulty-to-faulty, for residual settling before new detection). The first one, when $r(t) > \varepsilon_{f_1}$ a non-faulty-to-faulty case is detected, inducing a delay in the detection: Δt_{ds}. The

second one, when $r(t) > \varepsilon_{f_2}$ a faulty-to-non-faulty case is detected inducing a delay Δt_{de}. To reduce the possible false alarms between each fault a faulty-to-faulty *flag* is used that is activated if $r(t) < \varepsilon_{f_3}$. The conditionals of the algorithm are:

- **If** $r(t) > \varepsilon_{f_1}$ **and** flag=1 **and** FD=0 **Then** FD=1 **and** flag=0
- **If** $r(t) < \varepsilon_{f_3}$ **Then** flag=1
- **If** $r(t) > \varepsilon_{f_2}$ **and** flag=1 **and** $\mathrm{FD} = 1$ **Then** FD=0 **and** flag=0

Of course, the choice of such thresholds ε_{f_i}, $i = 1,2,3$ is a multi-constrained problem, minimizing false alarms and missed detection and maximizing good detections. For real-time applications, maximizing good detection consists in detecting the faults with unacceptable effects and ignoring low amplitude faults. Indeed, with different magnitudes of the residual, in our case, it is possible to infer the magnitude of the fault and to decide when it is convenient to disable the brake control.

3.2.2.4. Fault tolerant mechanism

Considering that the compensation is not always possible to perform (because of the wheel jamming), we need to disable the brake control on positive fault detection by releasing the brake, since it will unjam the wheel mechanically. Therefore, the control is deactivated, $u(t) = 0$, as soon as a fault is detected. This action will release the wheel after a short delay, stopping the fault with a time delay of Δt_{ft}, reducing the fault duration to a maximum of $\Delta t_{jam} = \Delta t_{ds} + \Delta t_{ft}$, *Fig. 3-5*. However, the control will not resume, and a new reference control will not be computed until the FD mechanism acknowledged full system recovery (the second blue vertical line in *Fig. 3-5*)

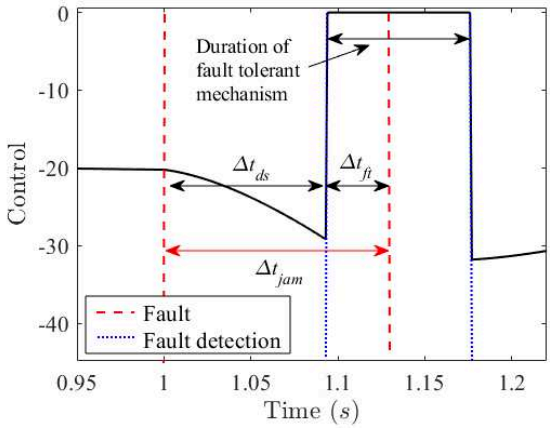

Fig. 3-5. Wheel release mechanism triggered by FTC action.

3.2.2.5. Convergence issues

In view of what has been explained, we can identify a cycle of four states, starting before fault occurrence and ending with system's recovery. Effectively, the system and the observer have two modes, faulty and fault-free, therefore, there are four cases to study, with transitions between cases as shown in the oriented graph of Fig. 3-6. For the vertices v_{ij}, the first index $i \in \{0,1\}$ corresponds to the system, the second $j \in \{0,1\}$ to the observer. "0" means fault-free, and "1" means a fault and in this case $u(t) = 0$ for the corresponding block (system or observer). For example v_{10} is the vertex with a fault on the system that is not detected by the observer; the system will lose control of the wheel, but the observer still uses the reference control. The arrows on the arcs indicate the possible paths.

Remember that the control u^* is considered as piecewise constant, and will be recomputed every time t_k such that both the observer and system are considered fault-free (see the algorithm given after equation (3.10)). This will happen at the time of the transition between v_{01} and v_{00} as indicated Fig. 3-6. We also write the time spent in each vertex as δt_{ij}.

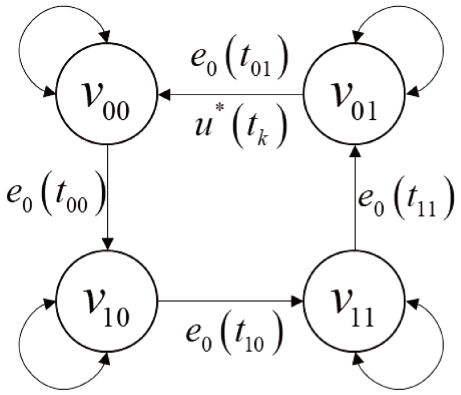

Fig. 3-6. The oriented graph of the fault occurrence and recovery for system and observer states

Let us write for each vertex the observer error dynamic. From (3.16), $\dot{\hat{x}} = A_o\hat{x} + K\left(\overline{y}_t - \hat{y}\right)$ corresponds to the faulty case and $\dot{\hat{x}} = A_o\hat{x} + B_o u + K\left(\overline{y}_t - \hat{y}\right)$ to the non-faulty one. For the system (3.15), $\dot{\overline{x}}_t = A_t\overline{x}_t$ is the faulty case. From these cases, we can infer how the error dynamic writes for the 4 vertices:

$$v_{00} \text{ and } v_{11}: \dot{e}_0 = \left(A_o - KC_o\right)e_0,\ t \in \left[t_{01}, t_{00}\right[\text{ and } t \in \left[t_{11}, t_{10}\right[\tag{3.19}$$

$$v_{10}: \dot{e}_o = \left(A_o - KC_o\right)e_o - Bu^*,\ t \in \left[t_{00}, t_{10}\right[\tag{3.20}$$

$$v_{01}: \dot{e}_o = \left(A_o - KC_o\right)e_o + Bu^*,\ t \in \left[t_{11}, t_{01}\right[\tag{3.21}$$

The basic idea is that as each vertex of the graph is stable, as it is driven by the poles of $A_o - KC_o$, thus the stability issue can be solved, whatever the transitions are. To simplify the notations, we will denote $A_o - KC_o = A_{cl}$. Let us begin with the constant input to reach the final position being $u(t) = u^*(t_k)$, so that the error in v_{00} writes:

$$e_o(t) = e^{A_{cl}(t-t_k)}e_o(t_k) \tag{3.22}$$

Suppose an error occurring at time t_{00}, and of course, the observer will not be able to detect it immediately and v_{10} is activated with $e_o(t_{00}) = e^{A_{cl}(t_{00}-t_k)}e_o(t_k)$. A solution to the observation error dynamic, (3.20), as $u(t) = u^*(t_k)$ is:

$$e_o(t) = e^{A_{cl}(t-t_{00})} e_o(t_{00}) - \int_{t_{00}}^{t} e^{A_{cl}(t-\tau)} d\tau B u^*(t_k) \tag{3.23}$$

And directly: $e_o(t) = e^{A_{cl}(t-t_{00})} e_o(t_{00}) + \left(1 - e^{A_{cl}(t-t_{00})}\right) A_{cl}^{-1} B u^*(t_k)$, from which it can be seen that even if the system stays in v_{10} we have: $\lim_{t\to\infty} e_o(t) = A_{cl}^{-1} B u^*(t_k)$. The initial condition will be $e_o(t_{00}) = e^{A_{cl}\delta t_{00}} e_o(t_k)$, with $t_{00} = t_k + \delta t_{00}$, and (3.23) renders:

$$e_o(t) = e^{A_{cl}(t-t_k)} e_o(t_k) + \left(1 - e^{A_{cl}(t-t_{00})}\right) A_{cl}^{-1} B u^*(t_k),\ t \in [t_{00}, t_{10}[\tag{3.24}$$

At time t_{10}, when the residual is bigger than the threshold ε_{f_1}, then the detection holds true and a transition to the vertex v_{11} occurs with $\delta t_{10} = t_{10} - t_{00}$. Its initial condition $e_o(t_{10})$ from (3.24) is: $e_o(t_{10}) = e^{A_{cl}(\delta t_{00} + \delta t_{10})} e_o(t_k) + \left(1 - e^{A_{cl}\delta t_{10}}\right) A_{cl}^{-1} B u^*(t_k)$. Thus, after time t_{10}:

$$e_o(t) = e^{A_{cl}(t-t_k)} e_o(t_k) + e^{A_{cl}(t-t_{10})} \left(1 - e^{A_{cl}(t_{10}-t_{00})}\right) A_{cl}^{-1} B u^*(t_k),\ t \in [t_{10}, t_{11}[\tag{3.25}$$

When the fault disappears, the observer will remain in the "faulty" mode, therefore v_{01} is activated through (3.21), with the initial condition given for $t = t_{11}$ in (3.25) and with $\delta t_{11} = t_{11} - t_{10}$. Then $e_o(t_{11}) = e^{A_{cl}(\delta t_{00} + \delta t_{10} + \delta t_{11})} e_o(t_k) + e^{A_{cl}\delta t_{11}} \left(1 - e^{A_{cl}\delta t_{10}}\right) A_{cl}^{-1} B u^*(t_k)$. Thus, after time t_{11}, similarly to (3.24), we will obtain:

$$e_o(t) = e^{A_{cl}(t-t_{11})} e_o(t_{11}) - \left(1 - e^{A_{cl}(t-t_{11})}\right) A_{cl}^{-1} B u^*(t_k),\ t \in [t_{11}, t_{01}[\tag{3.26}$$

Or equivalently;

$$e_o(t) = e^{A_{cl}(t-t_k)} e_o(t_k) + \left(e^{A_{cl}(t-t_{10})} - e^{A_{cl}(t-t_{00})} - 1 + e^{A_{cl}(t-t_{11})}\right) A_{cl}^{-1} B u^*(t_k),\ t \in [t_{11}, t_{01}[\tag{3.27}$$

Finally, when the residual will detect that the system has recovered from the fault, the transition to v_{00} ends the loop. Therefore, one cycle after we can write: $e_o(t) = e^{A_{cl}(t-t_{01})} e_o(t_{01}),\ t \geq t_{01}$ or:

$$e_o(t) = e^{A_{cl}(t-t_k)} e_o(t_k) + \left(e^{A_{cl}(t-t_{10})} - e^{A_{cl}(t-t_{00})} - e^{A_{cl}(t-t_{01})} + e^{A_{cl}(t-t_{11})}\right) A_{cl}^{-1} B u^*(t_k) \tag{3.28}$$

That can be rewritten as:

$$e_o(t) = e^{A_{cl}(t-t_k)} \left[e_o(t_k) + \left(e^{A_{cl}(t_k-t_{10})} - e^{A_{cl}(t_k-t_{00})} - e^{A_{cl}(t_k-t_{01})} + e^{A_{cl}(t_k-t_{11})}\right) A_{cl}^{-1} B u^*(t_k) \right] \tag{3.29}$$

Therefore, we can estimate a minimum time necessary to stay again in v_{00} that guarantees $\|e_o(t_{\min})\| \le \|e_o(t_k)\|$. Let us note $\varphi(t_k) = \left(e^{A_{cl}(t_k - t_{10})} - e^{A_{cl}(t_k - t_{00})} - e^{A_{cl}(t_k - t_{01})} + e^{A_{cl}(t_k - t_{11})}\right) A_{cl}^{-1} B$ to simplify the equation (3.29):

$$e_o(t) = e^{A_{cl}(t-t_k)} \left(e_o(t_k) + \varphi(t_k) u^*(t_k)\right) \tag{3.30}$$

A_{cl} being a stable Hurwitz matrix, it exists constants $\beta > 0$ and $m > 0$ such that: $\left\|e^{A_{cl}(t-t_k)}\right\| \le \beta e^{-m(t-t_k)}$ (see section 4.3.2 for developments). Therefore $\|e_o(t_{\min})\| \le \|e_o(t_k)\|$ corresponds to:

$$\|e_o(t_{\min})\| \le \beta e^{-m(t_{\min}-t_k)} \|e_o(t_k) + \varphi(t_k) u^*(t_k)\| \le \|e_o(t_k)\| \tag{3.31}$$

As $m > 0$, we obtain $e^{m(t_{\min}-t_k)} \ge \beta \dfrac{\|e_o(t_k) + \varphi(t_k) u^*(t_k)\|}{\|e_o(t_k)\|}$, and the minimum time to spend in v_{00} after a fault detection to ensure a decreasing error is:

$$t_{\min} \ge t_k + \frac{1}{m} \ln\left(\beta \frac{\|e_o(t_k) + \varphi(t_k) u^*(t_k)\|}{\|e_o(t_k)\|}\right) \tag{3.32}$$

Now, if we consider the next fault, we can write a discrete-like model between the fault instants, with t_{k+1} the instant of the new fault:

$$e_o(t_{k+1}) = e^{A_{cl}(\delta t_{00} + \delta t_{10} + \delta t_{11} + \delta t_{01})} e_o(t_k) + \left(e^{A_{cl}(\delta t_{11} + \delta t_{01})} \left(1 - e^{A_{cl}\delta t_{10}}\right) - \left(1 - e^{A_{cl}\delta t_{01}}\right)\right) A_{cl}^{-1} B u^*(t_k) \tag{3.33}$$

If $t_{k+1} \ge t_{\min}$ we ensure a decreasing error for $t \in [t_k, t_{k+1}[$. Notice also that if the fault detection is perfect, i.e. $\delta t_{10} = \delta t_{01} = 0$, then the estimation follows a simple stable exponential $e_o(t_{k+1}) = e^{A_{cl}(\delta t_{00} + \delta t_{11})} e_o(t_k)$ whatever is $u^*(t_k)$. Since all times are finite, and combined with decreasing exponentials and bounded input, then ISS property holds.

3.2.3. Simulations

This part just presents a preliminary study using a linear model in an ideal situation where the control input is known. It allows both giving a step-by-step procedure and pointing out the different issues that can occur, as well as showing that the proposed ideas are promising.

3.2.3.1. Fault-free tests

In this case, we are considering that all the parameters are known and the fault does not appear to test the part of the friction force estimated by the observer in ideal conditions. Therefore, the parameters for the train system and the reference system are: $w_0 = w_0^* = 0.01$, $w_1 = w_1^* = 0.1$, $w_2 = w_2^* = 0.001$, $b = b^* = 0.1$. The ideal braking control that is injected to the reference model is in this case $u^* = -26.22$, to brake from $v(t_0) = 30$ (*m/s*), to $v_{\min} = 0$ (*m/s*) in $100(m)$, i.e. from position $p(t_0) = 0$ (*m*), $t_0 = 0s$, to a final position $p(t_f) = 100$ (*m*), with an estimated arrival time $t_f = 7.62$ (*s*). The initial conditions for the observer are $\hat{\bar{x}}(t_0) = [30 \quad -0.91 \quad 0.13]^T$, and the gain matrix obtained by pole placement for the observer is $K = [101.4 \quad 2650 \quad 3750]^T$, with the poles $(-50, -50, -1.5)$. The time derivative order used for the unknown input estimation is $\rho = 2$. The gains obtained by pole placement for the controller are $L_1 = 1.4$ and $L_2 = 0.5$, with the poles $(-1, -0.5)$.

After simulation, the resulting final position error is $|x(t_f) - x_f| = 0.004$ *meters* as shown Fig. 3-7. The estimation of $d(v)$ in Fig. 3-8 is enough to obtain a smooth signal control, as it is shown Fig. 3-9. Then, for this case, the train stops in time at the targeted position with an acceptable error. Moreover, the FD block did not trigger any false fault detections. Fig. 3-10.

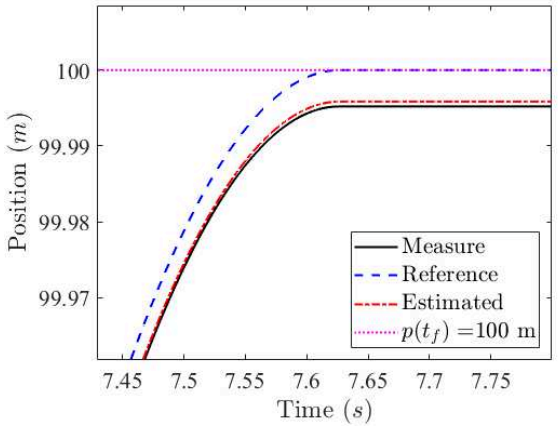

Fig. 3-7 Comparison of position without fault (zoom on stopping position).

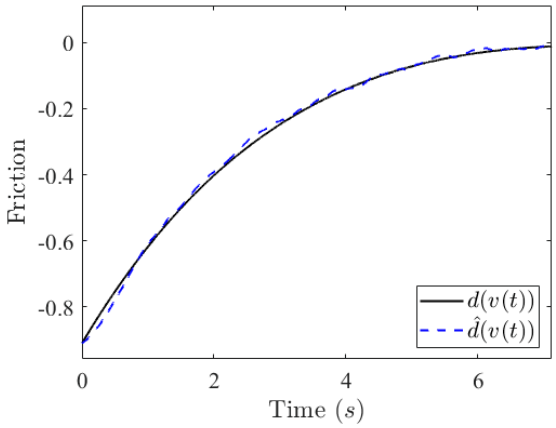

Fig. 3-8 Estimation of $d(v)$, without fault.

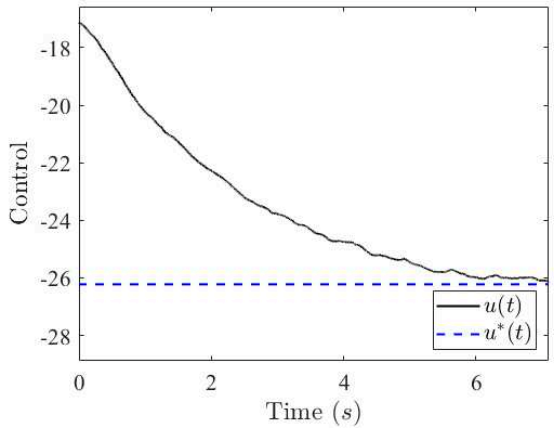

Fig. 3-9 Control signal without fault.

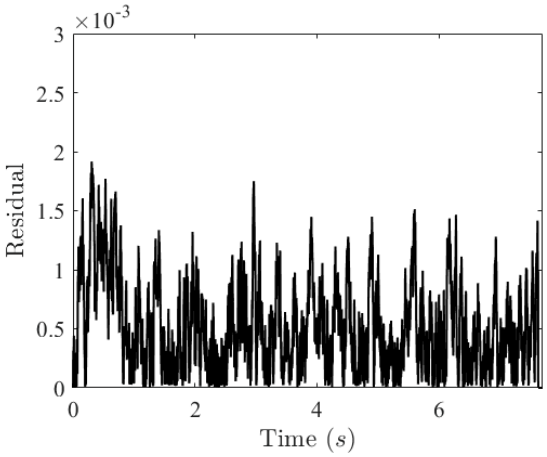

Fig. 3-10 Residual $r(t)$ without fault.

3.2.3.2. Faulty case and "classical" control (without compensation)

To show the effect of faulty situations, if not considered beforehand in the design of the control, we consider the same problem as the fault-free case, with the same simulation parameters, but including faults in the simulation. According to the previous notations, the fault duration is set to $\Delta t_{jam} = 200ms$. Then, we trigger four faults at 1s, 1.6s, 3s and 4s, *Fig. 3-11*.

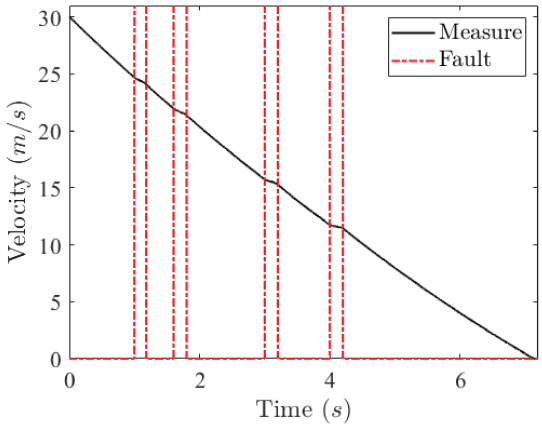

Fig. 3-11 Fault occurrence and duration during the braking phase.

Keeping the same control without compensation $\hat{d}$, i.e.:

$$\begin{cases} u = \frac{1}{b^*}\left(L_1\left(v - v_r\right) + L_2 p_i\right) + u^* \\ \dot{p}_i = v - v_r \end{cases}, \tag{3.34}$$

presents, of course, a wrong behavior. *Fig. 3-13* shows the position of the train and a stopping final position error of 0.12 meters. The first fault occurrence is shown Fig. 3-12. For illustration only, we provide the residual behavior during the fault, but in the "classical" control case we do not use any FD or FTC remediation of the fault's effect.

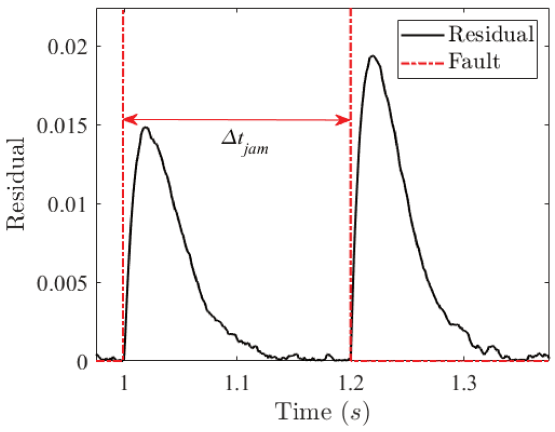

Fig. 3-12 Residual behavior during a fault

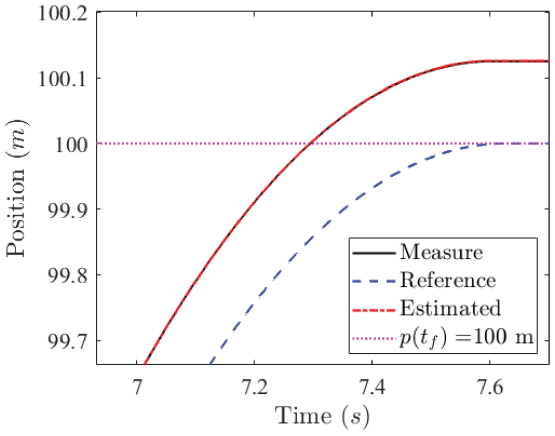

Fig. 3-13 Fault's impact on the final position using a classical controller.

3.2.3.3. Faulty case with Fault Tolerant Control

This simulation presents the application of the methodology. First of all, we apply the piecewise constant reference $u^*(t) = u^*(t_k)$ when $t \in [t_k, t_{k+1}[$, i.e. recomputed via the algorithm presented previously, where the times t_k correspond to the end of the detected jamming faults numbered $1,..,k$. Secondly, the control law (3.12) is applied to compensate for the disturbances $\hat{d}(t)$ estimated using the UIO PI-observer. The fault detection block uses a filtered residual $r(t) = |v(t) - \hat{v}(t)|$ with threshold values of $\varepsilon_{f_1} = 0.005$, $\varepsilon_{f_2} = 0.005$, and $\varepsilon_{f_3} = 0.001$, in order to trigger the FTC mechanism and to inhibit the fault.

Results are presented in Table 3.1 using fault durations Δt_{jam}, from 20%, i.e. $\Delta t_{jam} = 20ms$ to 100%. The second row presents the detection time delay's average Δt_{ds}, i.e. detection time minus beginning of the fault (known as we are in simulation). The last row of the table represents the relative error of the final position $e_{p\%} = \dfrac{|p(t_f) - p_f|}{l_{train}}$, assuming a train length of $l_{train} = 100m$. A comment must be made on the interpretation of the achieved improvement. While a single jamming without FTC remediation might lead in a small inaccuracy in the final position, in real conditions, they might be hundreds of random jamming during the braking phase, and the errors will accumulate. The FTC action will be especially beneficial in inhibiting the jamming as soon as possible, and consequently, in limiting its duration and its impact on stopping position. This is why the relative improvement obtained by FTC will grow with increased jamming duration, as shown in the table.

Taking the case shown in *Fig. 3-11*, with $\Delta t_{jam} = 200ms$ (100%) to be compared with the "classical" control, we have a final position error of 0.05 meters in

Fig. 3-16. The reduction on the error is achieved by the control signal in

Fig. 3-15, where the fault tolerant mechanism acts adequately when the fault is detected by the FD block, reducing the fault duration to $\Delta t_{jam} = 150ms$ with $\Delta t_{ds} = 4ms$,

Fig. 3-14.

Fig. 3-17 shows the train system following the reference with $u^*(t_k)$ recomputed at the instants t_k.

Table 3.1. Train stopping accuracy for different fault durations Δt_{jam}.

Δt_{jam} (ms)	40	80	120	160	200
Δt_{ds} (s)	0.002	0.002	0.001	0.002	0.001
Using FTC: $e_{p\%}$ $(\%)$	5.7×10^{-5}	1.8×10^{-4}	2.9×10^{-4}	3.3×10^{-4}	5.6×10^{-4}
Classical control: $e_{p\%}$ $(\%)$	1.7×10^{-3}	1×10^{-3}	3.5×10^{-4}	4.2×10^{-4}	1.2×10^{-3}

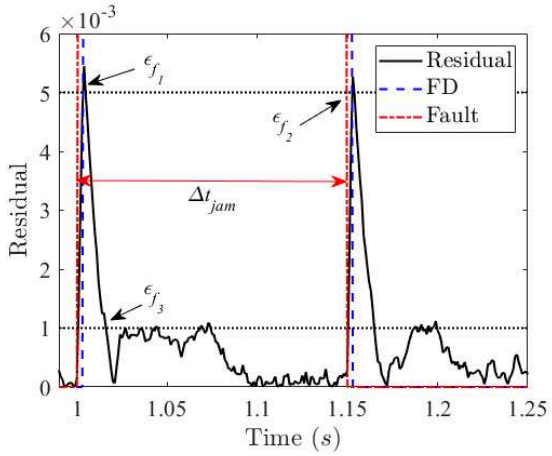

Fig. 3-14 Fault detection behavior.

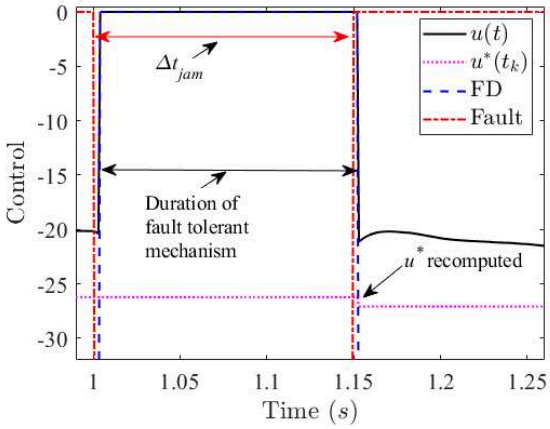

Fig. 3-15 FTC behavior during a fault.

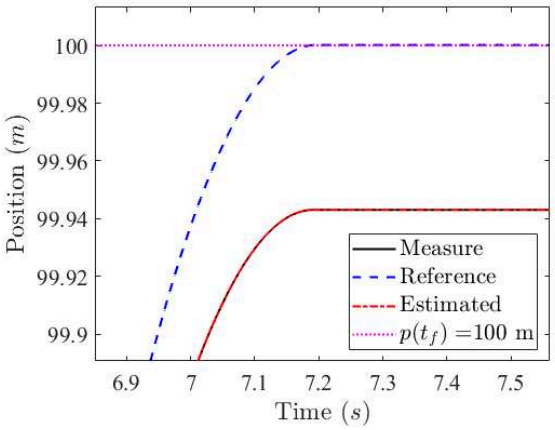

Fig. 3-16 Final position with FTC

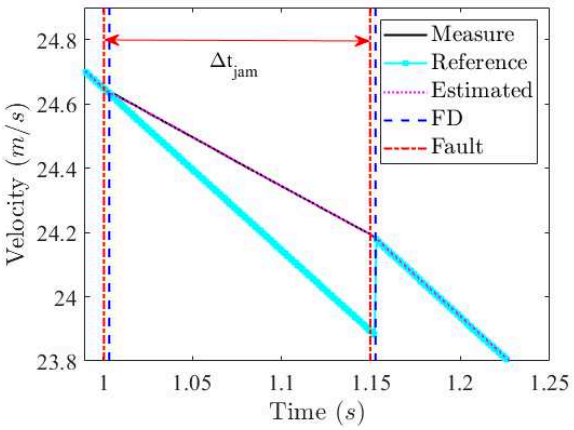

Fig. 3-17 velocity behavior.

3.2.4. Section discussion

This preliminary study showed that the proposed fault tolerant control with perturbation compensation can be efficiently used to improve accuracy of train's stopping when the braking wheel jams. The jamming faults were represented as actuator faults. As stated in the beginning of this section, the model taken into account (linear dynamic of the system, linear PI-observer, straight flat path during deceleration) and the assumptions (control input known) made this case as an "ideal" case, with the advantage to show the step-by-step procedure that was used to achieve our goals.

The assumptions made in this part, will now be removed in order to get close to real-time train operation. These assumptions were: knowledge of the effective braking control and accurate approximation of friction parameters.

3.3. Robust train position estimation under perturbation and sensor faults

In this section, we represent the wheel jamming as a sensor fault, motivated by the strong effect of the wheel jamming on speed measurements, which can lead to a temporary inaccessible velocity data, and the problem that might occur for real trains: if the on-board estimated position diverges significantly from the real position, an emergency brake might be issued by the ATP system for safety considerations. Indeed, if the estimated position is corrupted for some reason, it might indicate a malfunction in the train electronics, which can lead to the inability to stop the train in time at the right place. Then it is safer to stop the train immediately to investigate the malfunction. However, if the discrepancy between estimation and real positions is due bad wheel-rail contact that causes wheel's jamming, it is not a sensor malfunction but an intermittent fault that might lead to a big hit on the rolling stock and the infrastructure due to the emergency braking. In order to avoid this situation, a safety margin is applied on position estimation, and on the safe braking distances, which in turn reduces train frequency on the line, slows down the schedules and the travelers. Thus the need of a position estimation algorithm for the ATP with an improved robustness to sensor faults is required.

The comparison between the real and the estimated positions uses beacon-based position measurements for reference. The beacons are installed on the railway, at constant intervals, and their exact position is known. The beacons transmit the good position to the train when nearby, to reset the position estimation error, since the estimation relies solely on the odometer for velocity measurements and the following integration to obtain the position estimate. In order to improve position estimation for the ATP, we need to follow the constraints on the existing estimator and the ATP level systems: we consider that we have only access to the velocity sensors at the same rate that the ATP accesses the data bus, and that we do not know accurately the control signal, contrary to the previous section. This absence of measurement is partly compensated via the additional time-to-time beacon information that are used to reset the error of the position estimation.

The proposed approach is based on a sensor fault detection mechanism to identify and discard the corrupted measurements, and uses an UIO PI-observer. We consider also a more accurate train model based on a linear parameter varying (LPV) representation. Finally, robustness is considered with mixed H_∞/H_- approach for observer design. More specifically, mixed H_∞/H_- optimization is made, with H_∞ criteria for perturbation attenuation and H_- criteria for fault sensitivity. The design procedure is again expressed in terms of linear matrix inequalities (LMI), which are efficiently solved using convex optimization techniques (Boyd et al. 1994).

3.3.1. Problem statement and methodology

As explained in section 2.1.2 two types of sensors are used: the odometer located on the wheel, and the beacons fixed on the track. Wheel jamming occurs during braking phase and corrupts odometer measurements. The interest of beacons, that of course deliver a measurement independent of the jamming, is to give a time-to-time true measurement of the train position, i.e. each time the train crosses one of the beacon position, it corrects the odometer's corrupted measurements.

Based on the train dynamic taken from (Guzinski et al. 2009; Kaller and Allenbach 1995; Liu and Golovitcher 2003; Vijay 1984) analysed in section 2.1.1. We consider the following train model:

$$\begin{cases} \dot{v} = -w(v) + b_T u_T - b_B u_B - g(p) + \eta(t) \\ \dot{p} = v \end{cases}, \tag{3.35}$$

where v is the velocity *(m/s)*, p is the position of the vehicle *(meters)*, u_B is the braking force, u_T is the traction force, , $g(p)$ is the tangential force to the path or the force due to the declivity, $w(v)$ is the specific resistance to motion, b_B and b_T are constant coefficients and $\eta(t)$ represents the modelling errors. The dynamic friction has the same form as previously, i.e. $w(v) = w_0 + w_1 v + w_2 v^2$. Usually, we consider the declivity force $g(p) = g\sin(\theta(p))$, where $\theta(p)$ is the slope of the railway, and g is the gravity coefficient.

Similar to the section 0, an UIO from the PI-observer family is designed. As the speed coming from $w(v)$ is embedded into the system using a quasi-LPV framework, the unknown input will reconstruct the parts due to the modelling errors and to the force of the declivity. A second order, i.e. $\ddot{d}_R(t) \approx 0$ is also chosen to capture the unknown input, leading to the extended model:

$$\begin{cases} \dot{x} = A(z)x - Gw_0 - B_B u_B + B_T u_T + D\eta(t) \\ z = Cx \end{cases}, \tag{3.36}$$

where $x = \begin{bmatrix} v & d_R & \dot{d}_R \end{bmatrix}^T$ is the state vector, and: $A(z) = \begin{bmatrix} -w_1 - w_2 z & -1 & 0 \\ 0 & 0 & 1 \\ 0 & 0 & 0 \end{bmatrix}$, $B_T = \begin{bmatrix} b_T \\ 0 \\ 0 \end{bmatrix}$, $B_B = \begin{bmatrix} b_B \\ 0 \\ 0 \end{bmatrix}$, $G = \begin{bmatrix} 1 \\ 0 \\ 0 \end{bmatrix}$, $D = \begin{bmatrix} 1 & 0 & 0 \end{bmatrix}^T$ and $C = \begin{bmatrix} 1 & 0 & 0 \end{bmatrix}$. Notice that $A(z)$ depends on the measured variable $z = v$. A description of (3.36) can be done using a quasi-LPV (or the so-called Takagi-Sugeno) framework using a sector nonlinearity approach (Tanaka and Wang 2001); effectively as $z \in \left[\underline{z}, \overline{z}\right]$, a polytopic description can be written using the functions:

$$h_1(z) = \frac{\overline{z} - z}{\overline{z} - \underline{z}} \text{ and } h_2(z) = 1 - h_1(z). \tag{3.37}$$

that holds the convex sum property

$$\sum_{i=1}^{2} h_i(z) = 1,\ 0 \le h_i(z) \le 1. \tag{3.38}$$

Therefore, a quasi-LPV model of (3.36) has the following form:

$$\begin{cases} \dot{x} = \sum_{i=1}^{2} h_i(z) A_i x - Gw_0 - B_B u_B + B_T u_T + D\eta(t) \\ z = Cx \end{cases}. \tag{3.39}$$

Considering first that the fault occurs only during braking phases, i.e. when $u_B > 0$ and, second that it impacts the sensor; the jamming fault can be represented via the output equation as

$$y = z - Ff(t) \tag{3.40}$$

where $F \in [0,1]$ and $f(t) \in \mathbb{R}$, with $z = Cx$ corresponding to the fault-free output. Remember also that we consider only the braking phase, i.e. thereinafter we will consider $u_T = 0$, and as specified, the control u_B is not measured. An important remark has to be done therein.

Remark 3-1: as the speed signal is corrupted, we do not have the real output signal available anymore, i.e. the measured output is $y = z - Ff(t)$ whereas the parameter used in the quasi-LPV model is $z = Cx$. Therefore, if an observer has to be designed, it will enter in class of the so-called non-measurable parameters observer (Bergsten, Palm, and Driankov 2001; Yoneyama et al. 2001), which still is a challenging, theoretically unsolved problem.

A way to circumvent this issue is to transform $A(z)$ in $A(y)$, i.e. as $w_2 z = w_2(y + Ff(t))$, therefore we can introduce $A(y)$ in (3.39) and consider that the part $w_2 Ff(t)$ can be reconstructed via the unknown input d_R.

$$\dot{v} = -(w_1 + w_2 y)v - b_B u_B - w_0 + d_R + \eta(t) \tag{3.41}$$

It leads to the following model, being understood that the variable d_R (future unknown input for the observer) represents $d_R = g(p) + w_2 Ff(t)z$:

$$\begin{cases} \dot{x} = \sum_{i=1}^{2} h_i(y) A_i x - G w_0 - B_B u_B + D\eta(t) \\ z = Cx \\ y = z - Ff(t) \end{cases} \tag{3.42}$$

With the extended state vector $x = \begin{bmatrix} v & d_R & \dot{d}_R \end{bmatrix}^T$. At last, as we do not know the amplitude of u_B, we will use the same procedure as depicted section 0 (see Algorithm 3-1) , i.e. we will compute a piecewise control $\hat{u}_B = u^*$. Therefore, again we will consider that the difference

$u_B - u^*$ can be captured via the unknown input. These various issues will be discussed further on. Thus, the model used is:

$$\begin{cases} \dot{x} = \sum_{i=1}^{2} h_i(y) A_i x - G w_0 - B_B u^* + D\eta(t) \\ z = Cx \\ y = z - Ff(t) \end{cases} \tag{3.43}$$

With the extended state vector $x = \begin{bmatrix} v & d_R & \dot{d}_R \end{bmatrix}^T$ and the unknown input corresponding to: $d_R = g(p) + w_2 Ff(t) z + B_B(u_B - u^*)$.

3.3.2. Overview of the proposed sensor fault detection system

Recall that the force due to the declivity $g(p)$ and the control u_B are unknown, so the UI-Observer is designed to reconstruct it through the unknown input d_R. To reduce the effects of uncertainties, faults, and noise in the system, H_∞ attenuation criterion is applied with H_- index to make the residual sensitive to the fault and robust to the remaining disturbances. Fault detection module will trigger fault detection and system recovery signals, since jamming faults are intermittent. Therefore, the UIO will filter the jamming fault from the odometer measurements, based on estimated times of fault detection and recovery, and the correct trajectory will be reconstructed. Position estimation error is reset using the true position information that is received whenever a beacon is crossed. At the same time, $\hat{u}_B = u^*$ is computed following the algorithm proposed in section 3.1, using the exact position from the beacon and the velocity estimation of the observer. Therefore, if a beacon is crossed, then the constant control $u^*(t_0)$ is computed solving the nonlinear equation (3.10) from section 3.2.2.1, with $(t_0, p(t_0), v(t_0)) = (\bar{t}_k, p(\bar{t}_k), \hat{v}(\bar{t}_k))$, where $\bar{t}_k$, $k \in \{1,2,3,...,j\}$ is the instant when a beacon is crossed. In between two beacons, the measurement from the sensor and the estimation from the observer are used to compute a fault sensitive residual signal. This residual signal is

used with a fault detection algorithm explained after. The general structure of the integrated design is shown Fig. 3-18.

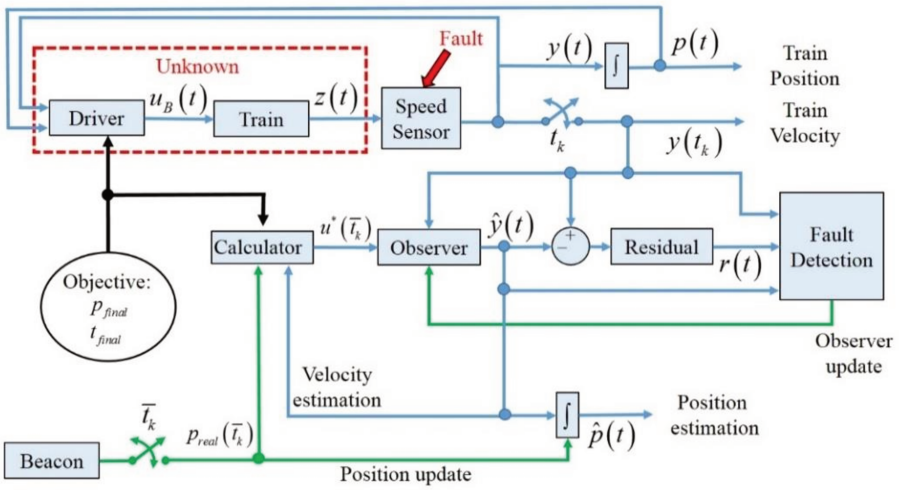

Fig. 3-18 General scheme.

3.3.3. Contribution

3.3.3.1. Observer design

The quasi-LPV-UIO for the system (3.43) has the following form:

$$\begin{cases} \dot{\hat{x}} = \sum_{i=1}^{2} h_i(y)\left(A_i\hat{x} - Gw_0 - B_B u^* + P^{-1}L_i\left(y-\hat{y}\right)\right) \\ \hat{y} = C\hat{x} \\ r = M\left(y-\hat{y}\right) \end{cases} \tag{3.44}$$

where $\hat{x} = \begin{bmatrix} \hat{v} & \hat{d}_R & \dot{\hat{d}}_R \end{bmatrix}^T$ is the state vector estimation, $\hat{y}$ is the output, r is the residual, $L_i \in \mathbb{R}^3$, $i = 1,2$ and $M \in \mathbb{R}$ are the observer gains and the residual gain, respectively. Defining the state estimation error as $e = x - \hat{x}$, the estimation dynamic error is:

$$\begin{cases} \dot{e} = \sum_{i=1}^{2} h_i(y)\left(\left(A_i - P^{-1}L_iC\right)e + P^{-1}L_iFf(t)\right) + D\eta(t) \\ r = MCe - MFf(t) \end{cases} \tag{3.45}$$

The goal is to design the gains L_i and M of the observer (3.44) to guarantee that the residual $r(t)$ is robust to $\eta(t)$ and sensitive to the fault $f(t)$. The design is made in two steps.

First consider $f(t)=0$. The robustness of the residual $r(t)$ to the noise $\eta(t)$ can be formulated as a classical H_∞ attenuation problem (Edelmayer, Bokor, and Keviczky 1994; Zhong et al. 2003), i.e. find a positive constant λ such that:

$$\|r(t)\|_2 < \lambda \|\eta(t)\|_2 \tag{3.46}$$

To ensure (3.46), a sufficient condition is:

$$\dot{V}(e(t)) + r(t)^T r(t) - \lambda^2 \eta(t)^T \eta(t) \le 0, \tag{3.47}$$

Integrating (3.47) gives:

$$V(e(\infty)) - V(e(0)) < \lambda^2 \int_0^\infty \left(\eta(t)^T \eta(t) - r(t)^T r(t)\right) dt, \tag{3.48}$$

Since the model is globally asymptotically stable $V(e(\infty))=0$, and considering initial conditions null, i.e. $V(e(0))=0$, (3.48) becomes $\int_0^\infty r(t)^T r(t)\,dt < \lambda^2 \int_0^\infty \eta(t)^T \eta(t)\,dt$ which corresponds to (3.46). Therefore, using a quadratic Lyapunov function $V(t)=e^T P e$, $P>0$, and using $r(t)=MCe$ (3.47) writes:

$$2e^T P\dot{e} + e(t)^T C^T M^T MCe(t) - \lambda^2 \eta(t)^T \eta(t) \le 0. \tag{3.49}$$

Using the expression (3.45), (3.49) will hold if:

$$\begin{bmatrix} e \\ \eta \end{bmatrix}^T \begin{bmatrix} PA(y) - L(y)C + (*) & PD \\ D^T P & 0 \end{bmatrix} \begin{bmatrix} e \\ \eta \end{bmatrix} + \begin{bmatrix} e \\ \eta \end{bmatrix}^T \begin{bmatrix} C^T M^T MC & 0 \\ 0 & -\lambda^2 \end{bmatrix} \begin{bmatrix} e \\ \eta \end{bmatrix} \le 0$$

with $(*)$ is the transpose quantity. Finally, recalling that $A(y)=\sum_{i=1}^{2} h_i(y) A_i$, $L(y)=\sum_{i=1}^{2} h_i(y) L_i$, a sufficient condition to have $r(t)$ robust to $\eta(t)$ is:

$$\sum_{i=1}^{2} h_i(y) \begin{bmatrix} PA_i - L_i C + (*) + C^T M^T MC & PD \\ D^T P & -\lambda^2 \end{bmatrix} \le 0 \tag{3.50}$$

Second, consider $\eta(t)=0$, we want to ensure that the residual $r(t)$ is sensitive to the fault $f(t)$. This goal can be achieved using H_- conditions from (J. L. Wang, Yang, and Liu 2007), i.e. finding a constant $\gamma>0$ such that:

$$\|r(t)\|_2 > \gamma \|f(t)\|_2. \tag{3.51}$$

Let us consider a function $V(e(t)) = e(t)^T P_f e(t)$, with $P_f = P_f^T$ a symmetric (non-necessary positive) matrix. Suppose that the following inequality is satisfied:

$$\int_0^\infty \left(r(t)^T r(t) - \gamma^2 f^T(t) f(t) - \dot{V}(e(t)) \right) dt + V(e(0)) > 0. \tag{3.52}$$

Knowing from the H_∞ part, that the error dynamic is GAS, i.e. $V(e(\infty)) = 0$, (3.52) is equivalent to $\int_0^\infty \left(r(t)^T r(t) - \gamma^2 f^T(t) f(t) \right) dt \geq 0$ which corresponds to condition (3.51). Therefore, a sufficient condition to ensure (3.51) holds true is:

$$r^T(t) r(t) - \gamma^2 f^T(t) f(t) - \dot{V}(e(t)) \geq 0 \tag{3.53}$$

And with $V(e(t)) = e(t)^T P_f e(t)$:

$$-2e(t)^T P_f e(t) - r(t)^T r(t) + \gamma^2 f^T(t) f(t) \leq 0 \tag{3.54}$$

The residual writes: $r(t) = \begin{bmatrix} MC & -MF \end{bmatrix} \begin{bmatrix} e \\ f(t) \end{bmatrix}$, from which (3.54) writes:

$$\begin{bmatrix} e^T \\ f(t)^T \end{bmatrix}^T \left(\begin{bmatrix} -P_f A(y) + L_f(y) C + (*) & L_f(y) F \\ F^T L_f(y)^T & \gamma^2 \end{bmatrix} - \begin{bmatrix} C^T M^T MC & -C^T M^T MF \\ -F^T M^T MC & F^T M^T MF \end{bmatrix} \right) \begin{bmatrix} e \\ f(t) \end{bmatrix} \leq 0$$

Or equivalently:

$$\begin{bmatrix} -P_f \left(A(y) - L_f(y) C \right) + (*) - M^2 C^T C & -M^2 C^T F + P_f L_f(y) F \\ -FM^2 C + F L_f{}^T(y) P_f & \gamma^2 - F^2 M^2 \end{bmatrix} \leq 0 \tag{3.55}$$

with P_f being symmetric and $L_f = \sum_{i=1}^{2} h_i(y) L_{f_i}$ being the gain matrix.

Remark 3-2: unlike the H_∞ attenuation conditions, P_f is not necessarily sign definite (J. L. Wang, Yang, and Liu 2007), this point is important for finding a solution to the general H_∞ / H_- problem. Effectively, it appears that searching for the same matrix, i.e. $P_f = P > 0$ (even if giving a strict LMI constraint problem) such in some works (Theilliol and Aberkane 2011) is extremely conservative. To give the example of the train, it results in a "no feasible" solution, whatever are the scalars $\gamma > 0$ and $\lambda > 0$.

Note that $M \in \mathbb{R}$ and $F \in \mathbb{R}$ are scalar, therefore if P_f is fixed, we will get LMI conditions using the convex sum property from (3.50) and (3.55); find $P > 0$, L_i, $\gamma > 0$, $\lambda > 0$ and $M > 0$ such that:

$$\begin{bmatrix} PA_i - L_i C + (*) + M^2 C^T C & PD \\ D^T P & -\lambda^2 \end{bmatrix} \leq 0 \tag{3.56}$$

$$\begin{bmatrix} -P_f \left(A_i - L_{f_i} C\right) + (*) - M^2 C^T C & -M^2 C^T F + P_f L_{f_i} F \\ -FM^2 C + F L_{f_i}^T P_f & \gamma^2 - F^2 M^2 \end{bmatrix} \leq 0 \tag{3.57}$$

with $i = 1, 2$. In order to reduce the magnitude of possible observer gains, a norm constraint $\left(L_h P^{-1}\right)^T P \left(P^{-1} L_h\right) \leq \alpha$ is added, where α is a positive constant value. Using Schur's complement and the convex sum property, the constraint is expressed as the following additional LMI condition:

$$\begin{bmatrix} -\alpha & L_i^T \\ L_i & -P \end{bmatrix} \leq 0, \; i = 1, 2. \tag{3.58}$$

Following *Remark 3-2*, the problem is not LMI. Therefore, there are several ways (suboptimal) to get solutions, based on two steps algorithm like in (J. L. Wang, Yang, and Liu 2007). For example, first fix the part that renders BMI the problem, for example P_f and then solve the LMI constraints problem, i.e. (3.56) and (3.58). Once a solution is obtained, fix L_{f_i} and solve the problem (3.56) and (3.57). Several loops can be used, and there is no proof of convergence to any optimal solution. In our case, after several trials-and-errors, a "good" option (that presented interesting results) was to run the following algorithm.

Algorithm 3-2:

Step 1: solve (3.56) and (3.58), i.e. find $P > 0$ and the observer gains L_i, $i = 1, 2$, minimizing $\lambda > 0$, while tuning $\alpha > 0$.

Step 2: let $L_{f_i} = L_i$ and solve (3.56) and (3.57), i.e. find $P_f = P_f^T$ and the residual gain $M > 0$, maximizing $\gamma > 0$.

As stated before, several loops may be necessary to get a satisfactory result. Especially, the acceptable compromise between $\lambda > 0$ that guarantees the robustness of residual $r(t)$ according to $\eta(t)$ and $\gamma > 0$ that guarantees its sensitivity to the fault $f(t)$.

3.3.3.2. Fault detection

After solving the H_∞ / H_- problem, we obtain the gain M using Algorithm 3-2 and we compute the residual from (3.45):

$$r(t) = M\left(y(t) - \hat{y}(t)\right) \tag{3.59}$$

Now, the fault detection algorithm uses the residual $r(t)$, a constant threshold ε_f determined using H_∞ / H_- results, the speed estimation $\hat{v}(t)$, and the measurement from the sensor $v(t_k)$, where t_k is the measurement instant. Therefore, based on the behavior of the fault from section 2.1.2, the fault detection is divided into three parts:

$$\text{Fault free } (N_f) \rightarrow \text{increasing fault } (F_f) \rightarrow \text{decreasing } (R_f) \rightarrow \text{Fault free } (N_f).$$

This give us additional information to improve fault detection and to filter corrupted sensor data.

- Fault free (N_f) *if* the observer estimation matches the sensor.
- Increasing fault (F_f) *if* the observer estimation and measurement are diverging.
- Decreasing fault (R_f) *if* the observer estimation and measurement are converging.

The main idea of the algorithm is shown in Fig. 3-19.

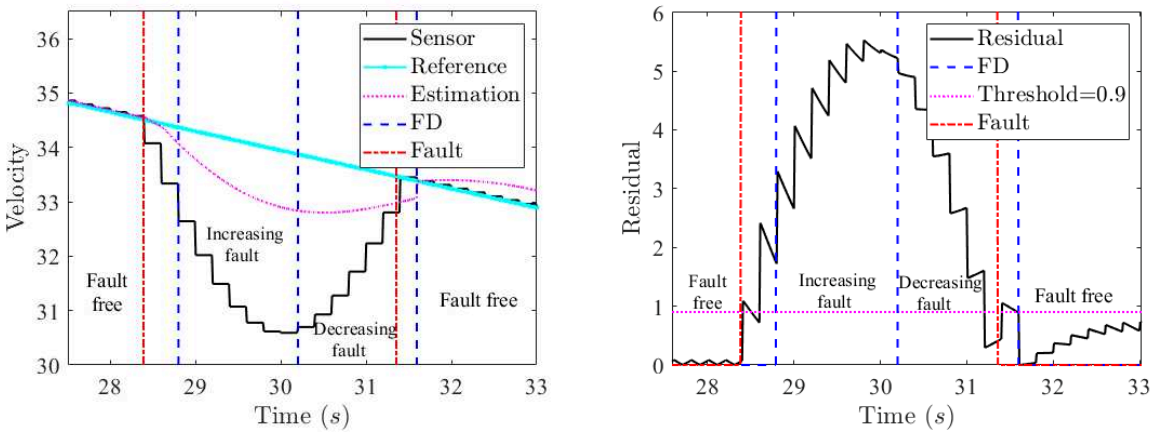

Fig. 3-19 Fault detection scheme: speed behavior (left), residual behavior (right).

The steps of the algorithm are the following:

Algorithm 3-3:

- If $r(t) > \varepsilon_f$ and $\hat{v}(t) > v(t_k)$ then $F_f(t_k+1) = 1$ and $N_f(t_k+1) = 0$

  Else $F_f(t_k+1) = F_f(t_k)$ and $N_f(t_k+1) = N_f(t_k)$
- If $F_f(t_k) = 1$ and $v(t_k-1) < v(t_k)$ then $R_f(t_k+1) = 1$

  Else $R_f(t_k+1) = R_f(t_k)$
- If $R_f(t_k) = 1$ and $v(t_k-1) > v(t_k)$ then $R_f(t_k+1) = 0$, $F_f(t_k+1) = 0$, and $N_f(t_k+1) = 1$
- If $N_f(t_k) = 1$ and $v(t_k-1) < v(t_k)$ then $R_f(t_k+1) = 1$, $F_f(t_k+1) = 1$, and $N_f(t_k+1) = 0$
- If $N_f(t_k) = 0$ and $v(t_k) = 0$ then $F_f(t_k+1) = 1$ and $N_f(t_k+1) = 0$

3.3.4. Simulations

The effectiveness of the proposed approach is demonstrated by simulation in two cases. The first case is fault free, to show the unknown input estimation d_R under ideal conditions. The

second case corresponds to a faulty case, to show the improvement in the position estimation with the proposed approach.

3.3.4.1. Fault-free case

Consider the quasi-LPV train model (3.42) with parameters $w_0 = 0.02$, $w_1 = 0.003$, $w_2 = -0.00024$, $b_B = b_T = 1$, $g(p) = 0.05\sin(0.1t)$. We assume that the speed is bounded: $y \in [0, 50]$ (m/s). The observer (3.44) parameters are supposed with a 20% of error in the friction parameters: $w_0 = 0.016$, $w_1 = 0.0024$, $w_2 = -0.000192$. The measurement update periodicity is 200ms. The position estimation error is reset with respect to the real position from the beacons each 200 *meters*.

Now, solving conditions (3.56), (3.57) and (3.58) via Algorithm 3-2 with $D = [0.01 \quad 0 \quad 0]^T$, $\alpha = 1$, $F = 1$, and minimizing λ, gives a result with $M = 2.3$, $\gamma = 1.58$, $\lambda = 0.031$, and with the gains $L_1 = [1.15 \quad -1.216 \quad -0.405]^T$ and $L_2 = [1.16 \quad -1.215 \quad -0.404]^T$.

The simulation results, with initial conditions $x(0) = [45 \quad 0.22 \quad 0]^T$ and $\hat{x}(0) = [44.1 \quad 0 \quad 0]^T$, shows that the observer follows the measurements, when there are no faults, as shown in

Fig. 3-20. Recall that the control $u(t)$ is unknown, and the only available information is about the train braking or not. We use each beacon (vertical blue lines on the figures) to compute a u^* as the solution to the problem presented (3.10). Fig. 3-23 presents the results of this procedure and shows that the computed control u^* is a realistic guess of the real control signal. The unknown input estimation is presented Fig. 3-22 and shows a very good capability to capture the dynamic of $d_R = g(p) + B_B(u_B - u^*)$. The position error, Fig. 3-24, is small even considering the noise signal,

Fig. 3-21 , benefiting from the accurate estimation of the disturbances. Finally, Fig. 3-25 shows the residual signal and, with a threshold of 0.9, as expected, there are no false alarm.

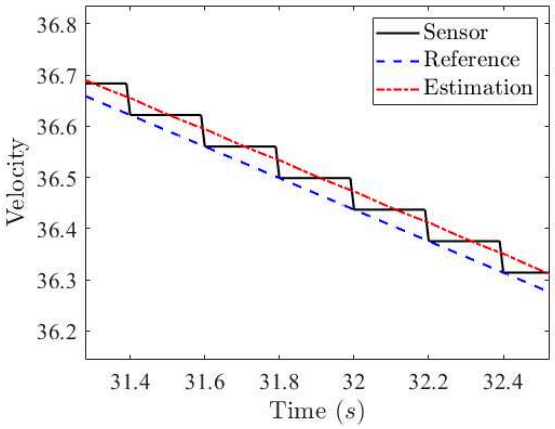

Fig. 3-20. Velocity comparison (fault-free).

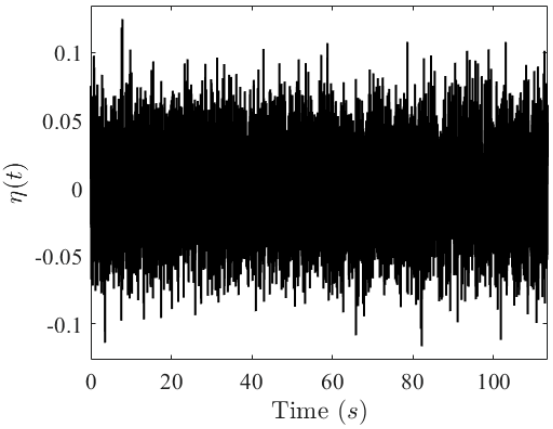

Fig. 3-21 Noise signal.

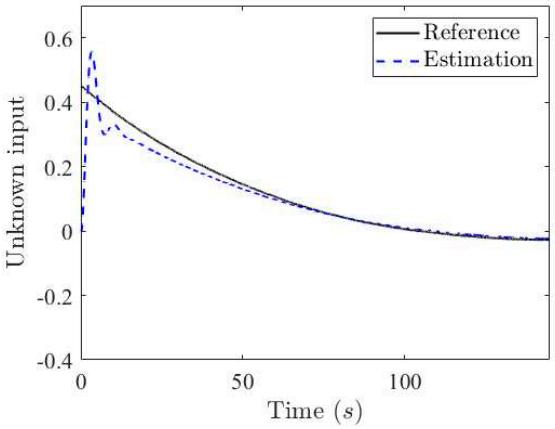

Fig. 3-22. Unknown input estimation (fault free)

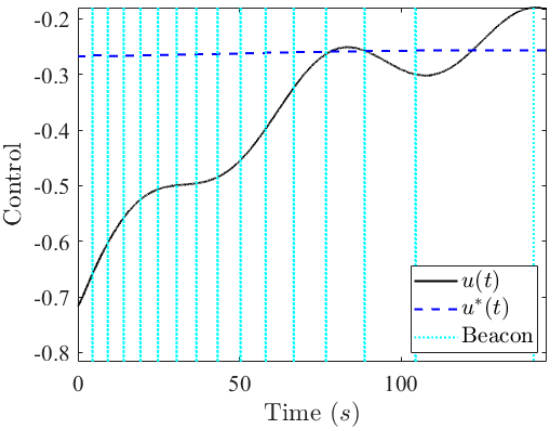

Fig. 3-23 Control signal.

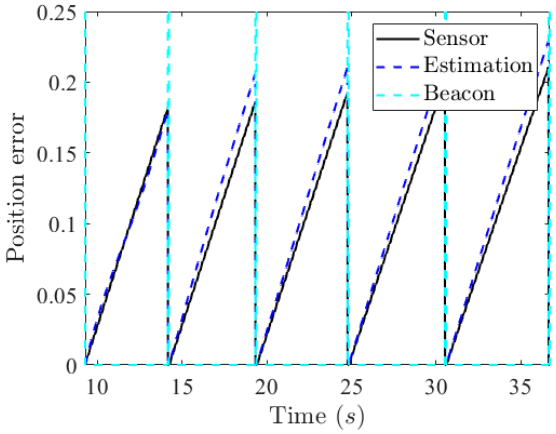

Fig. 3-24. Position error behavior (fault-free)

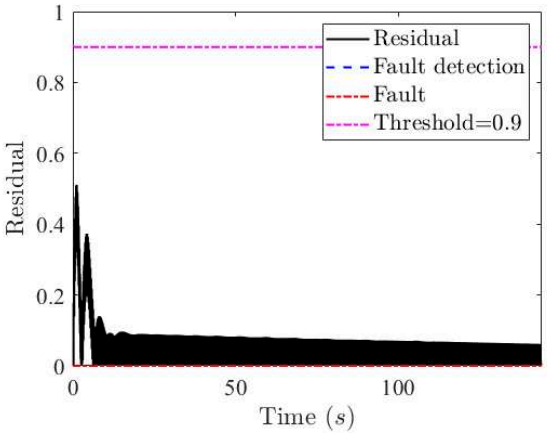

Fig. 3-25 Residual behavior (fault-free).

3.3.4.2. Faulty case

The example proposed therein introduces a jamming fault, Fig. 3-27, producing 10% error in comparison with the real velocity, Fig. 3-26. The algorithm for fault detection with a threshold of 0.9 is able to detect the fault with a time delay of 0.4s, as shown in Fig. 3-27. Moreover, the estimation of the unknown input $d_R = g(p) + w_2 Ff(t) z + B_B(u_B - u^*)$ converges to the real signal after fault occurrence, as shown in Fig. 3-29. Fig. 3-28 shows position error between two beacons (blue vertical lines). We can see that the position estimation error from the observer is 4 meters better (500%) than sensor-based estimation.

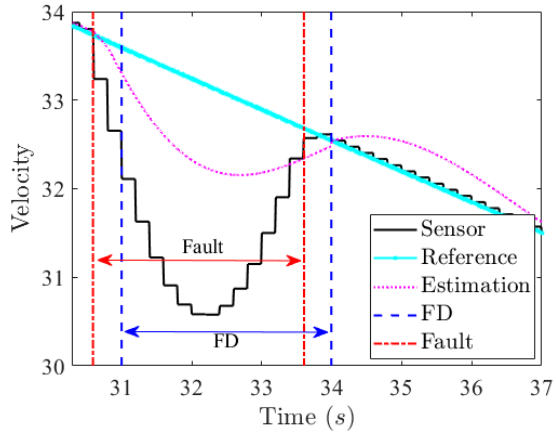

Fig. 3-26 Jamming fault impact on velocity

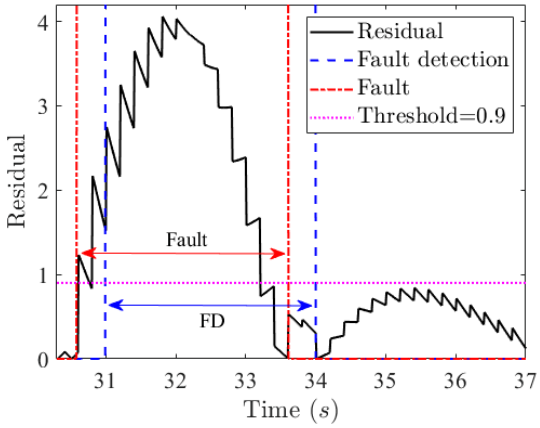

Fig. 3-27 Residual behavior for different fault amplitudes.

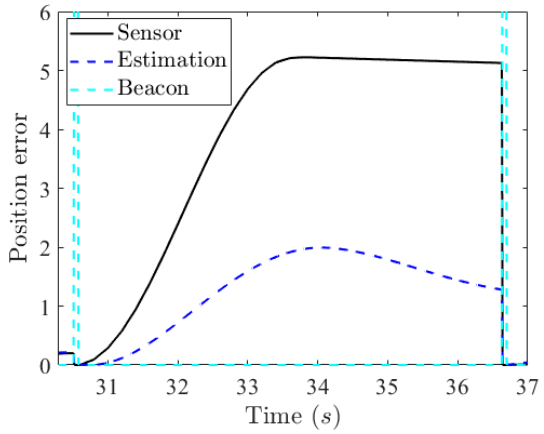

Fig. 3-28 Position error with fault.

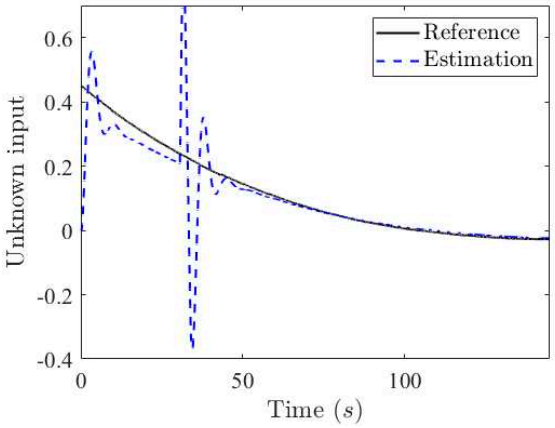

Fig. 3-29 UI estimation whit fault.

3.3.5. Section Discussion

This section presented the interest of a robust position estimation algorithm for the ATP system. Using only available noisy measurements at a low rate, with incomplete knowledge of parameters and control inputs, the quasi-LPV UI observer and the related fault detection module managed to successfully detect wheel jamming and to filter the corrupted measurements. We derived an algorithm and LMI conditions to design the observer with acceptable performance using H_∞/H_- optimization, and at the same time, the obtained norms will help with the choice of the appropriate fault detection threshold that insures an acceptable compromise.

However, these promising results need to be validated on an experimental data set, with stronger faults, and that will be addressed in the validation chapter.

Also, while the position estimation is improved, there is no guaranteed estimation error, i.e. it is impossible to predict how much the position error improved in order to appropriately determine the safety margin, or to allocate the exact bandwidth that is needed to insure some worst case position error bound. This topic will be addressed in the next chapter.

3.4. Conclusion

In this chapter, we presented two different contributions to help with automatic train operations. First of all, we addressed the problem of making the train stop accurately at the station, even if the brakes are intermittently unavailable because of faults. This application proposes a solution

for ATSC algorithm. Secondly, we considered the problem of robust position estimation, with imperfect knowledge of the system, perturbations, corrupted measurements and noise. This application is appropriate to improve ATO based position estimator.

From the methodological point of view, we addressed fault detection and fault tolerant control of intermittent faults (faults that appear and disappear), with two different formulations for the same wheel jamming fault. FD and FTC were performed, with realistic assumptions, considering imperfect knowledge of the system and the controls, and slow measurement updates.

Finally, we contributed to the design of an unknown input observer in proportional-integral form, and derived LMI conditions to formulate design conditions. We also used quasi-LPV system model, and H_∞/H_- optimization framework for that matter. Formal performance issues were discussed and solutions were proposed to ensure acceptable design performance.

Next chapter addresses possible worst case performance guarantees for the estimation error, considering the continuous-discrete dynamic nature of the system.

CHAPTER 4. Robust estimation for nonlinear continuous-discrete systems with missing outputs

4.1.Introduction

This chapter is about guaranteed state estimation of discrete output systems. The main motivation of this research is to obtain formal worst performance indicators for a continuous-time observer dynamic with sampled-time updates, considering constant sampling period and to some extent, variable sampling. The challenge here is that the system is impacted with perturbations together with a partial knowledge of the control input. As presented in the previous chapters, we use unknown input observers (UIO) (J. Chen, Patton, and Zhang 1996) to solve that issue. This makes possible the estimation of exogenous perturbations, and implementation of appropriate robust control techniques, based on disturbance compensation (Faieghi, Jalali, and Mashhadi 2014; Gao, Liu, and Chen 2016).

Therefore, this chapter addresses the performance of an observer of the continuous-discrete type with an UIO design, and how can we assess the worst-case error bound with respect to variable and partially unknown measurement sampling. A specific form of the so-called Gronwall inequality (Dragomir 2003) is necessary to compute the error bound, inspired by the Input to State Stability (ISS) / BIBO context and research on stability of systems (Lazarević and Spasić 2009) (Phat and Ratchagit 2011). Depending on the choice of the observer, i.e. constant gain or time-varying observer gain, different bounds can be obtained. Since the derived bounds can be over-conservative due to the assumptions and inequalities taken into account, we consider practical ways to relax the conservativeness using available knowledge on the observed physical system. The results are applied to the transport application, using the train mathematical model for simulation and validated in the next chapter by data acquired during field tests on a benchmark locomotive.

4.2. Continuous-discrete observer literature overview

Research works on continuous-discrete dynamics are popular when dealing with slow process dynamics, where fast measurements are not required, for example in the chemical industry (Astorga et al. 2002), (Tatiraju, Soroush, and Ogunnaike 1999), (Hernández and Alvarez 2003). For such cases, one will use the so-called continuous-discrete observers (CDO), with the objective to reconstruct the state between two samples. The study of CDO is also popular because in some situations, sensor measurements are available through a shared communication bus, and the allocated bandwidth is insufficient to transmit in real-time all the available measurements, which makes it difficult to implement observers that are fast enough to keep up with the system or controller rate.

Also, ideas to use CDO design to insure finite time performance of the estimation emerged recently (Mazenc, Ahmed, and Malisoff 2018). The continuous-discrete design problem, along with the similar multi-sampling rate design problem, is formulated in the linear case using either predictors in between samples (Ling and Kravaris 2017a) and (Mazenc and Dinh 2014) or classical sample and hold strategies (Moarref and Rodrigues 2014), with the objective to achieve exponential stability of the error dynamics, given a maximum sampling period, using LMI context and Lyapunov-Krassovskii-based conditions. This research is also extended to non-linear systems, like in (M. Farza et al. 2014b) and (Karafyllis and Kravaris 2009) using high gain observers and in (Ling and Kravaris 2017b), where the vector small-gain theorem was used (Karafyllis and Jiang 2011). In (Dinh et al. 2015), authors design CDO for continuous time Lipschitz system with sampled measurements, where the estimation error is bounded, which is useful for applications. Literature also contains results on the use of CD Kalman filter for stochastic systems (Jazwinski 2007).

4.3. Continuous discrete time observer design

4.3.1. Problem statement and preliminaries

Consider the following continuous-discrete nonlinear system

$$\begin{cases} \dot{x}(t) = A(y(t))x(t) + Bu(t_k) \\ y(t_k) = Cx(t_k) \end{cases} \tag{4.1}$$

where $x(t) \in \mathbb{R}^n$ is the state vector, $A(y(t)) \in \mathbb{R}^{n \times n}$, $B \in \mathbb{R}^{n \times n_u}$, and $C \in \mathbb{R}^{p \times n}$; the output $y(t_k) \in \mathbb{R}^p$ and the input $u(t_k) \in \mathbb{R}^{n_u}$ are measured every t_k sampling time with $k \in \mathbb{N}^+$, and we consider a possibly varying sampling time τ_M $(0 < t_{k+1} - t_k \le \tau_M < +\infty)$.

The proposed nonlinear observer in continuous-discrete time has the following form:

$$\begin{cases} \dot{\hat{x}}(t) = A(\hat{y})\hat{x}(t) + Bu(t_k) + K(\cdot)(y(t_k) - \hat{y}(t)) \\ \hat{y}(t) = C\hat{x}(t) \end{cases} \tag{4.2}$$

where $\hat{x}(t) \in \mathbb{R}^n$ is the state vector estimation, $\hat{y}(t) \in \mathbb{R}^p$ is the output estimation, and $K(\cdot) \in \mathbb{R}^{n \times p}$ is a matrix to be determined which form will be defined later on.

Remark 4-1: The problem written therein covers the case of the train where the measurements are done when it crosses the beacons, inducing a varying sampling time. Therefore, in (4.2) the choice of $K(\cdot)$ is twofold: whether it depends on the output at sampling instant t_k, i.e. $K(y(t_k))$ or on the observer–based output reconstruction $K(\hat{y}(t))$.

Considering the state observation error $e(t) = x(t) - \hat{x}(t)$, we obtain the following error dynamic:

$$\dot{e}(t, t_k) = (A(\hat{y}) - K(\cdot)C)e(t) + (A(y) - A(\hat{y}))x(t) + K(\cdot)(Cx(t) - y(t_k)). \tag{4.3}$$

From (4.3) we can see that the term $K(\cdot)(Cx(t) - y(t_k))$ appears and it needs to be bounded depending on the structure of $K(\cdot)$. The term $(A(y) - A(\hat{y}))x(t)$ will be handled using

robustness considerations for the case of the train, see section 4.3.3. Therefore, we consider the following bound on the error:

$$\left\| e\left(t,t_k\right) \right\| \le \mu\left(t,t_k\right). \tag{4.4}$$

If the value of $\mu\left(t,t_k\right)$ is determined, equation (4.4) guarantees a worst case performance for a Continuous-Discrete Observer design at time t, given that the last measurement update occurred at time t_k. Thus it is important to determine the most accurate estimation of $\mu\left(t,t_k\right)$, i.e. the smallest one, and the possible practical application of this bound. The studied cases are the following:

a) Design the Continuous Discrete PI-Observer that ensures the most favorable worst case estimation $\left\| e\left(t,t_k\right) \right\|$.

b) Determine what is impact of missing measurements (delayed or corrupted due to sensor faults) on $\left\| e\left(t,t_k\right) \right\|$

Another practical use of the bound $\mu\left(\cdot\right)$ is to determine the appropriate maximal measurement sampling time $\tau_M = t_{k+1} - t_k$ that ensures a given guaranteed worst-case performance. This case is a different formulation of case b), and will not be detailed.

4.3.2. Main result

First, an asymptotic convergence condition of the estimation error in the ideal case is required. This one is given by the following assumption, and holds in every case.

Assumption 4-1: For the homogeneous system

$$\dot{e}\left(t,t_k\right) = \left(A\left(\hat{y}\right) - K\left(\cdot\right)C\right)e\left(t,t_k\right), \tag{4.5}$$

it exists a matrix $K\left(\cdot\right)$ such that the convergence of the dynamical system $e\left(t,t_k\right)$ is exponentially guaranteed whatever the initial conditions are. For example, considering a quadratic Lyapunov function $V\left(e\right) = e^T P e$, $P = P^T > 0$ together with a gain observer written

as $K(\cdot)=P^{-1}M(\cdot)$, with $M(\cdot)\in\mathbb{R}^{n\times p}$ a matrix to be defined. Exponential convergence of the estimation error holds if:

$$PA(\hat{y})-M(\cdot)C+A(\hat{y})^{T}P-C^{T}M(\cdot)^{T}<0. \tag{4.6}$$

Therefore, *Assumption 4-1* ensures that it exists constants $\beta>0$ and $m>0$ such that the fundamental matrix solution $e(t,t_k)=\phi(t,t_k)e(t_k)$ satisfies the condition:

$$\|\phi(t,t_k)\|\le\beta e^{-m(t-t_k)},\ t\ge t_k. \tag{4.7}$$

The classical exponential decay rate for a quadratic Lyapunov function $V(e)=e^{T}Pe$, $P=P^{T}>0$ will be used in the sequel and is recalled thereafter. Consider a positive constant decay rate $\varepsilon>0$ (Duan and Yu 2013), thus for $t\ge t_k$:

$$V(e(t))\le V(e(t_k))e^{-\varepsilon(t-t_k)}. \tag{4.8}$$

Recall that $\underline{\lambda}_P\|e\|^2\le e^{T}Pe\le\overline{\lambda}_P\|e\|^2$, where $\underline{\lambda}_P$ and $\overline{\lambda}_P$ are respectively the minimum and maximum eigenvalue of P. Then (4.8) can be lower and upper bounded as:

$$\underline{\lambda}_P\|e(t)\|^2\le V(e(t))\le V(e(t_k))e^{-\varepsilon(t-t_k)}\le\overline{\lambda}_P\|e(t_k)\|^2e^{-\varepsilon(t-t_k)} \tag{4.9}$$

giving

$$\|e(t)\|^2\le\frac{\overline{\lambda}_P}{\underline{\lambda}_P}\|e(t_k)\|^2e^{-\varepsilon(t-t_k)} \tag{4.10}$$

Therefore, considering (4.7) gives directly the estimations: $\beta=\sqrt{\overline{\lambda}_P/\underline{\lambda}_P}$ and $m=\varepsilon/2$.

As already stated before (*Remark 4-1*), we consider the estimation of the bounds for the convergence of the error in two different cases, based on the matrix $K(\cdot)$ dependence. The first case corresponds to a matrix $K(y(t_k))$, i.e. taking into account only the discrete variable $y(t_k)$ measured at each sampling t_k, and is called Discrete Measurements Observer (DMO). The second corresponds to a matrix $K(\hat{y}(t))$, i.e. the matrix depends on the continuous-time estimated output $\hat{y}(t)$, and is called Continuous Discrete Observer (CDO).

Discrete measurements observer-based design (DMO)

As first result, we are using the system (4.1) and the observer (4.2) with $K(\cdot)$ depending on measured variables, i.e. $K\left(y\left(t_k\right)\right)$. Considering *Assumption 4-1*, the following theorem can be stated.

Theorem 4-1: Consider the system (4.1) and the observer (4.2). Under *Assumption 4-1*, it exists a matrix $K\left(y\left(t_k\right)\right)$ such that the convergence of the dynamical system (4.5) is exponentially guaranteed whatever the initial conditions are; the convergence of the observer error $e\left(t,t_k\right)$ is guaranteed with a bounded error defined as:

$$\left\|e\left(t,t_k\right)\right\| \le \beta e^{-m\left(t-t_k\right)}\left\|e\left(t_k\right)\right\| + \frac{\beta}{m}\left\|K\left(y\left(t_k\right)\right)\right\| M_y\left(1-e^{-m\left(t-t_k\right)}\right) \tag{4.11}$$

where β and m are positive constant values, and $M_y = \max\left(\left\|y_{\min} - y\left(t_k\right)\right\|, \left\|y_{\max} - y\left(t_k\right)\right\|\right)$.

Proof: Considering the error dynamic (4.3) with $K(\cdot) = K\left(y\left(t_k\right)\right)$:

$$\dot{e}\left(t,t_k\right) = \left(A\left(\hat{y}\right) - K\left(y\left(t_k\right)\right)C\right)e(t) + K\left(y\left(t_k\right)\right)\left(y(t) - y\left(t_k\right)\right) \tag{4.12}$$

From *Assumption 4-1*, the homogeneous system (4.12) is exponentially convergent and condition (4.7) holds with 2 constants $\beta > 0$ and $m > 0$. Introducing the second term $K\left(y\left(t_k\right)\right)\left(y(t) - y\left(t_k\right)\right)$, $t \in \left[t_k, t_{k+1}\right)$, the solution of (4.12) writes:

$$e\left(t,t_k\right) = \phi\left(t,t_k\right)e\left(t_k\right) + \phi\left(t,t_k\right)\int_{t_k}^{t}\phi\left(t_k,s\right)K\left(y\left(t_k\right)\right)\left(y(t) - y\left(t_k\right)\right)ds \tag{4.13}$$

with $\phi\left(t,t_k\right)\phi\left(t_k,s\right) = \phi\left(t,s\right)$, after passing at norms expression (4.13) and using (4.7), the following bound can be obtained:

$$\left\|e\left(t,t_k\right)\right\| \le \beta e^{-m\left(t-t_k\right)}\left\|e\left(t_k\right)\right\| + \beta e^{-mt}\int_{t_k}^{t} e^{ms}\left\|K\left(y\left(t_k\right)\right)\right\|\left\|y(s) - y\left(t_k\right)\right\| ds \tag{4.14}$$

According to the fact that $y(s) \in \left[y_{\min}, y_{\max}\right]$, thus $y_{\min} - y\left(t_k\right) \le y(s) - y\left(t_k\right) \le y_{\max} - y\left(t_k\right)$ it is easy to see that:

$$\left\| y(s) - y(t_k) \right\| \le \max\left(\left\| y_{\min} - y(t_k) \right\|, \left\| y_{\max} - y(t_k) \right\| \right), \tag{4.15}$$

That corresponds to the definition of M_y. Therefore, the expression (4.14) becomes:

$$\left\| e(t,t_k) \right\| \le \beta e^{-m(t-t_k)} \left\| e(t_k) \right\| + \beta \left\| K\left(y(t_k) \right) \right\| M_y \int_{t_k}^{t} e^{m(s-t)} ds$$

Or equivalently:

$$\left\| e(t,t_k) \right\| \le \beta e^{-m(t-t_k)} \left\| e(t_k) \right\| + \frac{\beta}{m} \left\| K\left(y(t_k) \right) \right\| M_y \left(1 - e^{-m(t-t_k)} \right) \tag{4.16}$$

Which concludes the proof. □

Remark 4-2: The DMO design problem is a tradeoff between the quality of the solution in terms of convergence speed, parameters β and m, and guaranteeing the largest possible time interval τ_M, i.e. minimizing $K\left(y(t_k) \right)$. The way to take into account this tradeoff will be discussed latter on.

Remark 4-3: As stated previously, the error bound in (4.11) can also be used:

- To estimate the bound on $\left\| e(t,t_k) \right\|$ at a time $t > t_k$, and for some value of M_y which can help the practitioner to know the worst case performance if some measurements are missing (corrupted or delayed).
- To determine the latest possible instant to request measurement updates for the observer, i.e. the time $\tau_M = t_{k+1} - t_k$ that will avoid the bound $\left\| e(t,t_k) \right\|$ to grow beyond a defined maximum value, in the case of limited bandwidth or energy saving strategy for the sensor (on-demand measurements).

Remark 4-4: Approximation of M_y in (4.15) corresponds to the worst case, without extended knowledge of the system, like its set-points, state and inputs range, etc. Of course, refinements on this bound are encouraged when possible and can be made if extra information are available. For example, in the case of the train application, in some operation mode (braking phase) the output will decrease at least with a known given rate $\xi > 0$. In this case, obviously, we can refine M_y using:

$$y(t) - y(t_k) \leq -\xi(t - t_k), \; t \geq t_k \tag{4.17}$$

From which:

$$\int_{t_k}^{t} e^{ms} \left\| y(s) - y(t_k) \right\| ds \leq \xi \int_{t_k}^{t} e^{ms} (s - t_k) ds \,. \tag{4.18}$$

Therefore, considering that $e^{-mt} \int_{t_k}^{t} e^{ms} (s - t_k) ds = \frac{1}{m}\left(t - t_k - \frac{1}{m}\left(1 - e^{-m(t-t_k)}\right)\right)$, the bound (4.11) can be replaced with:

$$\left\| e(t, t_k) \right\| \leq \beta e^{-m(t-t_k)} \left\| e(t_k) \right\| + \frac{\beta\xi}{m} \left\| K\left(y(t_k) \right) \right\| \left(t - t_k - \frac{\left(1 - e^{-m(t-t_k)}\right)}{m} \right). \tag{4.19}$$

Continuous-Discrete Observer (CDO)

In this case, the observation matrix $K\left(\hat{y}(t)\right)$ depends on the observer output estimation $\hat{y}(t)$. The following lemma corresponds to one of the Gronwall-like type inequality (it is a modified version of theorem 7 in (Dragomir 2003)), and it will be used to derive the bound.

Lemma 4-1: consider a continuous signal $x(t)$ defined on $[t_k, t]$ that satisfies:

$$\left| x(t) \right| \leq \beta e^{-m(t-t_k)} \left| x(t_k) \right| + \int_{t_k}^{t} e^{-m(t-s)} \left(a \left| x(s) \right| + b \right) ds \,, \tag{4.20}$$

where a, b and m are positive constants. Then the following inequality holds

$$\left| x(t) \right| \leq \beta e^{-(m-a)(t-t_k)} \left| x(t_k) \right| + \frac{b}{m-a}\left(1 - e^{-(m-a)(t-t_k)}\right). \tag{4.21}$$

Proof: The proof follows the classical Gronwall-like theorems. From (4.20) consider the quantity

$$\psi(t) = e^{-mt} \int_{t_k}^{t} e^{ms} \left(a \left| x(s) \right| + b \right) ds \tag{4.22}$$

Note that $\psi(t_k) = 0$. Derivative of (4.22) writes

$$\dot{\psi}(t) = -m\psi(t) + a \left| x(t) \right| + b \tag{4.23}$$

Using the inequality (4.20) gives

$$\dot{\psi}(t)+(m-a)\psi(t)\le a\beta e^{-m(t-t_k)}\left|x(t_k)\right|+b \tag{4.24}$$

Multiplying by $e^{(m-a)(t-t_k)}>0$ (4.24) is equivalent to:

$$\frac{d}{dt}\left[\psi(t)e^{(m-a)(t-t_k)}\right]\le a\beta e^{-a(t-t_k)}\left|x(t_k)\right|+be^{(m-a)(t-t_k)} \tag{4.25}$$

Now, integrating (4.25) on $\left[t_k,t\right]$ with $\psi(t_k)=0$ results in

$$\psi(t)e^{(m-a)(t-t_k)}\le\frac{b}{m-a}\left(e^{(m-a)(t-t_k)}-1\right)+\beta\left|x(t_k)\right|\left(1-e^{-a(t-t_k)}\right) \tag{4.26}$$

We obtain then

$$\psi(t)\le\frac{b}{m-a}\left(1-e^{-(m-a)(t-t_k)}\right)+\beta\left|x(t_k)\right|e^{-m(t-t_k)}\left(e^{a(t-t_k)}-1\right) \tag{4.27}$$

Now, considering that $\left|x(t)\right|\le\beta e^{-m(t-t_k)}\left|x(t_k)\right|+\psi(t)$ and replacing in (4.27) results in

$$\left|x(t)\right|\le\beta\left|x(t_k)\right|e^{-(m-a)(t-t_k)}+\frac{b}{m-a}\left(1-e^{-(m-a)(t-t_k)}\right) \tag{4.28}$$

That corresponds to (4.21) and ends the proof. □

The following theorem gives a bound for the CDO case using *Lemma 4-1*.

Theorem 4-2: Consider the system (4.1) and the observer (4.2). Under *Assumption 4-1*, it exists a matrix $K\left(\hat{y}(t)\right)$ such that the convergence of the dynamical system (4.5) is exponentially guaranteed whatever the initial conditions are. The convergence of the observer error $e(t,t_k)$ is guaranteed for a sampling time τ_M, with a bounded error defined as:

$$\left\|e(t,t_k)\right\|\le\beta e^{-m(t-t_k)}\left\|e(t_k)\right\|+\frac{\beta\lambda_{\hat{y}}M_{\hat{y}}}{m-\beta\lambda_{\hat{y}}\left\|C\right\|}\left(1-e^{-\left(m-\beta\lambda_{\hat{y}}\left\|C\right\|\right)(t-t_k)}\right) \tag{4.29}$$

where β and m are positive constant values, $M_{\hat{y}}=\max\left(\left\|\hat{y}_{\min}-y(t_k)\right\|,\left\|\hat{y}_{\max}-y(t_k)\right\|\right)$, and $\lambda_{\hat{y}}=\max\left(\left\|K\left(\hat{y}(t)\right)\right\|\right)$ for $t>t_k$.

Proof: Consider the expression:

$$e(t,t_k)=\phi(t,t_k)e(t_k)+\int_{t_k}^{t}\phi(t,s)K\left(\hat{y}(s)\right)\left(y(s)-y(t_k)\right)ds \tag{4.30}$$

Passing (4.30) at norms and using (4.7), an upper bound for (4.30) can be expressed as

$$\left\|e(t,t_k)\right\|\le\beta e^{-m(t-t_k)}\left\|e(t_k)\right\|+\beta\int_{t_k}^{t}e^{-m(t-s)}\left\|K\left(\hat{y}(s)\right)\left(y(s)-y(t_k)\right)\right\|ds \tag{4.31}$$

In order to use *Lemma 4-1*, the equation (4.31) is rewritten according to (4.20). First, consider that

$$\begin{aligned}y(s)-y(t_k)&=y(s)-\hat{y}(s)+\hat{y}(s)-y(t_k)\\&=Ce(s)+\hat{y}(s)-y(t_k)\end{aligned} \tag{4.32}$$

From where:

$$K\left(\hat{y}(s)\right)\left(y(s)-y(t_k)\right)=K\left(\hat{y}(s)\right)Ce(s)+K\left(\hat{y}(s)\right)\left(\hat{y}(s)-y(t_k)\right) \tag{4.33}$$

Therefore, passing at norms

$$\left\|K\left(\hat{y}(s)\right)\left(y(s)-y(t_k)\right)\right\|\le\left\|K\left(\hat{y}(s)\right)C\right\|\left\|e(s)\right\|+\left\|K\left(\hat{y}(s)\right)\right\|\left\|\hat{y}(s)-y(t_k)\right\| \tag{4.34}$$

According to the fact that $\hat{y}(s)\in\left[\hat{y}_{\min},\hat{y}_{\max}\right]$, thus $\hat{y}_{\min}-y(t_k)\le\hat{y}(s)-y(t_k)\le\hat{y}_{\max}-y(t_k)$, resulting in

$$\left\|\hat{y}(s)-y(t_k)\right\|\le\max\left(\left\|\hat{y}_{\min}-y(t_k)\right\|,\left\|\hat{y}_{\max}-y(t_k)\right\|\right) \tag{4.35}$$

which corresponds to the definition of $M_{\hat{y}}$, *Theorem 4-2*. In the same way, consider now that $\left\|K\left(\hat{y}(s)\right)\right\|\le\lambda_{\hat{y}}$, thus

$$\left\|K\left(\hat{y}(s)\right)\left(y(s)-y(t_k)\right)\right\|\le\lambda_{\hat{y}}\left(\left\|C\right\|\left\|e(s)\right\|+M_{\hat{y}}\right). \tag{4.36}$$

and,

$$\left\|e(t,t_k)\right\|\le\beta e^{-m(t-t_k)}\left\|e(t_k)\right\|+\lambda_{\hat{y}}\beta\int_{t_k}^{t}e^{-m(t-s)}\left(\left\|C\right\|\left\|e(s)\right\|+M_{\hat{y}}\right)ds \tag{4.37}$$

(4.37) is now in the form of (4.20), with $a=\beta\lambda_{\hat{y}}\left\|C\right\|$ and $b=\beta\lambda_{\hat{y}}M_{\hat{y}}$. Thus, from *Lemma 4-1*, an upper bound is obtained

$$\left\|e(t,t_k)\right\|\le\beta e^{-m(t-t_k)}\left\|e(t_k)\right\|+\frac{\beta\lambda_{\hat{y}}M_{\hat{y}}}{m-\beta\lambda_{\hat{y}}\left\|C\right\|}\left(1-e^{-\left(m-\beta\lambda_{\hat{y}}\left\|C\right\|\right)(t-t_k)}\right) \tag{4.38}$$

That concludes the proof. □

Remark 4-5: The idea of obtaining a form such as (4.20) through the bound (4.32) seems interesting. Nevertheless, we will see thereinafter that it can overestimate the bound. It is mainly due to the fact that the compromise between ε (convergence rate) and the conditioning of matrix P (via the parameter β), while limiting $\lambda_{\hat{y}}$, i.e. the norm $\left\|K\left(\hat{y}(s)\right)\right\|$, ends with ill-conditioned problems; see the *Proposition 4-1* and the examples in section 4.3.4. A way to correct this overestimation is to follow the work of (Mondher Farza, M'Saad, and Busawon 2015; Fall 2015b), using the so-called impulse continuous-discrete observer. It would resume in replacing $K\left(\hat{y}(s)\right)$ in the observer by $K\left(\hat{y}(s)\right)e^{-\eta(t-t_k)}$. It necessitates a new like-Gronwall lemma and new developments that are out of the scope of this work.

Remark 4-6: Following *Remark 4-4*, if some extra knowledge is available, a different bound can be obtained. Again, if the train is in a braking phase, we can consider (4.17): $y(t)-y(t_k)\leq -\xi(t-t_k)$ and obtain through the same procedure via (4.31) the inequality

$$\left\|e(t,t_k)\right\| \leq \beta e^{-m(t-t_k)}\left\|e(t_k)\right\| + \beta\xi\int_{t_k}^{t} e^{-m(t-s)}\left\|K\left(\hat{y}(s)\right)\right\|(t-t_k)\,ds\,. \tag{4.39}$$

Considering $\left\|K\left(\hat{y}(s)\right)\right\| \leq \lambda_{\hat{y}}$ a similar result to (4.19) is derived

$$\left\|e(t,t_k)\right\| \leq \beta e^{-m(t-t_k)}\left\|e(t_k)\right\| + \frac{\beta\xi\lambda_{\hat{y}}}{m}\left(t-t_k-\frac{\left(1-e^{-m(t-t_k)}\right)}{m}\right). \tag{4.40}$$

Performance design

As stated *Remark 4-2*, the goal is to find the largest possible interval τ_M together with guaranteed performances for the estimation error. The goal of this section is to propose a Linear Matrix Inequality (LMI) constraint problem writing. To introduce the decay rate in the conditions, for example in the linear case (4.6), we need to add the part εP, $\varepsilon > 0$ in the derivative of the quadratic Lyapunov function.

Next proposition summarizes a procedure to help to determine the parameters via a LMI performance constraints design. Only the second case (CDO) is presented, since the first one (DMO) can be deduced directly: it corresponds to a choice of a linear gain M (instead of $M(\hat{y})$) in the conditions.

Proposition 4-1: Consider the system (4.1) and the observer (4.2) under *Assumption 4-1* and a quadratic Lyapunov function. The convergence of the observer is guaranteed for a sampling time τ_M, under the smallest bound (4.11), with $\beta = \sqrt{\bar{\lambda}_P / \underline{\lambda}_P}$ and $m = \varepsilon/2$, if there exists matrices $P > 0$, $M(\hat{y})$ and scalars $\lambda_1 > 0$, $\lambda_2 > 0$ such that the following LMI constraints problem is verified, for given scalars $\alpha > 0$ and $\varepsilon > 0$:

Minimize $\lambda_2 - \lambda_1$ such that:

$$PA(\hat{y}) - M(\hat{y})C + A(\hat{y})^T P - C^T M(\hat{y})^T + \varepsilon P \le 0, \tag{4.41}$$

$$\begin{bmatrix} P & M(\hat{y})^T \\ M(\hat{y}) & \alpha I \end{bmatrix} > 0 \tag{4.42}$$

$$\lambda_2 I_n - P \ge 0 \tag{4.43}$$

$$P - \lambda_1 I_n \ge 0 \tag{4.44}$$

$$\lambda_2 - \lambda_1 \ge 0 \tag{4.45}$$

Proof: Inequality (4.41) is related to the convergence rate with a quadratic Lyapunov function and can be represented in various forms as a LMI constraint problem. The more direct being to consider a polytope on the vertices of $\hat{y}$, giving a set of finite LMI constraints (Boyd et al. 1994). The bigger $\varepsilon > 0$, the faster the convergence is. In opposition, the faster the convergence the bigger is $K(\cdot)$. Thus we need a compromise to limit $\|K(\cdot)\|$: considering $\alpha > 0$ such that $K(\cdot)^T P K(\cdot) \le \alpha I$ is one possibility, which is equivalent to $\left(P^{-1} M(\hat{y})\right)^T P \left(P^{-1} M(\hat{y})\right) \le \alpha I$ and to the use of Schur's complement to (4.42). The smallest α will lead to the smallest norm $\|K(\cdot)\|$, if P is well conditioned. Thus, the conditioning of matrix P has also to be taken into account, especially by restricting the parameter β. To reduce the magnitude of β, consider:

$\lambda_2 > \lambda_1 > 0$ and $\lambda_2 I_n \geq P \geq \lambda_1 I_n \geq 0$, corresponding to inequalities (4.43) and (4.44), thus minimizing the difference $\lambda_2 - \lambda_1$, which will act directly on the conditioning of matrix P. □

Thus, tuning the scalars $\alpha > 0$ and $\varepsilon > 0$ allows to set a procedure to obtain the "best" result for τ_M according to the problem.

4.3.3. Particular case of the train $\left(A(y) - A(\hat{y})\right)x(t)$

Recall that in (4.3) not only appears the extra term $K(\cdot)\left(Cx(t) - y(t_k)\right)$, but also the term: $\Delta = \left(A(y) - A(\hat{y})\right)x(t)$. This last term will be considered only for the case of the train; the general case is out of the scope of this work. It follows the idea proposed in (Blandeau et al. 2018b). Considering that: $A(y) = \begin{bmatrix} -w_1 + w_2 y & -1 & 0 \\ 0 & 0 & 1 \\ 0 & 0 & 0 \end{bmatrix}$, it is direct to see that Δ will consist in only one entry at position $(1,1)$, that writes: $\Delta = w_2 \begin{bmatrix} (y - \hat{y})\, y(t) \\ 0 \\ 0 \end{bmatrix} = w_2 \begin{bmatrix} y(t)\, e_1(t) \\ 0 \\ 0 \end{bmatrix}$. Therefore, it follows that:

$$A(\hat{y})e(t) + \Delta = \bar{A}(y, \hat{y}) = \begin{bmatrix} -w_1 + w_2 (y + \hat{y}) & -1 & 0 \\ 0 & 0 & 1 \\ 0 & 0 & 0 \end{bmatrix}. \tag{4.46}$$

Therefore (4.3), in the specific case of the train, is equivalent to

$$\dot{e}(t, t_k) = \left(\bar{A}(y, \hat{y}) - K(\cdot)C\right)e(t) + K(\cdot)\left(Cx(t) - y(t_k)\right). \tag{4.47}$$

Thus, all presented results hold by replacing $A(\hat{y})$ with $\bar{A}(y, \hat{y})$.

4.3.4. Simulations

The effectiveness of the proposed method is shown with the practical case of a locomotive robust position estimation, to be used at the ATC subsystems level, specifically for Automatic

Train Stop Control subsystem, which is a kind of autopilot for train station accurate parking. The complete description of the train has been presented in section 2.1; we recall therein that high level subsystems receive speed measurements at a lower rate than the effective acquisition rate, due to bandwidth allocation restrictions.

Therefore, consider again the dynamic of the train:

$$\dot{v}(t) = b_T\left(v(t)\right)u_T(t) - b_B\left(v(t)\right)u_B(t) - w\left(v(t)\right) + \eta(t) \tag{4.48}$$

where $v(t)$ is the velocity of the train *(m/s)*, $b_B\left(v(t)\right)$ is the coefficient of the braking force, $u_B(t)$ is the relative braking force, $b_T\left(v(t)\right)$ is the coefficient of the traction force, $u_T(t)$ is the relative traction force, $w\left(v(t)\right)$ is the resistance to motion and $\eta(t)$ represents the noise and the errors in modelling and control reconstruction.

We consider hereafter specifically the braking phase, during train final stage of coasting the station. If the ATSC receives corrupted sensor data, or misses measurement updates (because of discarded samples for example), then the train might stop before or after the targeted parking position, creating safety issues, and this situation should be avoided.

To begin with, several ***assumptions*** due to the real-time operating mode are to be carefully taken into account:

A1. As we consider the braking phase, the maximum traction and relative traction forces are null.

A2. The braking force coefficient $b_B\left(v(t)\right)$ is considered constant. It is not a strong assumption as we neither have the breaking force measurement $u_B(t)$.

A3. The relative braking force has a discrete nature and is partially unknown

$$u(t_k) = u_T + \Delta u \tag{4.49}$$

where u_T is piecewise constant and Δu is the unknown control part to be estimated.

A4. In (4.48), we consider the resistance to motion as a second order approximation of the dynamic friction $w\left(v\left(t\right)\right)=w_0+w_1v\left(t\right)+w_2v^2\left(t\right)$, where w_0, w_1 and w_2 are coefficients that vary depending on the type of the train and the condition of the tracks (shape, wetness, etc.). Recall that w_0 and w_1 are related to mechanical friction (impactful at low speed) and w_2 is related to aerodynamic resistance (impactful at high speed).

To deal with the robust estimation problem, an unknown input observer (PI-form) is designed to reconstruct a part of the dynamic friction $d\left(v\left(t\right)\right)=w_0+w_2v^2\left(t\right)+\Delta u$ and other possible uncertainties. The PI-form is a second order integrator:

$$\ddot{d}\left(t\right)\approx 0 \Leftrightarrow \begin{bmatrix}\dot{d}\left(t\right)\\ \ddot{d}\left(t\right)\end{bmatrix}=\begin{bmatrix}0 & 1\\ 0 & 0\end{bmatrix}\begin{bmatrix}d\left(t\right)\\ \dot{d}\left(t\right)\end{bmatrix}.$$

Now, (4.48) can be written in the form of (4.1) with an extended vector $x\left(t\right)=\begin{bmatrix}x_1\left(t\right) & x_2\left(t\right) & x_3\left(t\right)\end{bmatrix}^T$, where $x_1\left(t\right)=v\left(t\right)$, $x_2\left(t\right)=d\left(t\right)$, and $x_3\left(t\right)=\dot{d}\left(t\right)$. The matrices are:

$$A=\begin{bmatrix}-w_1 & -1 & 0\\ 0 & 0 & 1\\ 0 & 0 & 0\end{bmatrix},\ B=\begin{bmatrix}b_B\\ 0\\ 0\end{bmatrix}, \text{ and } C=\begin{bmatrix}1 & 0 & 0\end{bmatrix}.$$

For simulations we set the control input bounds to $u\left(t_k\right)\in\left[0,-1.7\right]$, the parameters of the train model: $w_0=0.0852$, $w_1=0.04$, $w_2=-5\times10^{-5}$ and $b_B=1$ (for simplicity).

Under LMI constraints of *Proposition 4-1*, a good compromise was found using $\varepsilon=0.2$ and $\alpha=4$, to obtain $\beta=1.9$, $m=0.1$, and the gain $K\left(\cdot\right)=\begin{bmatrix}2.9+w_1\left(\cdot\right) & -5.5 & -3.5\end{bmatrix}^T$. For simulations, the initial conditions are $v\left(0\right)=14$ for the system and $\hat{x}\left(0\right)=\begin{bmatrix}14.1 & 0 & 0\end{bmatrix}^T$ for the observer. Taking as sampling time $\tau_M=0.2s$ and a maximal possible braking force of $\xi=1.7$ (see *Remark 4-4* and *Remark 4-6*); we obtain an average error bound of

$e_v = \frac{1}{N}\sum_{k=0}^{N}\left\|e\left(\tau_M + t_k, t_k\right)\right\| \le 0.387$ for *Theorem 4-1* and $e_v = \frac{1}{N}\sum_{k=0}^{N}\left\|e\left(\tau_M + t_k, t_k\right)\right\| \le 0.386$ for *Theorem 4-2*. Fig. 4-1 and Fig. 4-2 show the evolution of the error bounds $\left\|e\left(t, t_k\right)\right\|$, $t \in \left[t_k, t_{k+1}\right[$ (red lines) respectively inequalities (4.19) and (4.40). Fig. 4-3 shows the behaviour of the bounds $\frac{1}{N}\sum_{k=0}^{N}\left\|e\left(\tau_M + t_k, t_k\right)\right\|$ varying the sampling time τ_M; we can see that CDO-based bound and DMO-based bound considering *Remark 4-4* and *Remark 4-6* are almost equivalent.

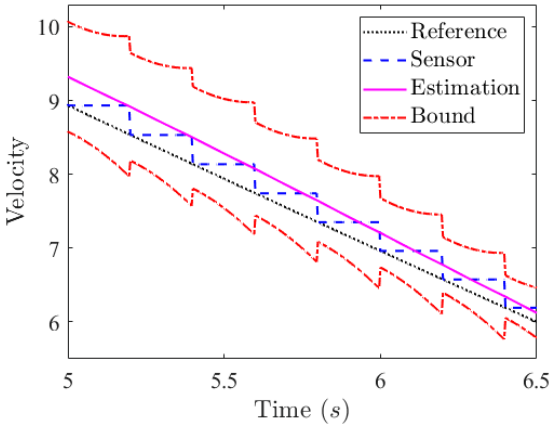

Fig. 4-1 Train speed (zoom) with error bound using DMO ($\tau_M = 0.2$)

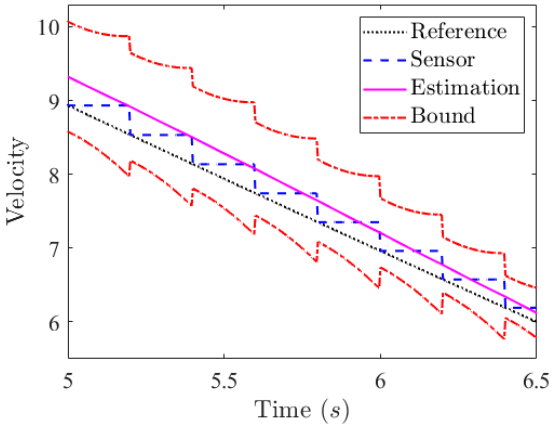

Fig. 4-2 Train speed (zoom) with error bound using CDO ($\tau_M = 0.2$)

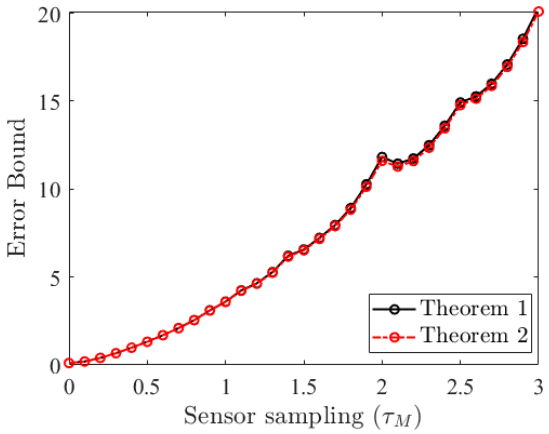

Fig. 4-3 DMO and CDO error bound e_v *for different update times* τ_M

Design trade-offs for the observer

Several tests were performed to study trade-offs between observer performance and favourable error bound. Two parameters are considered, $m \in \{0{,}1 \quad 0{,}5 \quad 1\}$ and $\alpha \in \{1 \quad 4 \quad 10 \quad 100\}$, to design the observer and the bounds, according to *Theorem 4-1* and *Theorem 4-2*. The different errors are computed as: $e_{UI} = \frac{1}{N}\sum_{i=1}^{N} \left| d(t_i) - \hat{d}(t_i) \right| / \left| d(t_i) \right|$ and $e_{est} = \frac{1}{N}\sum_{i=1}^{N} \left| \hat{y}(t_i) - y(t_i) \right| / \left| y(t_i) \right|$.

Of course, for e_{est} we stop the summation when the speed is under $1 m/s$.

Table 4.1 summarizes the results; the empty entries correspond to situations where the LMI algorithm is unable to reach a solution. Two columns appear for e_v, one is the result of the theorems without additional knowledge, the second is the result with the knowledge of the train braking. Due to the exponential nature of the bounds, the first case (e_v without knowledge) is over pessimistic; CDO being worse than DMO. As the structures of both observers are rather similar, the second case (e_v with knowledge) gives similar results. Now, considering the tradeoff between the dynamic of the observer and the upper bound, the best compromise is the pair $(m, \alpha) = (0.5; 100)$.

Table 4.1 DMO and CDO results using various parameter settings.

m	α	β	**DMO**				**CDO**			
			e_v Without *Remark 4-4*	e_v	e_{est}	e_{UI}	e_v without *Remark 4-6*	e_v	e_{est}	e_{UI}
0.1	100	1.91	3.29	0.59	0.05	0.35	1.23	0.59	0.05	0.35
	10	1.9	1.7	0.44	0.04	0.90	0.51	0.44	0.04	0.90
	4	**1.91**	**1.37**	**0.38**	**0.04**	**2**	**0.46**	**0.38**	**0.04**	**2.02**
	1	2.87	1.68	0.91	0.06	2	0.94	0.91	0.06	2
0.5	**100**	**2.80**	**5.32**	**0.86**	**0.05**	**0.27**	**7.61**	**0.86**	**0.05**	**0.28**
	10	3.52	3.24	0.82	0.04	0.6	1.32	0.82	0.04	0.61

	4	-	-	-	-	-	-	-	-	-
	1	-	-	-	-	-	-	-	-	-
1	100	7.1	14.7	2.2	0.05	0.33	2.2×10^{5}	2.2	0.05	0.34
	10	-	-	-	-	-	-	-	-	-
	4	-	-	-	-	-	-	-	-	-
	1	-	-	-	-	-	-	-	-	-

Fig. 4-4 presents the best case $(m,\alpha)=(0.5;100)$ and *Fig. 4-5* for sake of comparison shows $(m,\alpha)=(1;100)$. The red lines represent the bound $\|e(t,t_k)\|$, $t\in[t_k,t_{k+1}[$. We can see that the increase of m introduced an important increase in β resulting in a worse upper bound e_v, *Fig. 4-5*.

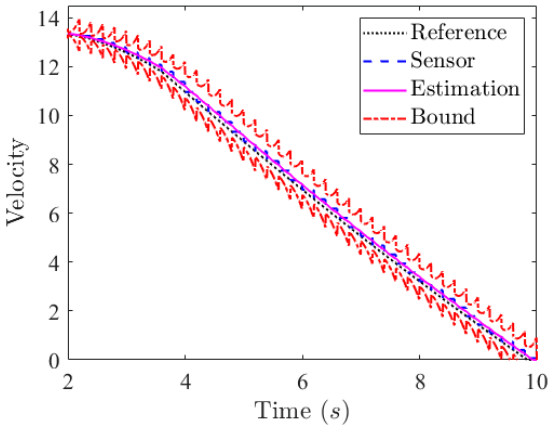

Fig. 4-4 Bound behavior for $(m,\alpha)=(0.5;100)$

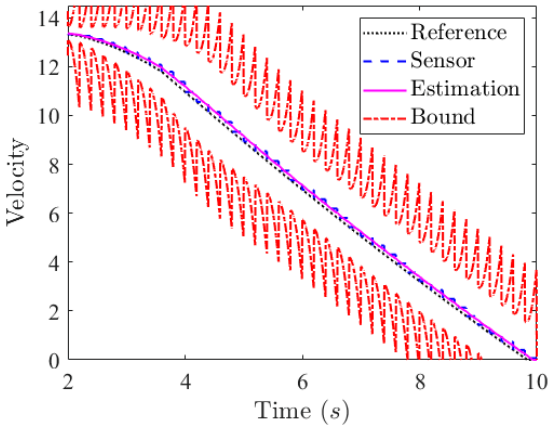

Fig. 4-5 Bound behavior for $(m,\alpha)=(1;100)$

4.3.5. Concluding remarks

An observer design approach for continuous-discrete time systems and the formal expression of the maximal bound of observer error have been investigated in this chapter. Two approaches to determine the bound are developed, based on a discrete measurement observer and a continuous discrete observer, using a special form of Gronwall inequality. A PI-observer design procedure is proposed in LMI form, with a tradeoff between the best guaranteed bound and

observer performance, to track both the state and the unknown input. Illustrations were provided by simulation of realistic scenarios. In the following chapter, the presented approach will be tested using data-sets obtained through experiments on real trains provided by Alstom company.

CHAPTER 5. Data validation

5.1. Introduction

This chapter will focus on the observer design, the results in robust estimation of position and of the upper bound of error estimation. Control issues are not concerned because we do not have possibility to test it in a real time framework. Nevertheless, we had access to sensor data acquired during multiple experimental runs performed by ALSTOM Transport, using different kind of brakes to stop, electrical and pneumatic. Moreover, the tests also included different speeds and wheel-track adherence conditions thus generating different fault frequencies and durations. Therefore, the validation can cover an interesting set of situations.

A sensor fault-based representation of the problem will be used together with a q-LPV UI-Observer presented in the previous chapters to design a fault detection strategy. We also formulate the problem of finding the best threshold for the collected data. Based on the γ and λ constants obtained through the mixed H_∞/H_- optimization procedure, we reconstruct the amplitudes of the occurring fault and obtain insights on what type of faults are more susceptible to occur based on different speed profiles, and what is the influence of both type of brakes on the fault occurrence frequency.

Then, we will investigate the behavior of the estimation error bound. Based on *Theorem 4-1*, *Theorem 4-2*, *Remark 4-4* and *Remark 4-6,* bound behavior will be shown for different speed profiles, for fault-free and faulty profiles.

A discussion on the strengths and weaknesses of the proposed solutions concludes the chapter.

5.2. Experimental setup

The data was obtained using a Coradia-type motor coach during tests to investigate the precision of the odometer-based measurement chain and to characterize particular behaviors of interest to determine the best configurations for the ATC system. ALSTOM Transport Company ran

twelve (12) experiments that correspond to combinations of different speed and adherence conditions: nine (9) experiments used electric brakes and three (3) used pneumatic brakes.

The considered speed profiles are:

- **HS**: High Speed profile with the maximum speed allowed, around 45 (*m/s*),
- **AS**: Average Speed profile around 66% of the allowed maximum speed, 30 (*m/s*),
- **LS**: Low Speed profile around 33% of the allowed maximum speed, around 17 (*m/s*).

The different levels of adhesion are defined as:

- **LoA**: Low Adhesion corresponding to rainy conditions (water on the rail).
- **BaA**: Bad Adhesion corresponding to rainy conditions and falling leafs.
- **EBA**: Extremely Bad Adhesion corresponding to the extremal skidding/jamming possible conditions.

The real time adhesion conditions were "artificially" obtained by proper configuration of the train devices and additional equipment that will pour water and soap on the track. The tracks are cleaned after each test.

The motor coach is equipped with the following sensors:

- 2 odometers (positioned on 2 different wheel axels)
- 1 radar (beneath the locomotive, oriented forward)
- 1 accelerometer (in cabin)

The speed is measured in *m/s* and the acceleration in m/s^2. The data is gathered using data-logger devices and CAN transmissions recording. The aggregated measurement data sampling time is 50*ms* (20*Hz*). The radar and accelerometer sensors are used only to give a "true measure" (the ground truth) in order to characterize odometer behavior. These sensors (radar and accelerometer) are not commonly used on commercial rolling stock for reasons that are out of the scope of this thesis. We need to point that, the measurements provided by the additional sensors are not used by TCU (Traction Control Unit), BCU (Braking Control Unit) and WSP (Wheel Sliding Protection) units of the motor coach. However, actions of the TCU, BCU and WSP obviously impact wheel behavior, causing (or masking) some effects of the wheel

jamming/skidding. For example, the WSP unit configuration is different depending on the configurations used for this experimental run: either all-or-nothing or progressive traction control behavior control to avoid skidding. The same applies for the BCU and braking in order to obtain the required jamming conditions for the test.

The tests were made only using the motor coach without additional vehicles, and only one cabin is used and active, the second cabin (for the reverse motion) is not used for the tests. The motor coach uses electric traction and two kind of brakes: †electric brakes and ††pneumatic brakes. Control signals from the TCU unit were not available for the study, thus some assumptions were made prior to the validation. These assumptions are explained thereafter. The procedure for generating these tests are rigorous, and will be omitted therein because of confidentiality issues. The scenario is the following:

Traction (Acceleration) phase: traction control is applied (maximum) until the required speed (HS, AS, or LS) is reached. The acceleration phase will be subject to degraded adhesion and skidding situations.

Maximum speed (Cruising) phase: stabilized maximal speed (for the test) is maintained using appropriate traction or braking actions during a short period (around 1 minute). This phase will benefit of normal adhesion conditions.

Braking (Deceleration) phase: braking control is applied (maximum) until the train completely stops. This phase will be under degraded adhesion conditions, and jamming situations.

The general scheme showing the test sequence is shown in Fig. 5-1.

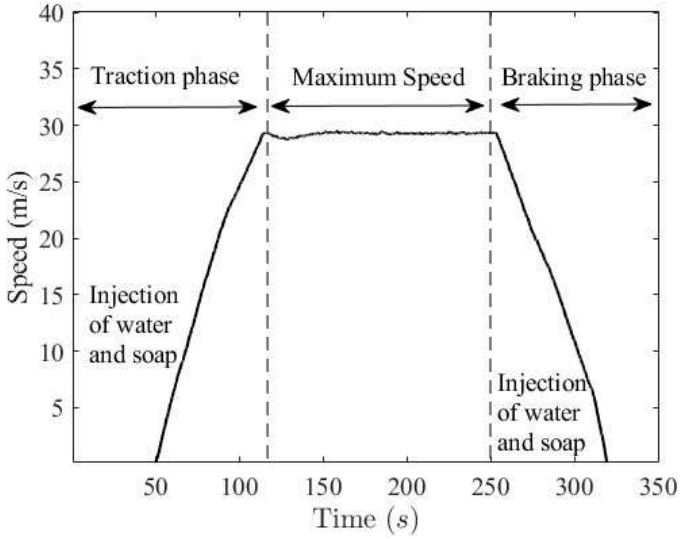

Fig. 5-1 Overview of the three test phases

Since the focus of the thesis is the jamming faults, we will analyze the data only during the braking phase. For illustration, Fig. 5-2 shows a braking sequence for both speed and position, where the ground truth is given by the radar (black line) and the accelerometer (pink line). We can see, left part of Fig. 5-2, that both odometers are heavily impacted by wheel-jamming faults, while the radar-based speed, and accelerometer-based speed, which is obtained by integration of the acceleration, are completely fault-free. The right figure shows position estimates obtained by integration (or double integration) of the sensor measurements. We can see that the impact can be important, with an error that can exceed 100 meters, for a motor coach length of 30m.

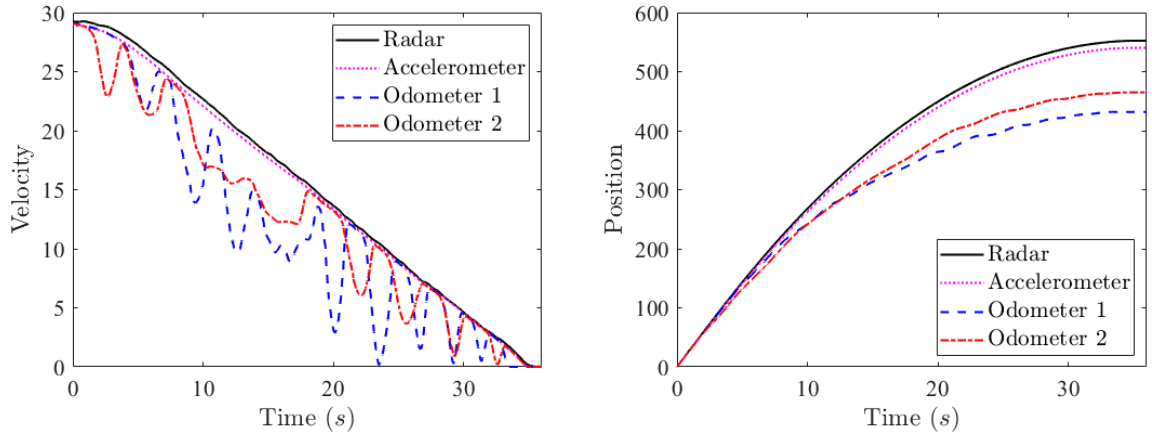

Fig. 5-2 Speed measurement (left) and position calculation (right) from sensors.

Thereafter, we introduce the assumptions made:

Assumption 1 (A1) Friction parameters

First of all, we need to determine the friction parameters w_0, w_1, and w_2 according to each adherence condition (LoA, BaA and EBA) that are unknown usually, and were not available in the data-set. The methods developed in the previous chapters rely on the approximate knowledge of these parameters. We will make the assumption that, an estimation algorithm will estimate the friction parameters w_0^*, w_1^*, and w_2^*, that are approximations of w_0, w_1, and w_2, during traction phase, using appropriate estimation techniques, for example (Hubbard et al. 2013; Onat, Voltr, and Lata 2017). Traction phase data is needed for the preliminary friction parameter estimation, because of the usual "persistence of excitation" assumption necessary for real-time parameter estimation algorithms. Of course, the data used for the estimation need to be filtered from faults. Therefore, to estimate the friction parameters, filtered measurements obtained during the traction phase are used, and acceleration is used as a reference to reconstruct the TCU control output. Considering the mechanical equality (Kaller and Allenbach 1995):

$$F_{in} - F_f = m\dot{v} \tag{5.1}$$

with F_{in} the train internal force (control), F_f the friction force, m the mass of the train (kg), and $\dot{v}$ the acceleration. Then, using the friction approximation relation $F_f = \bar{w}_0 + \bar{w}_1 v + \bar{w}_2 v^2$, where $\bar{w}_i$, $i \in \{0,1,2\}$ stands for the "true" coefficients of friction, we rewrite (5.1) as follows

$$\dot{v} = -\left(w_0 + w_1 v + w_2 v^2\right) + \bar{u} \tag{5.2}$$

where $w_i = \bar{w}_i / m$, $i \in \{0,1,2\}$ and $\bar{u} = F_{in}/m$.

Therefore, the values of w_0^*, w_1^*, and w_2^*, that are approximations of w_0, w_1, and w_2, are estimated from the data-set following the next steps – for a given adherence condition.

Under the assumption that the control $\bar{u}$ should be constant (since the traction is at maximum), then $u_{\max} - \dot{v} = w_0 + w_1 v + w_2 v^2$. This can help us to obtain an approximation of w_0, w_1 and w_2, with the assumption of $\bar{u} = u_{\max}$. The figure (Fig. 5-3) shows the graphic of the acceleration measurements with respect to the reference speed for a LoA adherence condition in 3

conditions: Low Speed (in green), Average Speed (in blue) and High Speed (black). The approximation with the polynomial from equation (5.2) will be made from $v > 5 m/s$ to the maximum speed, on the traction phase (top part of the graphic).

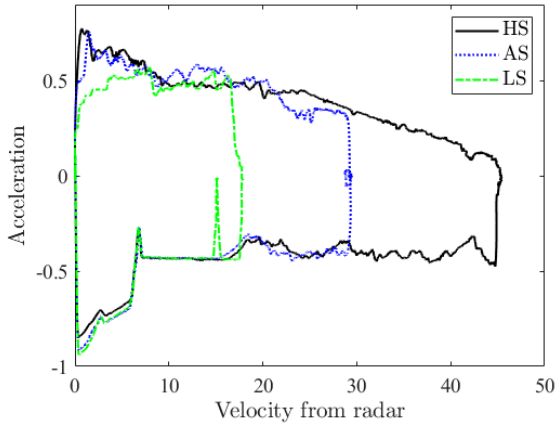

Fig. 5-3 Overview of the acceleration/speed trajectories (LoA).

In this case, we obtain $w_0^* = 0.46$, $w_1^* = 5.7 \times 10^{-3}$ and $w^*_2 = -2.4 \times 10^{-4}$. The final approximation (in red) is shown Fig. *5-4* superposed with the HS profile (left) and with all profiles (right).

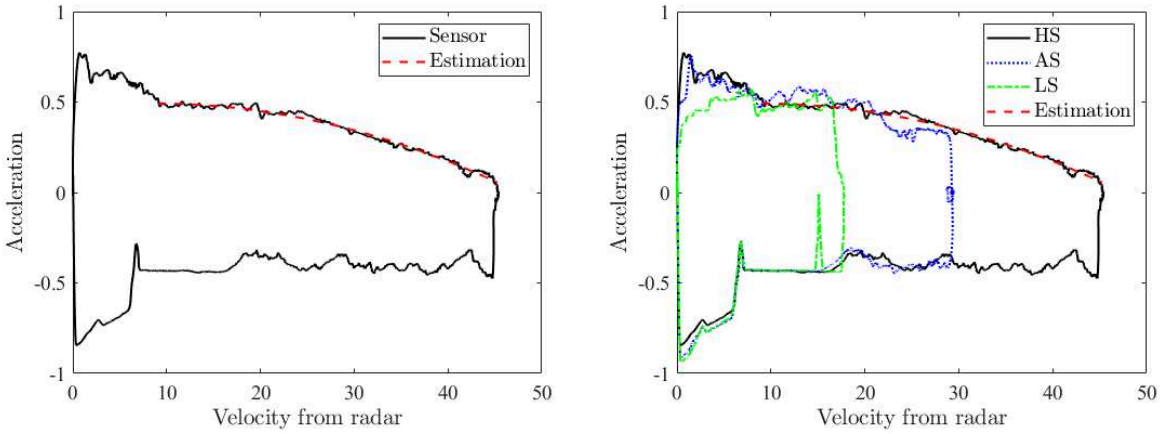

Fig. 5-4 Friction parameter estimation results.

Using this procedure, all friction parameters are estimated for the three adherence situations LoA, BaA and EBA, and results are shown Table 5.1. These estimates are obtained using reference data from radar and acceleration sensors, available in the data-set.

Table 5.1 Friction parameter estimations.

Parameters	LoA	BaA	EBA
w^*_0	0.46	0.35	0.25
w^*_1	5.7×10^{-3}	3×10^{-3}	5×10^{-3}
w^*_2	-2.4×10^{-4}	-1×10^{-4}	-2×10^{-4}

Assumption 2 (A2) Time-to-time position sensors: on-track position beacons

As explained section 2.1.2, time-to-time updates of the accurate train position are obtained via track-based position beacons. The beacon measurement updates are not available in the data-set, nevertheless as the reference sensor data are available, it is easy to construct and simulate "artificial" updates. We could even decide to test what would be an ideal positioning of beacons according to the observer design and bounds framework proposed. Therefore, we construct a set of a predetermined "artificial" beacons' positions $\left(p_B\right)$ from the radar sensor-based position. Thus, at each time an artificial beacon is crossed, the approximate "true" position $\left(p_B\right)$ is used to simulate the time-to-time position update.

Assumption 3 (A3) The TCU control signal

The TCU control signal would be helpful for outperforming the q-LPV UIO PI-observer performances, nevertheless, this information is never available, neither in the data set nor for the ATO in real conditions. Thus, the algorithm to construct the piecewise-constant control approximation $u^*(.)$ proposed in chapter 3, is used again; where $u^*(.)$ is updated at the times when a beacon is crossed or when the system has recovered from a fault. The procedure given from (3.5) to (3.10) will compute $u^*(t_0)$ from any initial position $\left(t_0, p(t_0), v(t_0)\right)$ to reach the final position $\left(t_f, p(t_f), 0\right)$. Since the final position and final time are known from the data set, then the control $u^*(\cdot)$ can be recomputed after a beacon update (and detected fault recovery) using the steps from *Algorithm 3-1*. Using position updates from the beacons and velocity

estimations from the observer, the piecewise-constant control $u^*(.)$ is updated at the time instants $\bar{t}_k$, based on $\left(\bar{t}_k, p_B(\bar{t}_k), \hat{v}(\bar{t}_k)\right)$, where the instants $\bar{t}_k$, $k \in \{1,2,3,...,j\}$ are the instants either when a beacon is crossed or when the system has recovered from a fault.

Now, considering the assumptions A1, A2 and A3, the results issued from the experimental study are presented to validate the methodology proposed in section 3.3, and section 4.3.

5.3. Quasi-LPV UIO-based robust position estimation

5.3.1. Preliminary discussion

In this section, we present the fault detection methodology validation, section 3.3 that improves the position estimation under jamming faults, and consequently reduces the stopping position error. The measurement sampling time of the odometers is 200*ms*, to match real conditions. The time-to-time true position updates are made considering that the beacons are placed on the path with 200 *meters* intervals. At the beacon crossing time $\bar{t}_k$, we update $u^*(\bar{t}_k)$, $k \in \{1,2,3,...,j\}$ based on the correct data.

The two-steps *Algorithm 3-2* based on the resolution of 2 LMI constraints problems based on conditions (3.56), (3.57) and (3.58), is performed, using $\alpha = 0.2$, $F = 1$, $D = \begin{bmatrix} 1 & 0 & 0 \end{bmatrix}^T$, and the friction parameters $w^*_0 = 0.46$, $w^*_1 = 5.7 \times 10^{-3}$, and $w^*_2 = -2.4 \times 10^{-4}$. The results obtained are: for the fault detection, a gain $M = 3.36$, for H_∞ / H_- parameters $\gamma = 2.32$, $\lambda = 0.1$ and the observer gains $L_1 = \begin{bmatrix} 2.41 & -1.34 & -0.22 \end{bmatrix}^T$ and $L_2 = \begin{bmatrix} 2.41 & -1.33 & -0.22 \end{bmatrix}^T$, which actually means that the parameter variation induced by $w^*_1 v$ is not significant. Therefore, for this set of parameters the q-LPV representation will not impact the results.

5.3.2. Determination of the best detection threshold

We split the tests into three groups based on the speed profiles: HS, AS, and LS. The different adherence levels are considered: LoA, BaA, and EBA. Now, we create two tables *Table 5.2* and *Table 5.3* with the fault detection information for each situation, in order to obtain maximum and minimum threshold values, with fault detection performance of *99%* of non-detected faults for the maximum possible threshold and *100%* detected faults with *50%* false alarms for the minimum possible threshold. Obviously, these values are unacceptable, and we must reach a fault detection rate of *100%* with no false alarms.

In this thesis, we will consider the three (3) markers to assess the performance of a fault detection algorithm. These markers are both popular and intuitive (Blanke et al. 2006; Isermann 2006; J. Zhang, Swain, and Nguang 2016), and are detailed below:

- **Fault detection rate (FDR):** It is the number of fault detections that correspond to real faults, divided by the number of total faults. This rate evaluates how close the results are to the objective of 100%.
- **Undetected faults rate (UFR):** Also referred to as non-detection rate, or missed faults rate. It is the number of undetected faults divided by the number of total faults. This rate has to be as close as possible to 0%.
- **False alarms rate (FAR):** Also referred to as bad-detection rate. It is the number of faults detections that do not correspond to real faults divided by the number of total detections. This rate has to be as close as possible to 0%.

When the number of total faults is unknown, the rate is computed based on the number of total detections. This is the usual situation in practice.

When a “real” fault is detected, another parameter that might be important is:

- **The fault detection delay** Δt_{ds}, or the time-delay from real fault occurrence moment until the moment when a “fault detected” decision is made by the fault detection system. The shorter this delay, the best the result is.

If the fault is intermittent, which means that the fault can disappear even if it is left unattended, then another indicator is considered:

- **The end-of-fault detection delay** Δt_{de} , or system recovery delay: it is the delay between the real disappearance of the fault and the moment when the end of detection occurs from the fault detection system. Again, the shorter this delay, the best the result is.

This last indicator is related to fault duration estimation, and can be replaced by the error in fault duration estimation.

Considering fault detection performance, we chose in this thesis to consider the number of faults and fault detections, in order to compute the rates and not the total duration of faulty periods and the total duration of good fault detections.

The last column of the *Table 5.2* and *Table 5.3* corresponding to the threshold ε_f gives the best threshold for each situation, that maximizes fault detection rate, and minimizes false alarms. The exploration of the interval was done iteratively.

Table 5.2. Thresholds for tests with electric brakes

Speed profile	**Adherence level**	**Threshold**		
		min	**Max**	ε_f
HS	**LoA**	0.58	1.12	0.65
	BaA	0.59	1.8	
	EBA	0.55	3.1	
AS	**LoA**	0.61	1.51	0.62
	BaA	0.51	2.3	
	EBA	0.45	13	
LS	**LoA**	0.2	1	0.4
	BaA	0.3	1.8	
	LoA	0.25	2	

Table 5.3. Thresholds for tests with pneumatic brakes

Speed profile	Adherence level	Threshold		
		min	Max	ε_f
HS	**BaA**	1	14	1.5
AS	**BaA**	1.2	18	
LS	**BaA**	1.2	20	

5.3.3. Fault detection performance for each case

Thereafter, the best detection threshold is used for each case. We consider that the threshold depends of the speed range as shown by the results of tables *Table 5.2* and *Table 5.3*. This result is compatible with real time application as in practice, the speed is both measured and estimated. Considering a unique threshold speed independent would be more conservative, it will correspond to the smallest one, and obviously will have worse fault detection rates. The main reason is that its higher sensitivity to noise will increase the rate of false detections FAR, and consequently decrease the rate of good detections FDR.

We consider in the following tables the time delay to detect the start $\left(\Delta t_{ds}\right)$, and the end $\left(\Delta t_{de}\right)$ of the fault on good detections; for the tables thereafter we present the average delay considering the whole deceleration phase. We also consider the false alarms FAR, and missed detections UFR. The FDR is omitted because it can be derived from the UFR value. The last two columns are dedicated to the relative position errors at the final position for both cases:

- without fault detection approach $e_p = \left| p_{ref}(t) - p_{sensor}(t) \right| \left(l_{train}\right)^{-1}$
- with the proposed approach $\hat{e}_p = \left| p_{sensor}(t) - \hat{p}(t) \right| \left(l_{train}\right)^{-1}$.

The relative errors are computed with respect to the coach length, which is fixed for the experiments to $l_{train} = 30m$. What we call final position, is the last position before beacon update, with contrast to stopping position which is the position when we want the train to stop.

5.3.3.1. High speed test case

Table 5.4 presents the results for the three HS tests using a threshold of $\varepsilon_f = 0.65$. It can be seen that all faults are correctly detected on the presented interval (*Fig. 5-5*) and that the position estimate is improved from 1% decrease for the less faulty case, to 8% for the worst case.

Table 5.4. Fault detection in HS with $\varepsilon_f = 0.65$.

Adherence level	**Detection delays (s)**		**Rate of undetected faults**	**Rate of false alarms**	e_p	$\hat{e}_p$
	Δt_{ds}	Δt_{de}				
LoA	0.4	0.17	0	0	0.126	0.113
BaA	0.19	0.41	0	0	0.123	0.106
EBA	0.22	0.3	0	0	0.193	0.115

Fig. 5-5 (a) shows the speed behavior for a situation with the worst adherence conditions EBA, which corresponds to the last line of *Table 5.4*. We can see an important jamming occurrences, varying for 1 to 2 seconds. The speed estimation manages to filter jamming impact on the measurement, using fault detection where the residual is able to detect the fault with a relatively small delays (*Fig. 5-5 (b)*: differences between vertical red – real fault – and blue lines – estimated faults and recovery).

Fig. 5-5 (c) shows the evolution of position estimation error during an interval of interest, i.e. 2 considered beacons. The blue lines correspond to the time-to-time beacon updates. The estimated error (dark blue line) is 3 meters better that the sensor measurement (black line), thus dividing by to the precision.

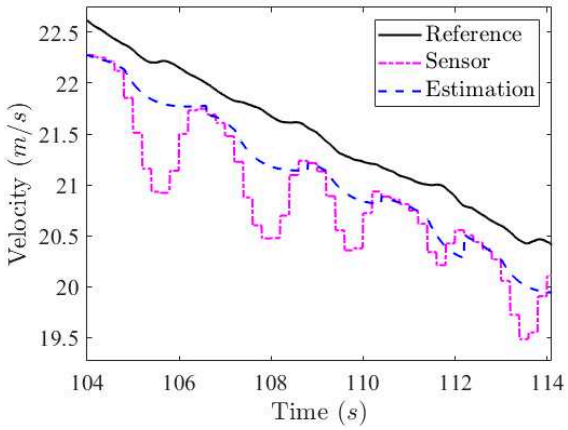

(a) Speed

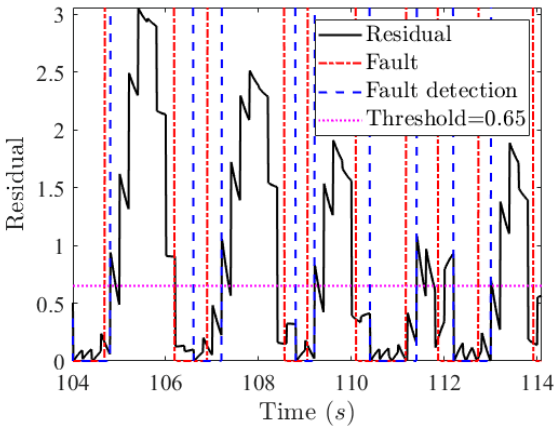

(b) Residual

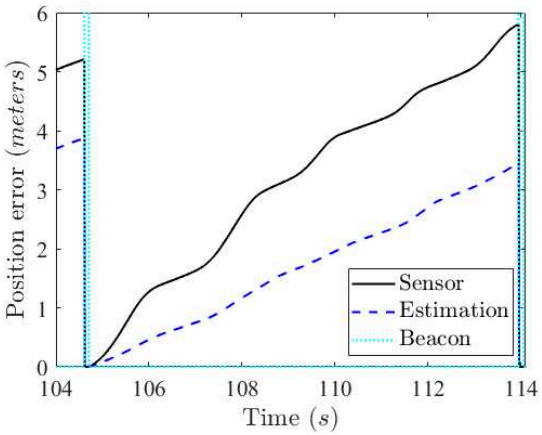

(c) Position error

Fig. 5-5 HS with EBA and $\varepsilon_f = 0.65$

In order to show the importance and the impact of the compromise that ends with the thresholds, next figure *Fig. 5-6* presents the same case conditions as *Fig. 5-5* with a threshold $\varepsilon_f = 1.5$. This value exhibits a sensitivity which is incompatible with the studied case that can end with an estimation worse than the one given by the corrupted sensor.

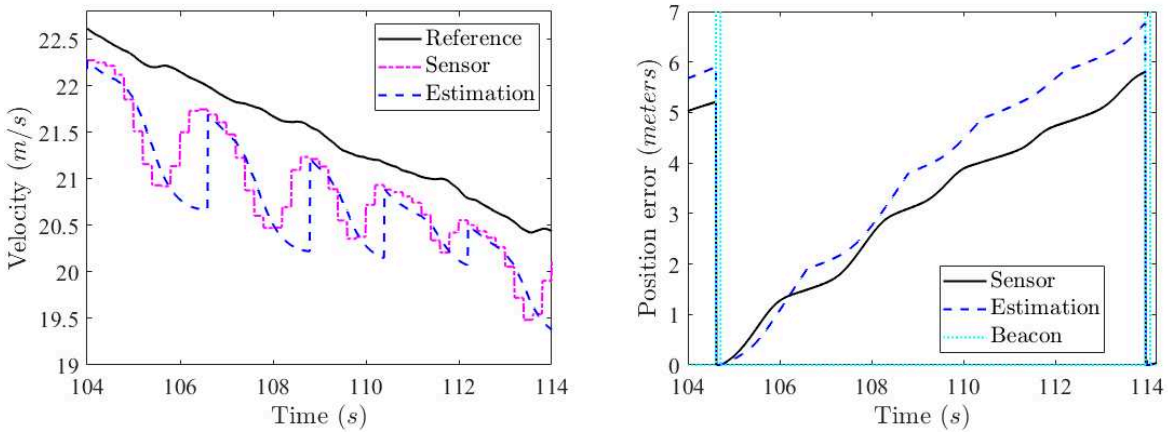

(a) Speed *(b) Position error*

*Fig. 5-6 HS with **EBA** and* $\varepsilon_f = 1.5$.

5.3.3.2. Average speed test case

An interval from the AS-test is studied thereafter and the results are shown *Table 5.5*: We see that the improvement is minor (2-3%) for the first two lines, and around 30% for the last line.

Table 5.5. Fault detection for AS with $\varepsilon_f = 0.62$.

Adherence level	**Detection delays (s)**		**Rate of undetected faults**	**Rate of false alarms**	e_p	$\hat{e}_p$
	Δt_{ds}	Δt_{de}				
LoA	0.1	0.2	0	0	0.14	0.11
BaA	0.56	0.16	0	0	0.16	0.14
EBA	0.2	0.2	0	0	0.58	0.19

Fig. 5-7 (a) shows two phenomena: a jamming in the beginning, and many micro-jammings during the whole period. Micro-jammings are jammings with shorter durations than the data sampling, causing a small decrease in speed measurement with respect to the reference. The same phenomenon was also present for the High Speed test, but was masked by the more important jammings. Micro-jammings can be seen especially *Fig. 5-7 (b)*, where the residual

shows multiple detections, but that will (a part from the first jamming) not correspond accurately to the behaviour of the fault. *Fig. 5-7 (c)* shows the position estimation errors.

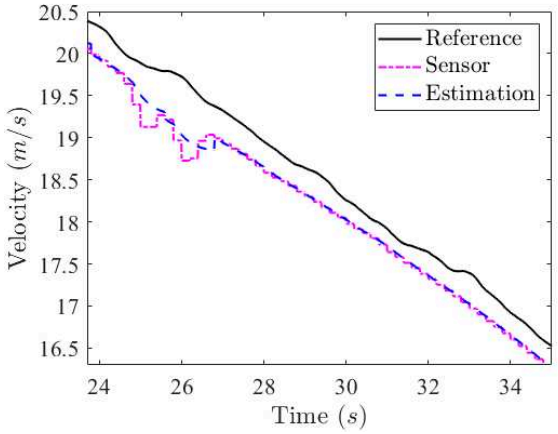

(a) Speed

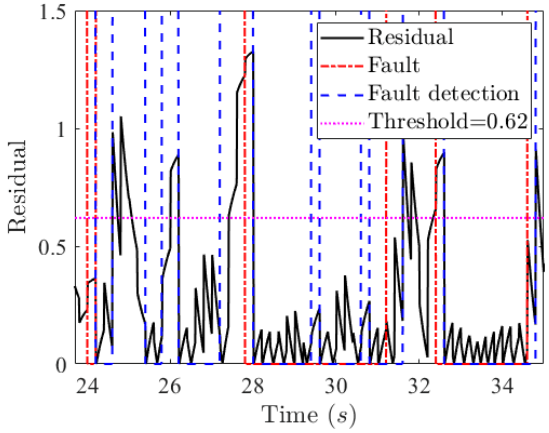

(b) Residual for

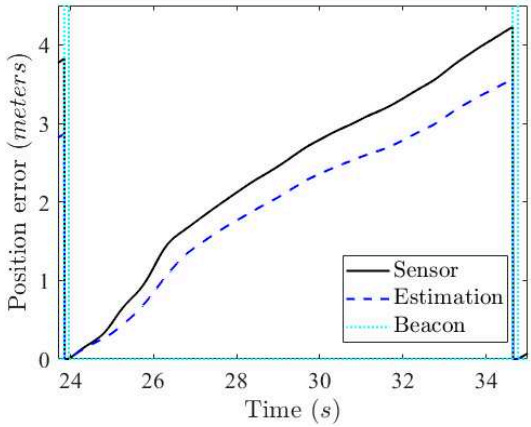

(c) Position error

Fig. 5-7 AS with BaA and $\varepsilon_f = 0.62$.

Changing the threshold will not solve the problem. For example, choosing a lower threshold $\varepsilon_f = 0.34$ will make it sensitive to noise and will trigger false detections, *Fig. 5-8).*

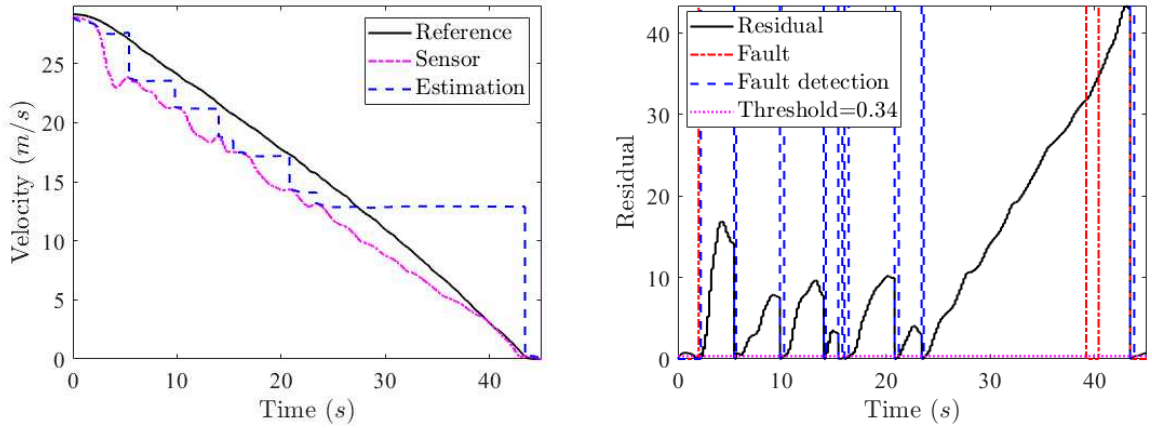

(a) Speed *(b) Residual*

Fig. 5-8 AS with EBA and $\varepsilon_f = 0.34$.

The case presented improves only in a small way the positioning result. In view of the figures, this case can be seen as a slowly varying measurement error (due to the micro-jammings), that cannot be detected by the residual set up for detecting jamming. Therefore, with only one "detectable" jamming amongst a lot of micro-jammings only a small the improvement can be obtained. Choosing a lower threshold wouldn't improve the result, since the residual for this observer was designed without knowledge of the micro-jammings.

5.3.3.3. Low speed test case

For the LS-tests, a lower threshold has to be preferred. From *Table 5.6*, we can see that the improvement in position estimation is around 2-3%.

Table 5.6. Fault detection in LS with $\varepsilon_f = 0.4$.

Adherence level	**Faults detected**		**Rate of undetected faults**	**Rate of false alarms**	e_p	$\hat{e}_p$
	Δt_{ds}	Δt_{de}				
LoA	No fault	No fault	No fault	No fault	0.06	0.03
BaA	0.2	0.2	0	0	0.15	0.13
EBA	0.14	0.2	0	0	0.18	0.13

Fig. 5-9 (a) shows that 7 jammings have occurred. The residual was able to sense them with some delay, *Fig. 5-9 (b)*. The position estimation is shown *Fig. 5-9 (c)*; since the jammings were short, there is nearly no impact on the position estimation error *Fig. 5-9 (c)*.

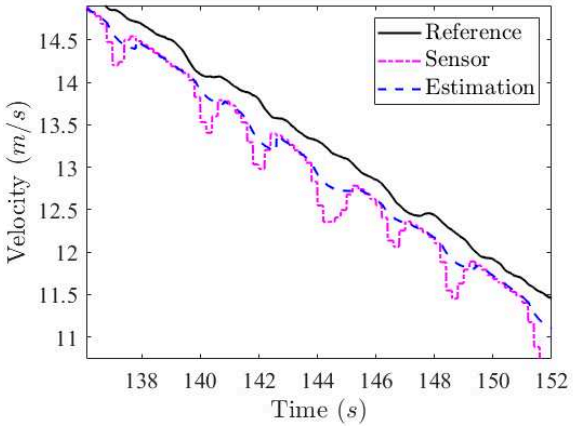

(a) Speed

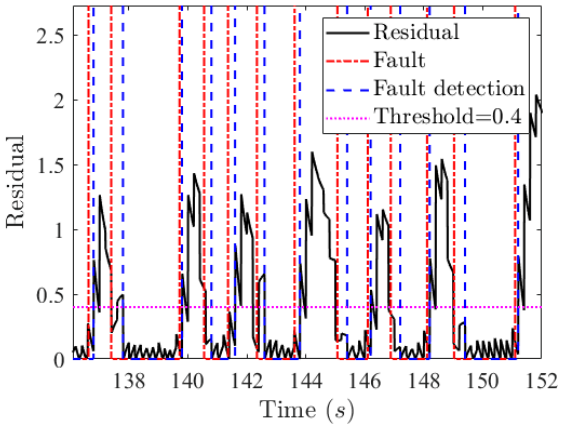

(b) Residual

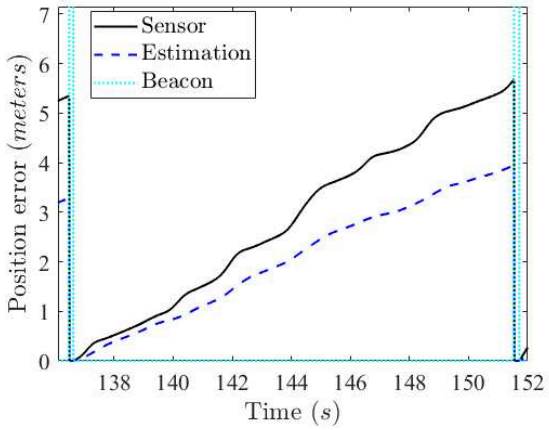

(c) Position error

Fig. 5-9 LS with EBA and $\varepsilon_f = 0.4$

5.3.3.4. Pneumatic brakes case

The last tests discussed here are those related to the use of pneumatic brakes. *Table 5.7* shows, that the LS-test is where fault detection is successful even with one small fault no detected, reducing the position error by nearly 90%.

Table 5.7. Fault detection with $\varepsilon_f = 1.5$ *and pneumatic brake.*

Speed profile	**Fault detected**		**Rate of undetected faults**	**Rate of false alarm**	e_p	$\hat{e}_p$
	Δt_{ds}	Δt_{de}				
HS	0.4	0.2	0	0	0.53	0.35
AS	0.2	0.2	0	0	0.66	0.15
LS	0.2	0.2	0.2	0	0.96	0.13

Fig. 5-10 shows that there are five important jammings that occur during the run, and the rate of success of the observer is able 4 on 5 (*Fig. 5-10 (b)*), thus, filtering their effects from the position estimation (*Fig. 5-10 c)*).

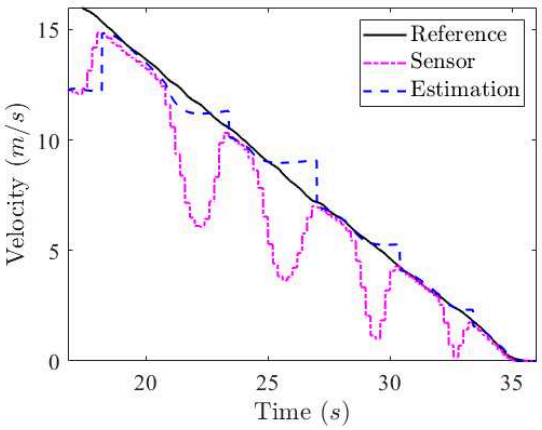

(a) Speed

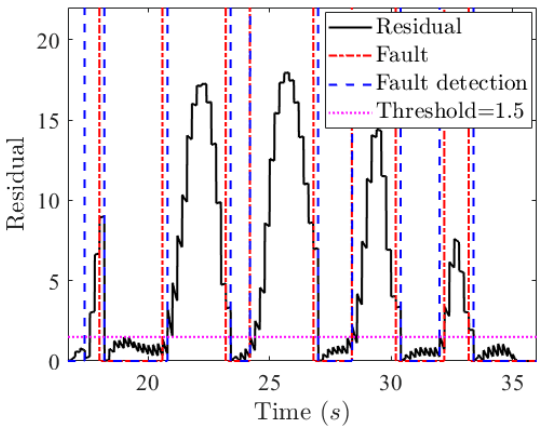

(b) Residual

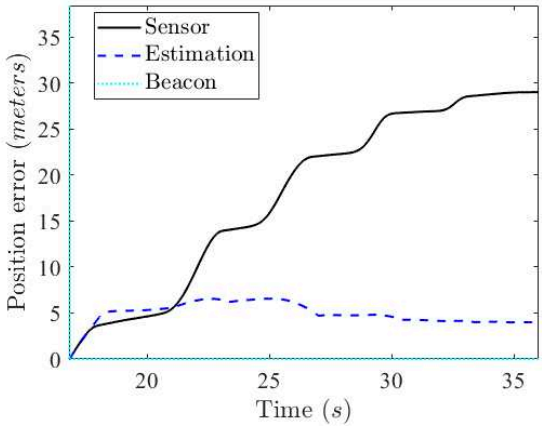

(c)Position error

Fig. 5-10 LS (pneumatic) with $\varepsilon_f = 1.5$

Fig. 5-11 shows a difficult case where two faults are occurring at the same time, and have their effects superposed. We can see in figure (a) that there is a characteristic jamming that is successfully detected and a slowly varying bias in the measured speed, caused probably by micro-jammings, which cannot be detected using this particular observer. The estimated speed is still closer to the reference.

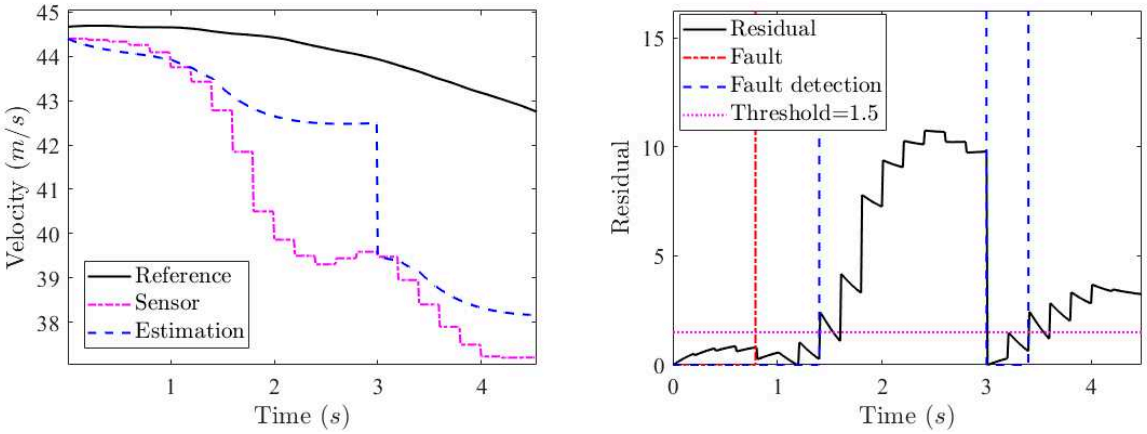

(a) Speed *(b) Residual*

Fig. 5-11 HS (pneumatic) with $\varepsilon_f = 1.5$

5.3.4. Discussion

The previous results show that the observer-based position estimation is at least as good as the measurement-based estimated position. When detectable faults occur, and on successful detection, the observer is able to greatly improve the accuracy of the position estimate.

The proposed approach has also its limits, since it is difficult to obtain a detection threshold that works on all speed ranges and for all configurations. Additionally, since the designs of both the observer and the fault detection are optimized for jamming detection, then the faults that are different will hardly be detected, and if successfully detected will be ill-interpreted. This actually shows that the fault detection is able to isolate jamming faults from other anomalies.

Another remark concerns the correlation between the speed and the jamming faults. It can be seen from the results that some jamming "types" are characteristic for specific speed ranges, which means that the residual should be chosen based on the speed of the train.

At the end we can turn back to the interpretation of the residual considering the H_∞ / H_- parameters $\gamma = 2.32$, and $\lambda = 0.1$. Since, on fault detection the relation $\epsilon_f \leq 2.32 \left\| f(t) \right\|$ is true, it means that the system is able theoretically for a threshold $\epsilon_f = 0.65$ to detect faults such as: $\left\| f(t) \right\| \geq 0.28$ for the specific case of HS range and electric braking. For pneumatic brakes, and $\epsilon_f = 1.5$, the minimum fault "amplitude" that is possible to detect, considering the same parameters, is $\left\| f(t) \right\| \geq \frac{1.5}{2.32} = 0.64$. This remark is consistent with the "poor" performance of the detection in some conditions. Also, if we want to detect jammings that are represented by a specific $f(t)$ value, it will imply a specific threshold or a specific γ to be considered at the design step. The same can be said about λ and the expected noise.

5.4. Continuous-discrete observer error bound estimation

5.4.1. Preliminary discussion

In this section, we will estimate the upper bound of the observation error on the same experimental data set as in the previous section. To achieve this goal, we will use the DMO and CDO observers and the methodology proposed in section 4.3. Therefore, considering the friction parameters ($w^*_0 = 0.46$, $w^*_1 = 5.7\times10^{-3}$, and $w^*_2 = -2.4\times10^{-4}$) identified previously, and using the LMI constraints of *Proposition 4-1*, a good compromise was found using the parameters $\varepsilon = 0.2$ for the observer decay rate estimation error and $\alpha = 80$ to limit the norm of the gains. The result ends with $\beta = 1.9$ (ratio of the maximum and minimum eigenvalues, for Lyapunov matrix P), $m = 0.5\varepsilon$ and the observer gain $K(\cdot) = \begin{bmatrix} 3.4 + w_1(\cdot) & -3.4 & -1.5 \end{bmatrix}^T$.

Thereafter, we will consider four (4) different cases to study the upper bound behaviour: nominal system (fault-free) case, and 3 other cases based on different fault types, small, medium and high severity.

The table 5.8 shows the average bounds computed based on the DMO (*Theorem 4-1*), CDO (*Theorem 4-2*) and improved DMO (i-DMO, corresponding to the *Remark 4-4* from the previous chapter). Improved CDO-based estimation was omitted, since it gives the same result as the i-DMO.

The table shows, as expected, that the i-DMO is the least conservative, for all situations, and the CDO the most conservative. However, even the best estimation remains, in some cases, conservative as it will be shown thereafter.

Table 5.9 CDO, DMO and i-DMO-based estimation of the observer error upper bound

Fault type	Duration (s)	DMO	CDO	i-DMO
Fault free	0	5.3	4.96	0.7
Small	0.2	6	10	1.28
Medium	1	26.11	2.2×10^6	13.4
Big	1.4	40.49	7×10^9	33.3

5.4.2. Fault-free case

For the fault-free situation the measurements are "exact", and updates of the observer are done as expected. *Fig. 5-12* shows the behavior of the different bounds: i-DMO *(Fig. 5-12 (a))*, DMO (*Fig. 5-12 (b)*) and CDO (*Fig. 5-12 (c)*). The dynamic bounds are represented by the red lines. Their exponential nature has been presented equations (4.11), (4.29), and both (4.19) and (4.40). We can see that the reference is contained in the range of the estimation.

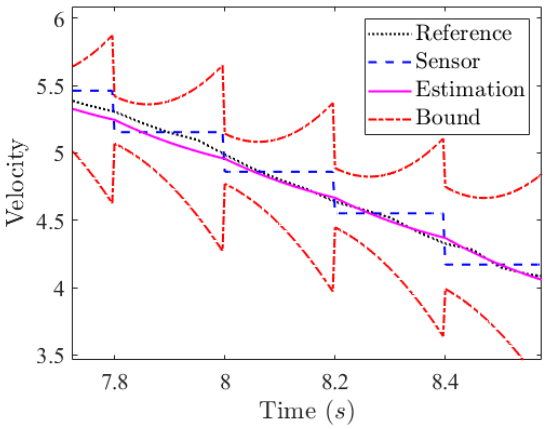

(a) i-DMO bound

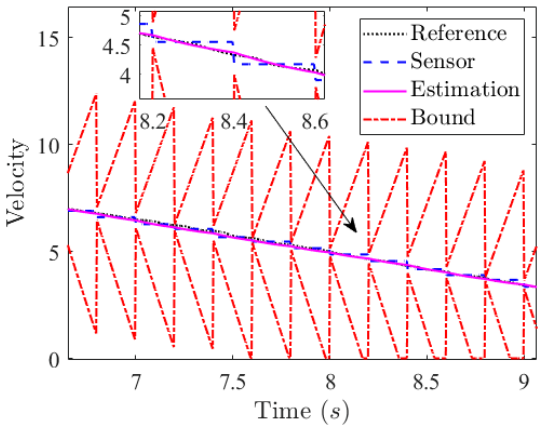

(b) DMO bound

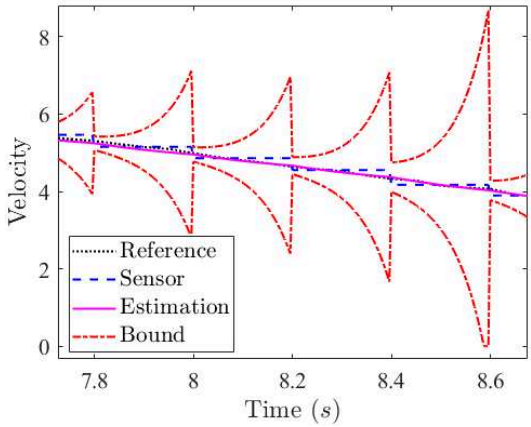

(c) CDO bound

Fig. 5-12 Fault free

5.4.3. Small fault case

Small jamming faults are considered in this case (*Fig. 5-13* again with the 3 cases i-DMO *(a)*, DMO *(b)* and CDO *(c)*), which means that their duration is less than a measurement sample. Here also, no measurement is discarded, a slight decrease can be observed for the measurement with respect to the reference. The observer will not be able to detect the fault that fast, and with a quite small residual. The bound values are similar to the fault free case.

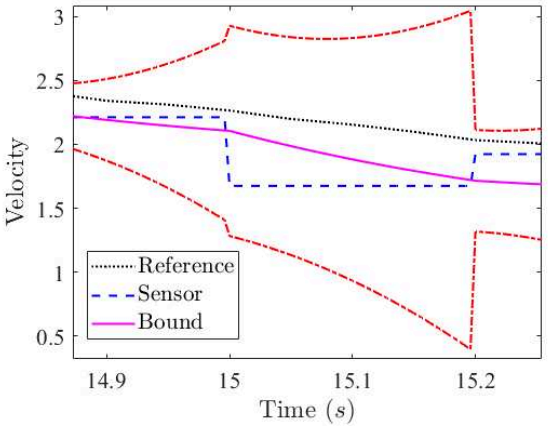

(a) i-DMO bound

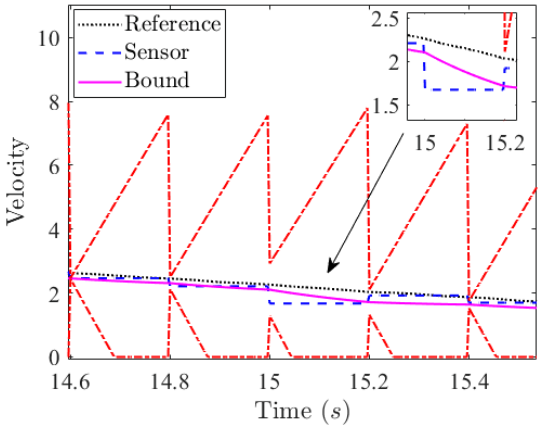

(b) DMO bound

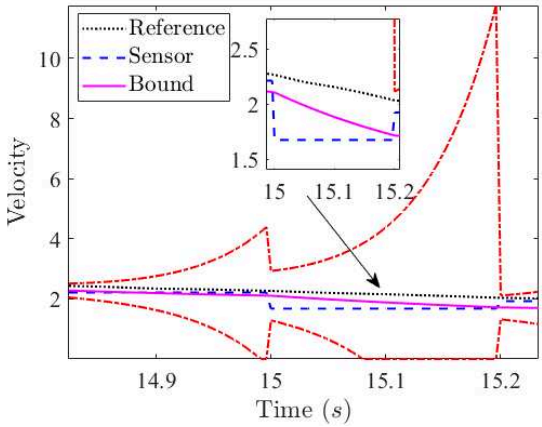

(c) CDO bound

Fig. 5-13 Small fault

5.4.4. Medium fault case

This case corresponds to a jamming duration between 3 and 6 samples. Some measurements are discarded from observer updates, which implies that the bound will continue to increase in an exponential way (*Fig. 5-14*). The reference remains in the bound, as expected.

Notice that for the i-DMO, the first corrupted measurement is on the edge of the bound (*Fig. 5-14 (a)* zoom top left), which makes sense: an unexpected external signal impacting the system will change its behavior, potentially invalidating the bound.

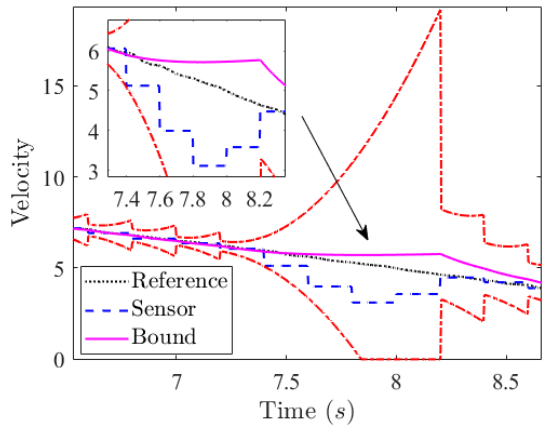

(a) i-DMO bound

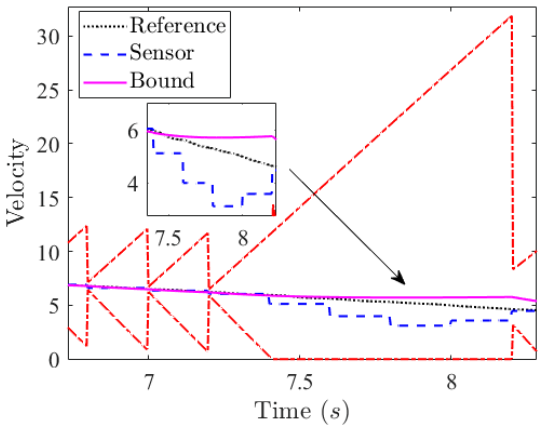

(b) DMO bound

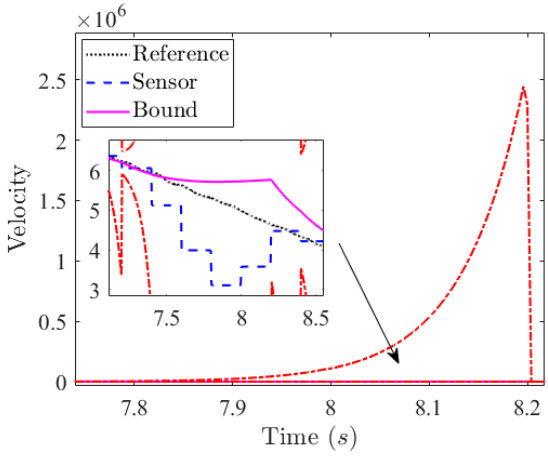

(c) CDO bound

Fig. 5-14 Medium fault

5.4.5. Big fault case

Big faults are those which duration is more than 6 samples. More measurements are discarded, and the exponential nature of the dynamic bounds (*Fig. 5-15*) will quickly render them inadequate, especially for the CDO case.

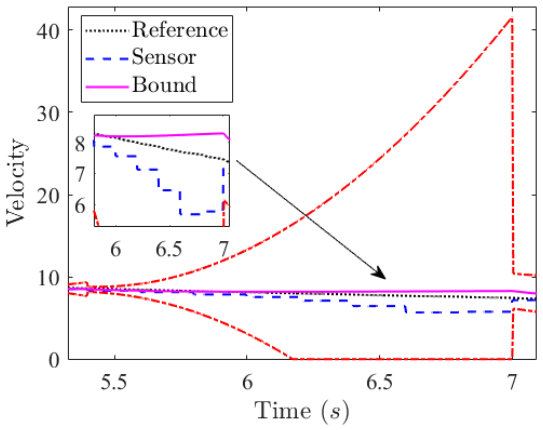

(a) i-DMO bound

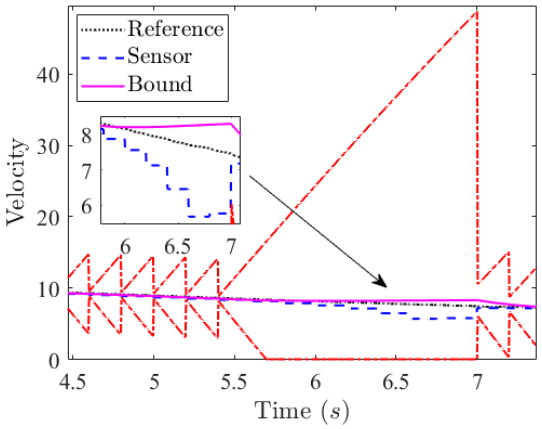

(b) DMO bound

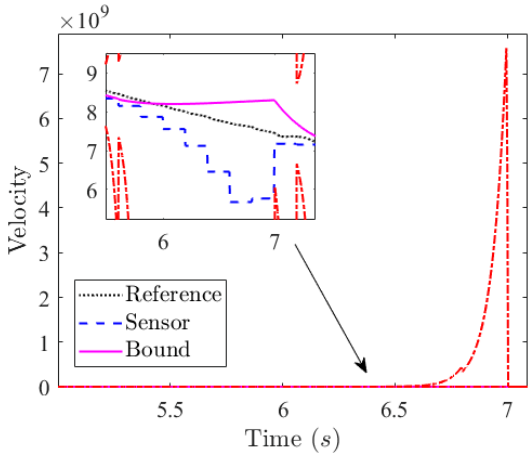

(c) CDO bound

Fig. 5-15 Big fault

5.4.6. Discussion

This short section aimed to show the bound estimation applied to real data, and to discuss its behavior. The exponential nature of the dynamic bounds renders them quickly inappropriate if too many measurements are discarded. In a sense, this is perfectly normal, it takes into account the worst possible case at each instant, therefore cumulating them can result in estimations far from reality. Improvements should come at hand, trying to reduce the gains of the exponential parts, introducing more knowledge in the design of these bounds, using different observer, for example based on a forgetting factor, i.e. the further from a measurement, the less credible the estimation.

5.5. Concluding Remarks

This chapter discusses practical applications of the unknown input observer and the associated fault detection system. First of all, the experimental setup was described, and a preliminary study to identify parameters based on the proposed assumptions was performed. Then, the data set was investigated to determine the adequate threshold for the best fault detection performance, considering the highest fault-detection and lowest undetected fault rates. Case per case discussion was then presented, to show the results and the limits of the proposed algorithms. The ending sections discussed the practical application of the estimated upper bound of observation error, focusing on cases ranging from fault free to various severity jamming faults, when some corrupted measurement updates were discarded.

As expected, when faults are successfully and timely detected, the proposed solution improves the position estimation, with some limitations, concerning mainly faults that do not match the expected model. The estimated bound is conservative, as expected, but is matching the measurements. However, to be useful, less conservativeness is needed, using more extra-information or another form of observer design.

CHAPTER 6. Final words

Conclusion

This thesis dealt with the development of advanced observation and control algorithms and their practical application for railway systems automatic operations, considering uncertain system parameters, limited communication bandwidth, and faults in the system. Two faulty situations were considered in particular: wheel jamming during braking and wheel skidding during traction.

The main result of this research was the design of an unknown input observer in proportional-integral form, with a continuous-discrete update dynamic. This observer can be used for disturbance estimation and fault detection, and is a major component in the proposed fault tolerant control scheme.

There are four contributions in the thesis:

The first contribution was the design of an active fault tolerant braking control, where the main contribution is an integrated approach using an unknown input observer, fault detection, and disturbance compensation control with a reference model for train stopping, with some assumptions on the system. The design of such a system and a discussion on the convergence properties was provided.

The second contribution dealt with the design of a robust position estimation algorithm based on the unknown input observer with a quasi-LPV representation. The assumptions on the system were relaxed with respect to the previous case, as the observer assumed a nonlinear system model, and an unknown control.

The third contribution explored a novel Gronwall-like bound for the observer error, in continuous-discrete dynamic. The unknown input observer was designed in a quasi-LPV framework with a piecewise constant input. Practical considerations on how to improve the bound with extra information from the system were discussed.

The last contribution concerns experimental study: the designed observers were tested on data sets acquired during real time experiments provided by ALSTOM Transport Company. Several situations were studied, considering different speeds and different wheel-track adherence

conditions. The performances of the developed observers were discussed for the presented scenarios, and strategies for observer parameters choice were proposed.

Overall, the proposed approach showed promising results, and needs to be embedded for real-time tests. The Gronwall-like bound formulation and use in such applications is a novel idea, that was proved to be feasible, but needs further investigations to obtain less "pessimistic" estimation for the upper bound of the error.

Perspectives

Both theoretical and applicative perspectives are to be considered:

The applicative perspectives are centered on the real-time exploitation of the algorithms, in a dedicated data acquisition environment, to validate real-time performance of the algorithms: robustness, speed, numerical issues, etc. A complete discretization is considered in order to facilitate the transition.

Another applicative development is the use of a more accurate representation of the train, with a proper dynamic of each vehicle and their interconnections. The model will consider wagons and locomotives separately, with distinct braking controls for each vehicle, and with the traction control remaining exclusive to locomotives.

The following application perspective is related to the exploitation of the existing wheel-track contact cartography and other models of wheel-track adherence to improve the model that is used to derive the observer.

Finally, the practical use of the estimated upper observer error bound for the optimization of the safety intervals and train timetable scheduling must be investigated, among other possibilities.

The theoretical developments are related again to the estimation of the upper observer error bound, and ways to make it less conservative. A promising idea to correct this overestimation is to follow the work of (Mondher Farza, M'Saad, and Busawon 2015; Fall 2015b), using the so-called impulse continuous-discrete observer. It would resume in replacing the gain $K\left(\hat{y}(t)\right)$

in the observer by $K\left(\hat{y}(t)\right)e^{-\eta(t-t_k)}$. It will require a new like-Gronwall lemma, and probably a different approach in the observer design methodology.

Another possible theoretical development is the transposition of the results to the multi-sampling rate framework, and consider dedicated discrete time observer design tools. For example, this could help to improve the design procedure for the robust position estimator discussed in the second section of the third chapter.

References

Aguiar, Braulio, Denis Berdjag, Bernard Demaya, and Thierry Marie Guerra. 2017. "A Robust and Fault Tolerant Approach for Automatic Train Stop Control System Design." In *The 20th IFAC World Congress*, Toulouse, France, 8879–84.

Allan, John J., and E. Arias. 2008. *Multi-Objective Optimization Method for the ATO System Using Cellular Automata*. WIT Press.

Allotta, B et al. 2001. "Distance and Speed Evaluation from Odometric Measurements."

Allotta, B, V Colla, and M Malvezzi. 2002. "Train Position and Speed Estimation Using Wheel Velocity Measurements." *Proceedings of the Institution of Mechanical Engineers, Part F: Journal of Rail and Rapid Transit* 216(3): 207–25.

Astorga, C. -M. et al. 2002. "Nonlinear Continuous–Discrete Observers: Application to Emulsion Polymerization Reactors." *Control Engineering Practice* 10(1): 3–13.

Barna, G. 2011. "Theoretical Analysis of Wheel Slide Protection Controllers for Rail Vehicles." In *2011 16th International Conference on Methods Models in Automation Robotics*, , 230–35.

Bergsten, P., R. Palm, and D. Driankov. 2001. "Fuzzy Observers." In *10th IEEE International Conference on Fuzzy Systems. (Cat. No.01CH37297)*, , 700–703 vol.3.

Blandeau, M. et al. 2018a. "Fuzzy Unknown Input Observer for Understanding Sitting Control of Persons Living with Spinal Cord Injury." *Engineering Applications of Artificial Intelligence* 67: 381–89.

———. 2018b. "Fuzzy Unknown Input Observer for Understanding Sitting Control of Persons Living with Spinal Cord Injury." *Engineering Applications of Artificial Intelligence* 67: 381–89.

Blanke, Mogens, Michel Kinnaert, Jan Lunze, and Marcel Staroswiecki. 2006. *Diagnosis and Fault-Tolerant Control*. Springer Science & Business Media.

Boyd, Stephen, Laurent El Ghaoui, Eric Feron, and Venkataramanan Balakrishnan. 1994. *Linear Matrix Inequalities in System and Control Theory*. SIAM.

C. Johnson. 1968. "Optimal Control of the Linear Regulator with Constant Disturbances." *IEEE Transactions on Automatic Control* 13(4): 416–21.

———. 1970. "Further Study of the Linear Regulator with Disturbances--The Case of Vector Disturbances Satisfying a Linear Differential Equation." *IEEE Transactions on Automatic Control* 15(2): 222–28.

Callahan, Bernard E., and Edward A. Christianson. 1978. “Slip-Slide Detector System for Railway Car Wheels.” https://patents.google.com/patent/US4071282A/en (April 11, 2019).

Cecati, Carlo. 2015. “A Survey of Fault Diagnosis and Fault-Tolerant Techniques—Part II: Fault Diagnosis With Knowledge-Based and Hybrid/Active Approaches.” https://ricerca.univaq.it/handle/11697/94240#.XLi_tzAzaJA (April 18, 2019).

Chen, D., R. Chen, Y. Li, and T. Tang. 2013. “Online Learning Algorithms for Train Automatic Stop Control Using Precise Location Data of Balises.” *IEEE Transactions on Intelligent Transportation Systems* 14(3): 1526–35.

Chen, Jie, Ron J. Patton, and Hong-Yue Zhang. 1996. “Design of Unknown Input Observers and Robust Fault Detection Filters.” *International Journal of Control* 63(1): 85–105.

Chibani, A., M. Chadli, P. Shi, and N. B. Braiek. 2017. “Fuzzy Fault Detection Filter Design for T–S Fuzzy Systems in the Finite-Frequency Domain.” *IEEE Transactions on Fuzzy Systems* 25(5): 1051–61.

Colla, V., M. Vannucci, B. Allottay, and M. Malvezziy. 2003. “Estimation of Train Speed via Neuro–Fuzzy Techniques.” In *Artificial Neural Nets Problem Solving Methods*, Lecture Notes in Computer Science, eds. José Mira and José R. Álvarez. Springer Berlin Heidelberg, 497–503.

Colla, Valentina, Marco Vannucci, B Allotta, and Monica Malvezzi. 2003. “Comparison of Traditional and Neural Systems for Train Speed Estimation.” In , 401–6.

Darouach, M., M. Zasadzinski, and S. J. Xu. 1994. “Full-Order Observers for Linear Systems with Unknown Inputs.” *IEEE Transactions on Automatic Control* 39(3): 606–9.

Delrot, Sabrina, Thierry Marie Guerra, Michel Dambrine, and François Delmotte. 2012. “Fouling Detection in a Heat Exchanger by Observer of Takagi–Sugeno Type for Systems with Unknown Polynomial Inputs.” *Engineering Applications of Artificial Intelligence* 25(8): 1558–66.

Dinh, T. N., V. Andrieu, M. Nadri, and U. Serres. 2015. “Continuous-Discrete Time Observer Design for Lipschitz Systems With Sampled Measurements.” *IEEE Transactions on Automatic Control* 60(3): 787–92.

Dong, H., B. Ning, B. Cai, and Z. Hou. 2010. “Automatic Train Control System Development and Simulation for High-Speed Railways.” *IEEE Circuits and Systems Magazine* 10(2): 6–18.

Douglas, Heather et al. 2017. “Method for Validating the Train Motion Equations Used for Passenger Rail Vehicle Simulation.” *Proceedings of the Institution of Mechanical Engineers, Part F: Journal of Rail and Rapid Transit* 231(4): 455–69.

Dragomir, Sever Silvestru. 2003. *Some Gronwall Type Inequalities and Applications*. Rochester, NY: Social Science Research Network. SSRN Scholarly Paper. https://papers.ssrn.com/abstract=3158353 (April 23, 2018).

Duan, Guang-Ren, and Hai-Hua Yu. 2013. *LMIs in Control Systems: Analysis, Design and Applications*. CRC Press.

Edelmayer, A., J. Bokor, and L. Keviczky. 1994. "An H Infin; Filtering Approach to Robust Detection of Failures in Dynamical Systems." In *Proceedings of 1994 33rd IEEE Conference on Decision and Control*, , 3037–39 vol.3.

Faieghi, Mohammadreza, Aliakbar Jalali, and Seyed Kamal-e-ddin Mousavi Mashhadi. 2014. "Robust Adaptive Cruise Control of High Speed Trains." *ISA Transactions* 53(2): 533–41.

Fall, Mamadou Lamine. 2015a. "Synthesis of Observers for Nonlinear Systems - Application to the Control and Diagnosis of Bioreactors." Ph. D. thesis. Université de Caen. https://hal.archives-ouvertes.fr/tel-01148795.

———. 2015b. "Synthesis of Observers for Nonlinear Systems - Application to the Control and Diagnosis of Bioreactors." Ph. D. thesis. Université de Caen. https://hal.archives-ouvertes.fr/tel-01148795.

Farza, M. et al. 2014a. "Continuous-Discrete Time Observers for a Class of MIMO Nonlinear Systems." *IEEE Transactions on Automatic Control* 59(4): 1060–65.

———. 2014b. "Continuous-Discrete Time Observers for a Class of MIMO Nonlinear Systems." *IEEE Transactions on Automatic Control* 59(4): 1060–65.

Farza, Mondher, Mohammed M'Saad, and Krishna Busawon. 2015. "Continuous–Discrete-Time Observers for a Class of Uniformly Observable Systems." In *Hybrid Dynamical Systems: Observation and Control*, eds. Mohamed Djemai and Michael Defoort. Cham: Springer International Publishing, 261–75. https://doi.org/10.1007/978-3-319-10795-0_10.

Gao, Z., C. Cecati, and S. X. Ding. 2015. "A Survey of Fault Diagnosis and Fault-Tolerant Techniques -Part I: Fault Diagnosis With Model-Based and Signal-Based Approaches." *IEEE Transactions on Industrial Electronics* 62(6): 3757–67.

Gao, Z., S. X. Ding, and C. Cecati. 2015. "Real-Time Fault Diagnosis and Fault-Tolerant Control." *IEEE Transactions on Industrial Electronics* 62(6): 3752–56.

Gao, Z., X. Liu, and M. Z. Q. Chen. 2016. "Unknown Input Observer-Based Robust Fault Estimation for Systems Corrupted by Partially Decoupled Disturbances." *IEEE Transactions on Industrial Electronics* 63(4): 2537–47.

Garcia-Rivera, M., R. Sanz, and J. A. Perez-Rodriguez. 1997. "An Antislipping Fuzzy Logic Controller for a Railway Traction System." In *Proceedings of 6th International Fuzzy Systems Conference*, , 119–24 vol.1.

Guzinski, J. et al. 2009. "Application of Speed and Load Torque Observers in High-Speed Train Drive for Diagnostic Purposes." *IEEE Transactions on Industrial Electronics* 56(1): 248–56.

Hernández, Héctor, and Jesús Alvarez. 2003. "Robust Estimation of Continuous Nonlinear Plants with Discrete Measurements." *Journal of Process Control* 13(1): 69–89.

Hiscox, Leonard Ramsay. 1976. "Wheel Slide Protection System." https://patents.google.com/patent/US3936941A/en (April 11, 2019).

Howlett, P. G., I. P. Milroy, and P. J. Pudney. 1994. "Energy-Efficient Train Control." *Control Engineering Practice* 2(2): 193–200.

Hubbard, Peter, Chris Ward, Roger Dixon, and Roger Goodall. 2013. "Real Time Detection of Low Adhesion in the Wheel/Rail Contact." *Proceedings of the Institution of Mechanical Engineers, Part F: Journal of Rail and Rapid Transit* 227(6): 623–34.

"Incremental Encoders - Lenord+Bauer." https://www.lenord.com/products/incremental-encoders/?L=34.

Isermann, Rolf. 2006. *Fault-Diagnosis Systems An Introduction from Fault Detection to Fault Tolerance*. 1st ed. Springer-Verlag Berlin Heidelberg. https://www.springer.com/us/book/9783540241126.

Iwnicki, Simon. 2006. *Handbook of Railway Vehicle Dynamics*. Taylor & Francis.

Izumi, Hasegawa, and Uchida Seigo. 1999. "Braking Systems." *Japan Railway and Transport*: 52–59.

Jazwinski, Andrew H. 2007. *Stochastic Processes and Filtering Theory*. Courier Corporation.

Jee, Sung Chul, Ho Jae Lee, and Young Hoon Joo. 2012. "Sensor Fault Detection Observer Design for Nonlinear Systems in Takagi–Sugeno's Form." *Nonlinear Dynamics* 67(4): 2343–51.

Jesussek, Mathias, and Katrin Ellermann. 2013. "Fault Detection and Isolation for a Nonlinear Railway Vehicle Suspension with a Hybrid Extended Kalman Filter." *Vehicle System Dynamics* 51(10): 1489–1501.

José A. Lozano. 2012. "Railway Traction." In *Reliability and Safety in Railway*, ed. Jesús Félez. Rijeka: IntechOpen, Ch. 1. https://doi.org/10.5772/36339 (May 5, 2019).

Kaller, Roger, and Jean-Marc Allenbach. 1995. *Traction Électrique*. Lausanne, Suisse: Presses polytechniques et universitaires romandes.

Karafyllis, I., and Z.-P. Jiang. 2011. “A Vector Small-Gain Theorem for General Non-Linear Control Systems.” *IMA Journal of Mathematical Control and Information* 28(3): 309–44.

Karafyllis, I., and C. Kravaris. 2009. “From Continuous-Time Design to Sampled-Data Design of Observers.” *IEEE Transactions on Automatic Control* 54(9): 2169–74.

Kowalczuk, Z. 1993. “Discrete Approximation of Continuous-Time Systems: A Survey.” *IEE Proceedings G - Circuits, Devices and Systems* 140(4): 264–78.

Lazarević, Mihailo P., and Aleksandar M. Spasić. 2009. “Finite-Time Stability Analysis of Fractional Order Time-Delay Systems: Gronwall’s Approach.” *Mathematical and Computer Modelling* 49(3–4): 475–81.

Lendek, Zs. et al. 2010. “Adaptive Observers for TS Fuzzy Systems with Unknown Polynomial Inputs.” *Fuzzy Sets and Systems* 161(15): 2043–65.

Li, L. et al. 2018. “Diagnostic Observer Design for T–S Fuzzy Systems: Application to Real-Time-Weighted Fault-Detection Approach.” *IEEE Transactions on Fuzzy Systems* 26(2): 805–16.

Ling, Chen, and Costas Kravaris. 2017a. “Multi-Rate Observer Design for Process Monitoring Using Asynchronous Inter-Sample Output Predictions.” *AIChE Journal* 63(8): 3384–94.

———. 2017b. “Multi-Rate Sampled-Data Observers Based on a Continuous-Time Design.” In *2017 IEEE 56th Annual Conference on Decision and Control (CDC)*, Melbourne, Australia: IEEE, 3664–69. http://ieeexplore.ieee.org/document/8264198/ (May 1, 2019).

Liu, Rongfang (Rachel), and Iakov M. Golovitcher. 2003. “Energy-Efficient Operation of Rail Vehicles.” *Transportation Research Part A: Policy and Practice* 37(10): 917–32.

Makhortova, N., and Y. Vivdenko. 2012. “Rail Vehicle Wheels Common Faults Characteristic.” *Teka Komisji Motoryzacji i Energetyki Rolnictwa* 4(12). https://www.infona.pl//resource/bwmeta1.element.agro-b2955fba-4524-4934-8442-d4b03945ec9f (March 29, 2019).

Malvezzi, Monica et al. “Train Position and Speed Estimation by Integration of Odometers and IMUs.” : 11.

Marx, B., D. Koenig, and J. Ragot. 2007. “Design of Observers for Takagi–Sugeno Descriptor Systems with Unknown Inputs and Application to Fault Diagnosis.” *IET Control Theory & Applications* 1(5): 1487–95.

Mazenc, Frédéric, Saeed Ahmed, and Michael Malisoff. 2018. “Finite Time Estimation through a Continuous-Discrete Observer.” *International Journal of Robust and Nonlinear Control* 28(16): 4831–49.

Mazenc, Frédéric, and Thach Ngoc Dinh. 2014. "Construction of Interval Observers for Continuous-Time Systems with Discrete Measurements." *Automatica* 50(10): 2555–60.

Miyatake, Masafumi, and Hideyoshi Ko. 2010. "Optimization of Train Speed Profile for Minimum Energy Consumption." *IEEJ Transactions on Electrical and Electronic Engineering* 5(3): 263–69.

Moarref, Miad, and Luis Rodrigues. 2014. "Stability and Stabilization of Linear Sampled-Data Systems with Multi-Rate Samplers and Time Driven Zero Order Holds." *Automatica* 50(10): 2685–91.

Nadri, M., H. Hammouri, and C. Astorga. 2004. "Observer Design for Continuous-Discrete Time State Affine Systems up to Output Injection." *European Journal of Control* 10(3): 252–63.

Nadri, M., H. Hammouri, and R. M. Grajales. 2013. "Observer Design for Uniformly Observable Systems With Sampled Measurements." *IEEE Transactions on Automatic Control* 58(3): 757–62.

Onat, Altan, Petr Voltr, and Michael Lata. 2017. "A New Friction Condition Identification Approach for Wheel–Rail Interface." *International Journal of Rail Transportation* 5(3): 127–44.

Pazera, M., and M. Witczak. 2016. "Towards Robust Process Fault Estimation for Uncertain Dynamic Systems." In *2016 21st International Conference on Methods and Models in Automation and Robotics (MMAR)*, , 877–82.

Phat, V.N., and K. Ratchagit. 2011. "Stability and Stabilization of Switched Linear Discrete-Time Systems with Interval Time-Varying Delay." *Nonlinear Analysis: Hybrid Systems* 5(4): 605–12.

Rath, Heinrich B. 1984. "Wheel Slide Protection System." https://patents.google.com/patent/US4456309A/en (April 11, 2019).

Ridolfi, Alessandro et al. 2011. "Train Position and Speed Estimation by Integration of Odometers and IMUs."

Rochard, B P, and F Schmid. 2000. "A Review of Methods to Measure and Calculate Train Resistances." *Proceedings of the Institution of Mechanical Engineers, Part F: Journal of Rail and Rapid Transit* 214(4): 185–99.

S. A. Ali, A. Christen, S. Begg, and N. Langlois. 2016. "Continuous–Discrete Time-Observer Design for State and Disturbance Estimation of Electro-Hydraulic Actuator Systems." *IEEE Transactions on Industrial Electronics* 63(7): 4314–24.

Saab, S. S., G. E. Nasr, and E. A. Badr. 2002. "Compensation of Axle-Generator Errors Due to Wheel Slip and Slide." *IEEE Transactions on Vehicular Technology* 51(3): 577–87.

Sandidzadeh, Mohammad Ali, and Ali Khodadadi. 2011. "Optimization of Balise Placement in a Railway Track Using a Vehicle, an Odometer and Genetic Algorithm." *JSIR Vol.70(03) [March 2011]*. http://nopr.niscair.res.in/handle/123456789/11088 (April 8, 2019).

Sheppard, Charles W. 1969. "Combined Anti-Slip and Anti-Spin Control for Vehicle Wheels." https://patents.google.com/patent/US3482887A/en (April 11, 2019).

"Speed Sensors - Lenord+Bauer." https://www.lenord.com/products/speed-sensors/.

Sutton, Christopher John. 1977. "Vehicle Wheel Slide Protection Systems." https://patents.google.com/patent/US4018486A/en (April 11, 2019).

Tan, C., G. Tao, H. Yang, and L. Wen. 2018. "An Adaptive Switching Based Actuator Failure Compensation Scheme for Control of High-Speed Trains." In *2018 IEEE 14th International Conference on Control and Automation (ICCA)*, , 857–62.

Tanaka, Kazuo, and Hua O. Wang. 2001. *Fuzzy Control Systems Design and Analysis: A Linear Matrix Inequality Approach*. John Wiley & Sons.

Tatiraju, Srinivas, Masoud Soroush, and Babatunde A. Ogunnaike. 1999. "Multirate Nonlinear State Estimation with Application to a Polymerization Reactor." *AIChE Journal* 45(4): 769–80.

"The Railway Technical Website." *The Railway Technical Website | PRC Rail Consulting Ltd*. http://www.railway-technical.com/signalling/automatic-train-control.html.

Theilliol, D., and S. Aberkane. 2011. "Design of LPV Observers with Immeasurable Gain Scheduling Variable under Sensor Faults." *IFAC Proceedings Volumes* 44(1): 7613–18.

Tractive Effort, Acceleration and Braking. 2004. The Mathematical Association.

Verbert, K., B. De Schutter, and R. Babuška. 2016. "Fault Diagnosis Using Spatial and Temporal Information with Application to Railway Track Circuits." *Engineering Applications of Artificial Intelligence* 56: 200–211.

Vijay, Garg. 1984. *Dynamics of Railway Vehicle Systems*. Academic Press.

Wang, Jian Liang, Guang-Hong Yang, and Jian Liu. 2007. "An LMI Approach to H- Index and Mixed H-/H∞ Fault Detection Observer Design." *Automatica* 43(9): 1656–65.

Wang, Zhenhua, Cheng-Chew Lim, Peng Shi, and Yi Shen. 2017. "H-/L∞ Fault Detection Observer Design for Linear Parameter-Varying Systems." *IFAC-PapersOnLine* 50(1): 15271–76.

Watanabe, T. et al. 1997. "Optimization of Readhesion Control of Shinkansen Trains with Wheel-Rail Adhesion Prediction." In *Proceedings of Power Conversion Conference - PCC '97*, , 47–50 vol.1.

Wei, Xiukun, Limin Jia, and Hai Liu. 2013. "A Comparative Study on Fault Detection Methods of Rail Vehicle Suspension Systems Based on Acceleration Measurements." *Vehicle System Dynamics* 51(5): 700–720.

Witczak, M. et al. 2015. "A Robust $\mathcal{H}\infty$observer Design for Unknown Input Nonlinear Systems: Application to Fault Diagnosis of a Wind Turbine." In *2015 23rd Mediterranean Conference on Control and Automation (MED)*, , 162–67.

Wood, James A., and Richard J. Mazur. 1990. "Electronic Adhesion Adaptive Wheel Slide Protection Arrangement Function." https://patents.google.com/patent/US4941099A/en (April 11, 2019).

Wu, Qing, Maksym Spiryagin, and Colin Cole. 2016. "Longitudinal Train Dynamics: An Overview." *Vehicle System Dynamics* 54(12): 1688–1714.

Wu, Yunkai, Bin Jiang, and Peng Shi. 2016. "Incipient Fault Diagnosis for T–S Fuzzy Systems with Application to High-Speed Railway Traction Devices." *IET Control Theory & Applications* 10(17): 2286–97.

Yang, Hui, Ya-Ting Fu, Kun-Peng Zhang, and Zhong-Qi Li. 2014. "Speed Tracking Control Using an ANFIS Model for High-Speed Electric Multiple Unit." *Control Engineering Practice* 23: 57–65.

Yin, Jiateng et al. 2017. "Research and Development of Automatic Train Operation for Railway Transportation Systems: A Survey." *Transportation Research Part C: Emerging Technologies* 85: 548–72.

Yoneyama, Jun, Masahiro Nishikawa, Hitoshi Katayama, and Akira Ichikawa. 2001. "H_ Infinity Control for Takagi-Sugeno Fuzzy Systems." *International Journal of Systems Science* 32(7): 915–24.

Zhang, Jian, Akshya Kumar Swain, and Sing Kiong Nguang. 2016. *Robust Observer-Based Fault Diagnosis for Nonlinear Systems Using MATLAB®*. Springer.

Zhang, Q. 2002. "Adaptive Observer for Multiple-Input-Multiple-Output (MIMO) Linear Time-Varying Systems." *IEEE Transactions on Automatic Control* 47(3): 525–29.

Zhong, Maiying, Steven X. Ding, James Lam, and Haibo Wang. 2003. "An LMI Approach to Design Robust Fault Detection Filter for Uncertain LTI Systems." *Automatica* 39(3): 543–50.

Zhou, Meng, Mickael Rodrigues, Yi Shen, and Didier Theilliol. 2017. "H − /H ∞ Fault Detection Observer Design Based on Generalized Output for Polytopic LPV System." *Journal of Physics: Conference Series* 783(1): 012002.

Zhou, Yu Wei. 2012. "Research of Multi-Sensor Integration System for Train Speed and Position Measurement." *Applied Mechanics and Materials* 105–107: 1920–25.